How to weld:
Energies, weldings and driving functions

Tim Mesikepp

A dissertation
submitted in partial fulfillment of the
requirements for the degree of

Doctor of Philosophy

University of Washington

2021

Reading Committee:
Steffen Rohde, Chair
Donald Marshall
Jayadev Athreya

Program Authorized to Offer Degree:
Mathematics

University of Washington

Abstract

How to weld:
Energies, weldings and driving functions

Tim Mesikepp

Chair of the Supervisory Committee:
Professor Steffen Rohde
Department of Mathematics

We prove a variant of the welding zipper algorithm converges for curves $\gamma \subset \mathbb{H} \cup \{0\}$ that have Loewner driving functions $\xi \in C^{3/2+\epsilon}$. Convergence holds whether one "zips up" with straight line segments, circular arc segments orthogonal to $\mathbb{R}$, or either of two energy-minimizing curve families, or any combination of these. One of the energy-minimizing families is new, and we also prove some new properties of the known minimizing family. We furthermore show the Loewner energy of a curve can be computed by means of the conformal welding through the *zipper welding energy*. Lastly, we generalize a result of Bishop from T_2 Weil-Petersson quasicircles to the p-integrable Teichmüller space T_p, showing $\gamma \in T_p$ if and only if γ has p-summable β-numbers, for $p > 2$.

TABLE OF CONTENTS

ACKNOWLEDGMENTS

I owe a tremendous debt to my advisor Steffen Rohde for the enormous amount of time he has invested in me. It is hard to quantify how much I have learned from him, and I gratefully acknowledge that precious little in these pages could be done without his assistance. It was both a privilege and pleasure to work with an advisor who was so generous with his time and ideas. I am also very thankful to Don Marshall for many stimulating conversations and ideas about the zipper (not to mention his invention of the algorithm), and for his very careful reading of this thesis. Thanks also to Yilin Wang for helpful discussion of Loewner energy and energy-minimizing curves, and to Chris Bishop for generous explanations and discussion related to β-numbers and Teichmüller space.

I am grateful to have done grad school alongside my academic siblings Peter Lin, Camilo Posse and Zijian Li. Thanks, gentlemen, for being great brothers.

I do not think I would have survived grad school in any healthy sense of the term without the support of my friends in the Ravenna community group of Trinity Church Seattle. Thank you for praying for me, holding me accountable, and meeting faithfully on Thursday nights to study the Scriptures. I thank God for you all.

I know I would not have survived grad school without the support and prayers of my wife Leigh, who gracefully handled the stress of both COVID-19 and my last year of grad school, all during our first year of marriage and her third year of graduate study. What a remarkable woman, and what a gift. Thank you, dear.

Lastly, I give praise and thanksgiving to my Creator and Redeemer, the Triune God, for the opportunity to study and explore the wonderful world of mathematics. "Great are the works of the LORD, studied by all who delight in them." - Psalm 111:2.

Chapter 1
INTRODUCTION

While two components Ω, Ω^* of the complement $\hat{\mathbb{C}}\backslash\gamma$ of a Jordan curve $\gamma = \partial\Omega = \partial\Omega^*$ are conformally equivalent to the unit disk by Riemann's famous theorem, the conformal maps are rarely explicitly computable. Numerical approximations can be important in practice, and the *zipper algorithm* is an umbrella term for two such computational methods. Both give an approximate conformal map $f : \mathbb{D} \to \Omega$; one through a discretization $\{z_1, \ldots, z_n\}$ of γ itself, and the other through a discretization $\{(x_j, \varphi(x_j)\}$ of the conformal welding φ of γ. We call these the *domain zipper* and *welding zipper*, respectively.

This thesis presents a partial proof of the convergence of the welding zipper algorithm.* We consider the problem from the point of view of the Loewner differential equation and prove that a small variation of the algorithm convergences for curves $\gamma \subset \mathbb{H} \cup \{0\}$ with Loewner driving function $\xi \in C^{3/2+\epsilon}$. In what follows, we explain the welding zipper in §1.1 and then describe our convergence result and proof strategy in §1.2. We outline the remaining results in the thesis in §1.3.

1.1 The welding zipper

Consider a welding φ determined by a finite Jordan arc $\gamma \subset \mathbb{H} \cup \{0\}^\dagger$, discretized at the nth stage into pairs $\{(x_{nj}, y_{nj})\}_{j=1}^{N(n)}$, where $y_{nj} = \varphi(x_{nj})$ and

$$x_{n,N(n)} < x_{n,N(n)-1} < \cdots < x_{n1} < 0 < y_{n1} < y_{n2} < \cdots < y_{n,N(n)}.$$

*Marshall and Rohde have convergence results for the domain zipper. Since our focus is exclusively on the welding zipper, we do not discuss their work here, but refer the reader to [28].

†The usual context for conformal welding is $\mathbb{S}^1$, but we formulate the problem in $\mathbb{H}$ because it is a natural setting for programming the algorithm. Weldings on the circle can be approximated in this way by first transferring them to the real line.

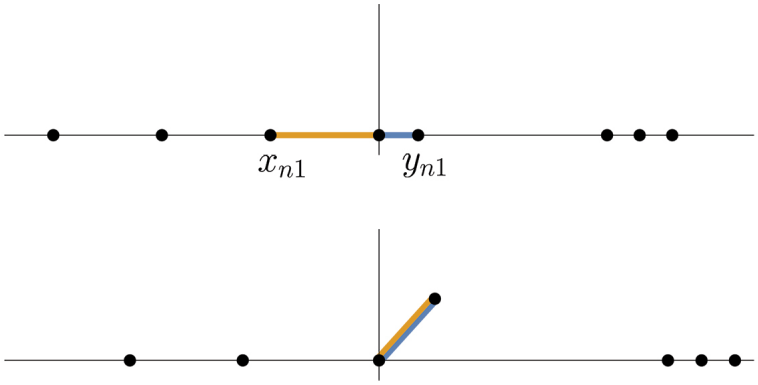

Figure 1.1: One zipper step with the straight slit family; the two intervals on either side of the origin are welded together to a single line segment, with the data points x_{n1}, y_{n1} joined at the origin. The process is then repeated for the next closest points to zero. See Figure 1.3 for other curve options for a single zip.

How can you construct a curve γ_n^c such that γ_n^c's welding φ_n^c satisfies $\varphi_n^c(x_{nj}) = y_{nj}$ for all $1 \leq j \leq N(n)$? The welding zipper algorithm, invented by Don Marshall in collaboration with Lennart Carleson in the early 1980's, answers this by iteratively "zipping up" pairs of data points. The idea is to fix a family of curves, such as straight line segments, and begin with the pair $x_{n1} < 0 < y_{n1}$ closest to zero. "Zip up" the interval $[x_{n1}, y_{n1}]$ with the line segment $\tilde{\gamma}_{n1}$ that welds x_{n1} to y_{n1} together at 0 and sends 0 to the tip, by means of applying the corresponding conformal map $F_{n1} : \mathbb{H} \to \mathbb{H}\backslash\tilde{\gamma}_{n1}$. This welds the interval $[x_{n1}, 0]$ to $[0, y_{n1}]$, taking them to the left- and right-sides of the curve, respectively, as in Figure 1.1.

After applying F_{n1} to the data there are new points closest to the origin. Now repeat, zipping up the next pair $F_{n1}(x_{n2}) < 0 < F_{n1}(y_{n2})$ with the curve which welds these together. Iterate these zips to form a conformal map $F_n^c := F_{n,N(n)} \circ \cdots \circ F_{n1}$ to the complement of the constructed curve γ_n^c.

As the mesh $\{(x_{nj}, y_{nj})\}$ is refined as n increases, do the γ_n^c converge to γ? By construction, the computed weldings φ_n^c agree with the true welding φ at all x_{nj}, and since they are also monotonic, it immediately follows that the φ_n^c converge uniformly to φ; this much

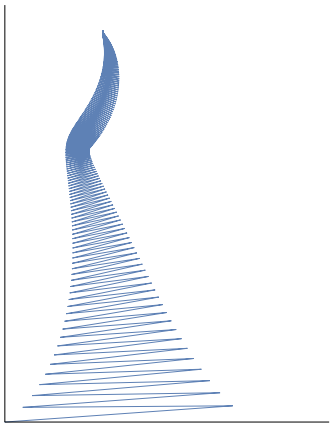

Figure 1.2: A curve constructed with a zipper-like process converging to a set with non-empty interior.

is trivial. Numerical examples, however, show that this need not imply that γ_n^c converges to γ. The question of convergence is basically whether or not the errors in γ_n^c spiral out of control, leading to extreme oscillations and sub-sequential limits with non-empty interior, as in Figure 1.2. The question of how to handle these errors is vexing, and up to this point there have been scant convergence results for the welding zipper, even though it behaves extremely well numerically.

1.2 Convergence result and the flow of the argument

Our approach is to broaden the viewpoint and also consider the Loewner driving functions of γ_n^c and γ, not just their weldings. Using tools from the Loewner theory, we prove that the welding zipper algorithm converges when run from a careful perturbation of the data which replaces the welding discretization $\{(x_{nj}, y_{nj})\}$ with shifted points $\{(x_{nj} + \delta_{nj}^x, y_{nj} + \delta_{nj}^y)\}$, which we call the *equilibria points*.

Theorem 1.1. *Let γ be a finite Jordan arc in $\mathbb{H} \cup \{0\}$ with welding $\varphi : [-a, 0] \to [0, b]$ and*

driving function $\xi \in C^{3/2+\epsilon}([0,T])$ *for some* $\epsilon > 0$. *Let*

$$\{\mathcal{P}_n = (x_{n,N(n)}, x_{n,N(n)-1}, \ldots, x_{n1})\}_{n=1}^{\infty}$$

be any sequence of partitions of $[-a,0]$ *that become finer and finer, in the sense that the half-plane capacities of the corresponding curve segments satisfy*

$$\lim_{n\to\infty} \max_{2\le j\le N(n)} \mathrm{hcap}_{\gamma}(x_{nj}, x_{n,j-1}) = 0. \tag{1.1}$$

There exists a small perturbation $\{(x_{nj}+\delta_{nj}^x, y_{nj}+\delta_{nj}^y)\}_{j=1}^{N(n)}$ *of the discretization* $\{(x_{nj}, y_{nj})\}_{j=1}^{N(n)}$ *of the welding* φ *such that the welding zipper algorithm run on the perturbed points converges, in the sense that the constructed curves* γ_n *converge uniformly to* γ *in their capacity parametrizations on compact subsets of* $[0,T)$.

Convergence holds whether one zips up with straight line segments, circular arcs, either of the two energy-minimizing curve families, or any combination of these curve families.

See Chapter 2 for unexplained terminology and notation. The idea behind the equilibria points is to nudge the data so that the constructed driving function ξ_n^c on each zipper increment has the same ending value as the driver ξ for the true curve on the corresponding increment. We explain the intuition behind this choice and how to carefully construct the shifts $\delta_{nj}^x, \delta_{nj}^y$ at the start of Chapter 6. It follows almost immediately that running the zipper from these shifted points builds curves γ_n^c whose drivers ξ_n^c converge to the true driving function ξ, as we also show in Chapter 6. This is more data in our hand than mere welding convergence. In fact, we prove in Chapter 4 that driver convergence is stronger than welding convergence, a result we have jointly with V. Margarint and Y. Yuan. Combined with tools from quasiconformal mappings and known results in Loewner theory, we show in Chapter 7 that the convergence $\xi_n^c \to \xi$ is robust enough to yield convergence of the constructed curves $\gamma_n^c \to \gamma$, completing the proof of Theorem 1.1.

The organization of the rest of the thesis is as follows. We lay introductory groundwork in Chapter 3 by giving infinitesimal expansions for the points welded by ξ at time $t+\epsilon$ in terms of $\dot{\xi}(t)$. These receive heavy use, and enable us to precisely describe the *equilibria shifts* $\delta_{nj}^x, \delta_{nj}^y$.

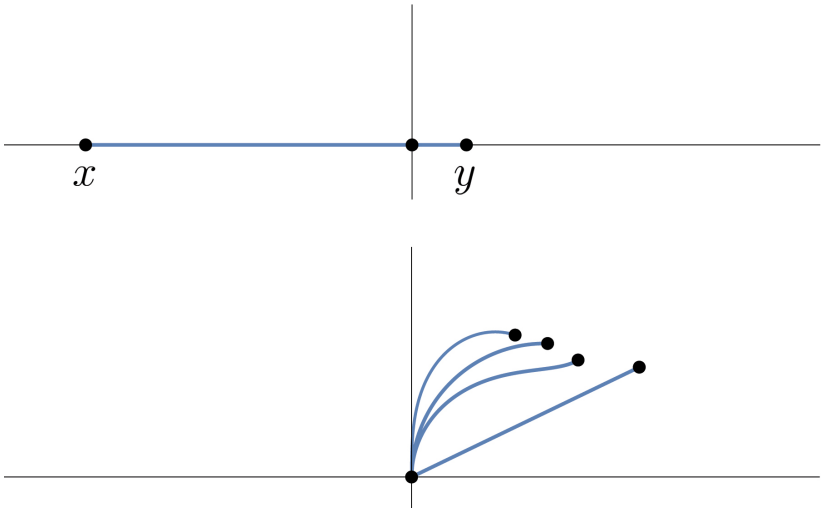

Figure 1.3: The four curve families in Theorem 1.1 welding the same points $x < 0 < y$. From left to right in the lower picture: the EMW family, the circular arc family, the Wang minimizers, and the straight slit family. See Chapter 5.

In Chapter 5 we discuss the four curve families appearing in the statement of Theorem 1.1, which are illustrated in Figure 1.3. In particular, we offer deterministic proofs for some known properties of the curve from 0 to a point $z \in \mathbb{H}$ which minimizes Loewner energy among all such curves, the *Wang minimizer*, and prove several new properties, including explicitly calculating its driving function; see Theorem 5.2. We also introduce a new family and prove the existence and uniqueness of the curve which minimizes the Loewner energy among all curves welding $x < 0 < y$, the *EMW curve*. We compute its energy and show that all such curves, up to scaling and reflection, come from a single planar curve; see Theorem 5.5 and Figure 5.3. We also show in Lemma 5.7 that the orthogonal circular arc is, curiously, a factor of exactly 9/8 away from the energy usage of both the above minimizing families. We close Chapter 5 in §5.7 by discussing the slowest and fastest ways to weld $x < 0 < y$ with a monotonic driver, which yields some interesting and open questions about what curve families produce a convergent zipper algorithm.

1.3 Other results

This thesis also includes several auxiliary results. In Chapter 8 we introduce two ways to compute the Loewner energy of a curve through the zipper algorithm, which we call *welding energies*. We show in Theorems 8.2 and 8.8 that the ℓ^2-deviation from 1/2 of the "zipping angle" $\frac{y}{y-x}$ of the next two equilibria points $x+\delta < 0 < y+\delta$ to be zipped up, what we call the *zipper welding energy*, converges to a multiple of the Loewner energy. In Chapter 9 we consider regularity of quasicircles γ in the p-integrable Teichmüller space T_p, and show that $\gamma \in T_p$ if and only if the β-numbers for γ are in ℓ^p, for $p > 2$. This generalizes a result of Bishop [5] from the case $p = 2$.

Chapter 2
PRELIMINARIES AND NOTATION

In this chapter we discuss the background material of conformal welding, the Loewner equation, driving functions, Loewner energy, quasiconformal mappings and $C^{n,a}$-classes. This provides introductory explanation for the non-expert, establishes our notation, and sets the stage for chapters 3 to 8. Because Chapter 9 is thematically distinct and uses notation not found elsewhere in the thesis, we begin that chapter by reviewing pertinent background and notation rather than including that material here.

2.1 Conformal welding

Consider a (closed) Jordan curve $\Gamma \subset \mathbb{C}$, dividing the plane into a bounded component Ω and an unbounded component Ω^*. These domains are simply-connected regions in $\hat{\mathbb{C}}$, and hence have associated Riemann maps $f : \mathbb{D} \to \Omega$ and $g : \mathbb{D}^* \to \Omega^*$, where $\mathbb{D}^* := \hat{\mathbb{C}} \backslash \overline{\mathbb{D}}$. Because Γ is Jordan both f and g extend to be homeomorphisms of $\mathbb{T} := \partial\mathbb{D}$ onto Γ, and so one may define the *conformal welding associated to* Γ as the increasing homeomorphism $h : \mathbb{T} \to \mathbb{T}$ given by $g^{-1} \circ f$. Of course without further restrictions h is not unique: for any two Möbius maps $\varphi_1, \varphi_2 \in \mathrm{Aut}(\mathbb{D}) = \mathrm{Aut}(\mathbb{D}^*)$,

$$\varphi_2^{-1} \circ g^{-1} \circ f \circ \varphi_1 \tag{2.1}$$

is another welding associated to Γ. But if one fixes a normalization on both sides, such as $f(0) = w \in \Omega$, $f'(0) > 0$ and $g(\infty) = \infty$, $g'(\infty) > 0$, then all degrees of freedom in Riemann maps, and hence the welding, are removed.

An intuitive way to think about the welding h is as an equivalence relation between the boundaries of two copies of $\mathbb{D}$. Or, in the older, more picturesque vocabulary, a way

of "sewing" the disks together. When you "sew" along h, the resulting topological space $X := \mathbb{D} \coprod \mathbb{D} / \sim_h$ is a real 2-manifold homeomorphic to $\mathbb{S}^2$. But the fact that h arose from conformal boundary data yields consistent complex coordinates on X, i.e. X is also a Riemann surface. Indeed, the coordinates are obvious on the interior of either disk, and for a point $\zeta \sim h(\zeta)$ on the boundary, pull back a small disk D around $f(\zeta) = g(h(\zeta))$ into a piece $B := f^{-1}(\overline{\Omega} \cap D)$ and $B^* := g^{-1}(\overline{\Omega^*} \cap D)$. Then $B \coprod B^* / \sim_h$ is the neighborhood of $\zeta \sim h(\zeta)$. Being a simply-connected, compact Riemann surface, X is thus conformally the sphere, and the uniformization map $\psi : X \to \hat{\mathbb{C}}$ draws a conformal image of Γ as $\psi(\partial\mathbb{D})$. More poetically, ψ smooths out the "wrinkles and folds" caused by sewing via h, yielding the conformally-embedded version of the curve $\Gamma = \psi(\mathbb{T})$.

Moving between weldings and curves

The association between Γ and h is rich merits further reflection. In the direction of $\Gamma \mapsto h$, it is worth noting that, even after modding out by Möbius maps as in (2.1), the map is not one-to-one. See [44], for example, for discussion of some of the subtleties of this question. In the other direction, moving from h to Γ, a deep question is what homeomorphisms h of $\mathbb{T}$ arise from weldings. In other words, for which h is there a Jordan curve Γ and Riemann maps f, g from $\mathbb{D}$ to the two components of $\hat{\mathbb{C}} \backslash \Gamma$ such that $h = g^{-1} \circ f$? It is not possible for *every* h. However, the "Sewing Theorem" of Lehto-Virtanen and Pfluger, for instance, states that it suffices for h to be quasisymmetric. But this is not necessary. In fact, Bishop [6] has shown that every orientation-preserving homeomorphism h of $\mathbb{T}$ is almost a welding, in that it agrees with a welding on subsets of $\mathbb{T}$ of measure arbitrarily close to 2π. The actual statement is slightly stronger: there is a sequence of welding homeomorphisms $\{H_n\}$ such that H_n and H_n^{-1} converge in measure to h and h^{-1}, respectively. Or, put probabilistically, H_n and H_n^{-1} both converge to h and h^{-1} in probability, with respect to the uniform distribution on $\mathbb{T}$. Hence welding homeomorphisms are dense in measure among all homeomorphisms, and perhaps this suggests that there is no clean way to characterize them.

Curve weldings

There is a similar notion of welding for Jordan arcs. Consider a simple (finite) curve $\gamma = \gamma([0,T]) \subset \mathbb{H} \cup \{0\}$ with $\gamma \cap \partial\mathbb{H} = \{0\}$. Then $\mathbb{H}\backslash\gamma$ is simply connected, so there is a conformal map $f : \mathbb{H}\backslash\gamma \to \mathbb{H}$ with $f(\infty) = \infty$ and $f(\gamma(T)) = 0$, unique up to dilation, which "opens up" γ onto two intervals about zero. More precisely, since γ is locally connected, f^{-1} extends to be continuous on $\mathbb{R}$, and there are two intervals $I_1 = [a, 0]$ and $I_2 = [0, b]$ with $a < 0 < b$ such that $f^{-1}(I_1) = f^{-1}(I_2) = \gamma$, and each point of γ has exactly two pre-images, one in $[a, 0]$ and one in $[0, b]$, with the exception of $\gamma(T)$, whose only preimage is zero. This establishes a decreasing homeomorphism h of $[a, b]$ defined via $h(x) = y$ if and only if $f^{-1}(x) = f^{-1}(y)$. Furthermore, h is idempotent and has zero as a unique fixed point. We will call such a homeomorphism h a *curve welding*, or, when the context is clear, simply a *welding*.

The situation is similar for an infinite Jordan arc $\gamma \subset \mathbb{H} \cup \{0, \infty\}$, $\gamma \cap \mathbb{H} = \{0, \infty\}$ (a situation we subsequently abbreviate by writing "γ is a curve in $(\mathbb{H}, 0, \infty)$"). Just take a Riemann map $\varphi : \hat{\mathbb{C}}\backslash\gamma \to \mathbb{H}$ which fixes 0 and ∞. As above, this will "open up" or "unzip" γ into two halves, but now corresponding to the infinite intervals $[-\infty, 0]$ and $[0, \infty]$, and the resulting homeomorphism h is defined on all of $\mathbb{R}$.

From a welding on $\mathbb{T}$ to a welding on $\mathbb{R}$

Note that after approximation we may always consider ourselves to be in the case of a welding on $\mathbb{R}$ as above, even starting with a welding on $\mathbb{T}$. The idea is just to transfer the welding h to $\mathbb{R}$ via Möbius maps. Indeed, pick two nearby points $\theta_1, \theta_2 \in \mathbb{T}$ and let A_1 and A_2 be the associated arcs $A_1 := \{e^{i\theta} : \theta_1 \leq \theta \leq \theta_2\}$, $A_2 := \{e^{i\theta} : h(\theta_1) \leq \theta \leq h(\theta_2)\}$. Find conformal maps $f : \mathbb{D} \to \mathbb{H}$ and $g : \hat{\mathbb{C}}\backslash\overline{\mathbb{D}} \to -\mathbb{H}$ such that $f(A_1) = g(A_2) = \mathbb{R}_{\geq 0}$. The original welding h now gives an identification between the two copies of $\mathbb{R}$ belonging to $\mathbb{H}$ and $-\mathbb{H}$. Now isometrically weld (the images of) A_1 to A_2 by replacing this with the identity map between the two copies of $\mathbb{R}_{\geq 0}$. Then apply $i\sqrt{z}$, $\arg(z) \in (-\pi, \pi]$, to open up the identification on the copies of $\mathbb{R}_{\leq 0}$ to one between $\mathbb{R}_{\leq 0}$ and $\mathbb{R}_{\geq 0}$. This gives a decreasing

idempotent homeomorphism of $\mathbb{R}$, just as in the case of the "curve welding" above. The price paid is the isometric welding approximation on $A_1 \to A_2$, which now corresponds to the imaginary axis.

Another equivalent approach to this transferring is the following: given a (closed) Jordan curve $\Gamma \subset \mathbb{C}$, approximate a small piece by a line segment, yielding a new closed curve $\tilde{\Gamma}$, and then map the two components of the complement $\hat{\mathbb{C}}\backslash\tilde{\Gamma}$ to $\mathbb{H}$ and $-\mathbb{H}$, with the image of the line segment going to $\mathbb{R}_{\geq 0}$ in both cases. Then apply $i\sqrt{z}$.

The point is that, so long as a small approximation is acceptable, we may always consider ourselves to be in the case of a welding h on $\mathbb{R}$: a decreasing, idempotent map with a unique fixed point at zero.

2.2 The Loewner equation, driving functions and Loewner energy

The Loewner equation and the correspondence between driving functions and simple curves $\gamma \subset \mathbb{H} \cup \{x\}$, $x \in \mathbb{R}$ is fundamental for our approach, and the story begins by considering the Riemann map $g : \mathbb{H}\backslash\gamma \to \mathbb{H}$ which fixes ∞. Note that since $\gamma \subset \mathbb{H} \cup \{x\}$, $\mathbb{H}\backslash\gamma$ is simply-connected and many such maps exist. Schwartz-reflecting across $\mathbb{R}$ yields a map which we can view as defined on the Riemann sphere $\hat{\mathbb{C}}$ save γ and its conjugation $\gamma^* := \{\bar{z} \ : \ z \in \gamma\}$, and which thus has a Taylor series at $z = \infty$. Because g maps $\mathbb{R}$ to $\mathbb{R}$ and is injective, we obtain

$$g(z) = a_{-1}z + a_0 + \frac{a_1}{z} + O\Big(\frac{1}{z^2}\Big), \qquad z \to \infty,$$

for some $a_j \in \mathbb{R}$. We have two degrees of freedom in g if our only stipulation is that $g(\infty) = \infty$, and by post-composing by an appropriate Möbius map $T(z) = az+b \in \mathrm{Aut}(\mathbb{H}) = PSL_2(\mathbb{R})$ that fixes ∞, we obtain the unique *hydrodynamically-normalized* $g_\gamma : \mathbb{H}\backslash\gamma \to \mathbb{H}$ that has expansion

$$g_\gamma(z) = z + \frac{b_1}{z} + O\Big(\frac{1}{z^2}\Big), \qquad z \to \infty, \tag{2.2}$$

for some $b_j \in \mathbb{R}$. Note that g_γ is the unique element of the coset $\mathrm{Aut}_\infty(\mathbb{H}) \circ g$ that satisfies

$$\lim_{z\to\infty} g_\gamma(z) - z = 0,$$

where $\mathrm{Aut}_\infty(\mathbb{H}) = \{T \in \mathrm{Aut}(\mathbb{H}) : T(\infty) = \infty\}$, i.e. all complex-affine maps with real coefficients.

2.2.1 Half-plane capacity

We define the coefficient b_1 in (2.2) as the *half-plane capacity* $\mathrm{hcap}(\gamma)$ of γ. This is a measurement of the size of γ within $\mathbb{H}$, "as seen from infinity," in the sense that

$$\mathrm{hcap}(\gamma) = \lim_{z\to\infty} z(g_\gamma(z) - z),$$

and in several other senses that we will see below. The half-plane capacity is strictly monotonic: if $\gamma_1 \subsetneq \gamma_2$, then $\mathrm{hcap}(\gamma_1) < \mathrm{hcap}(\gamma_2)$ [15, §A.4], and this allows us to parametrize our curve γ so that

$$\mathrm{hcap}(\gamma([0,t])) = 2t, \tag{2.3}$$

which we call the *Loewner-* or *half-plane-capacity-parametrization* of γ. Whenever we deal with a curve and its driving function, defined below, we assume that it is thus parametrized by capacity, and if we refer to the "time" or "Loewner time" or "capacity time" of a curve, we mean t in this parametrization. Note the Loewner time of $\gamma([0,t])$ is $\frac{1}{2}\,\mathrm{hcap}(\gamma([0,t]))$ by the normalization choice (2.3).

We sometimes wish to specify the half-plane capacity corresponding to a segment of the welding $\varphi : [a,0] \to [0,b]$ of a curve γ. If $[x_1,x_2] \subset [a,0]$, we write

$$\mathrm{hcap}_\gamma(x_1,x_2) := t_2 - t_1,$$

where when we weld by φ to create the curve γ, x_2 corresponds to $\gamma(t_2)$ and x_1 corresponds to $\gamma(t_1)$.

It is simple but important to note how capacity changes under conformal maps $T \in \mathrm{Aut}_\infty(\mathbb{H})$. If $b \in \mathbb{R}$, we see from (2.2) that the hydrodynamically-normalized map is

$$g_{\gamma+b}(z) = g_\gamma(z-b) + b,$$

and so $\mathrm{hcap}(\gamma + b) = \mathrm{hcap}(\gamma)$. If $a > 0$, we similarly have $g_{a\gamma}(z) = a g_\gamma(z/a)$, and so $\mathrm{hcap}(a\gamma) = a^2 \,\mathrm{hcap}(\gamma)$.

We mention in passing two other interesting expressions for $\mathrm{hcap}(\gamma)$ that can be derived from (2.2). First, the Poisson integral formula yields

$$\mathrm{hcap}(\gamma) = \frac{1}{\pi} \int_{-\infty}^{\infty} \mathrm{Im}\, g_\gamma^{-1}(x) dx,$$

see [15, §A.4]. There is also a probabilistic interpretation from Lawler [17, Prop. 3.41], which says

$$\mathrm{hcap}(\gamma) = \lim_{y \to \infty} y \mathbb{E}^{iy}(\mathrm{Im}(B_\tau)), \tag{2.4}$$

where $\mathbb{E}^{iy}(\mathrm{Im}(B_\tau))$ is the expected value of the imaginary part of a two-dimensional Brownian motion, started at iy, $y > 0$, and stopped at the first time τ it leaves the domain $\mathbb{H}\backslash\gamma$. Note that this equivalently says

$$\mathbb{E}^{iy}(\mathrm{Im}(B_\tau)) = \frac{\mathrm{hcap}(\gamma)}{y} + o(y^{-1}), \qquad y \to \infty. \tag{2.5}$$

We give a similar stochastic interpretation of the driving function below in Lemma 2.2. Compare (2.4) and (2.5) with (2.8) and (2.7), respectively.

There are also purely geometric interpretations of half-plane capacity. Rohde and Wong proved, for instance, that $\mathrm{hcap}(\gamma)$ is comparable to the Euclidean area of the hyperbolic neighborhood of γ of radius one, and this leads to several other equivalent geometric descriptions, see [34].

While there are other notions of capacity in complex analysis, in this thesis we always mean "half-plane capacity" when referring to capacity unless we explicitly state otherwise. Half-plane capacity can also be defined by (2.2) for any *compact* $\mathbb{H}$*-hull* K, that is, a bounded set $K \subset \mathbb{H}$ that is relatively closed in $\mathbb{H}$ with $\mathbb{H}\backslash K$ simply connected. It can be further generalized for sets where $\mathbb{H}\backslash K$ is not simply connected through (2.4).

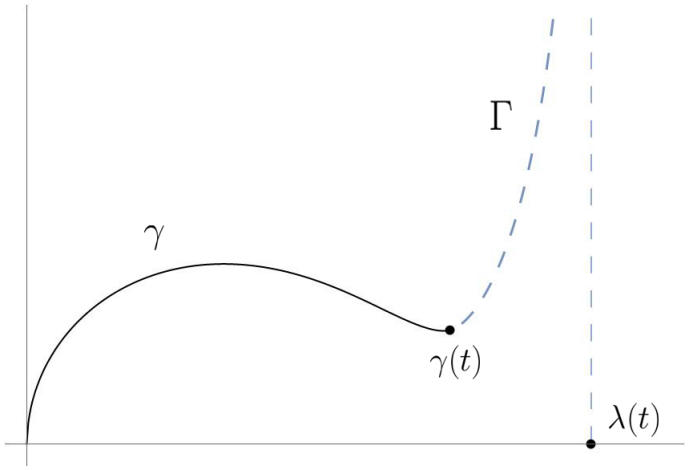

Figure 2.1: The driving function $\lambda(t)$ of $\gamma([0,t])$ is where the attached hyperbolic geodesic "hangs from infinity." See Lemma 2.1.

2.2.2 Three viewpoints on the driving function

When γ is parametrized by capacity, we define $g_t := g_{\gamma([0,t])}$ as the conformal map which "maps down" the first part $\gamma([0,t])$ of γ in the hydrodynamic normalization. The *driving function* $\lambda(t)$ of γ is the image of the tip of the curve under g_t,

$$\lambda(t) := \lim_{\substack{z \to \gamma(t) \\ z \in \mathbb{H} \setminus \gamma}} g_t(z). \tag{2.6}$$

When $\gamma : [0,T] \to \mathbb{H} \cup \{x\}$ is a simple curve, this is a well-defined, real-valued and continuous function on $[0,T]$ with $\lambda(0) = x$ [17, Lemma 4.2]. The driving function encodes γ as a real-valued function, as we will see below. While the most natural and intuitive definition of the driver is as the image of the tip of the curve (2.6), we also present two other viewpoints. The first is as the x-coordinate of how $\gamma([0,t])$ "hyperbolically hangs from infinity." The idea is the following: enlarge $\gamma([0,t])$ by attaching the hyperbolic geodesic Γ in $\mathbb{H} \setminus \gamma([0,t])$ from $\gamma(t)$ to ∞. Then $\lambda(t)$ is the asymptotic x-value of Γ as you head to ∞, as formalized in the following Lemma and pictured in Figure 2.1. This was observed independently by the author and by Rohde and Wang [33, Lemma 2.8]. Parametrize the curve $\gamma \cup \Gamma$ by capacity.

Lemma 2.1. $\lim_{s\to\infty} \mathrm{Re}(\Gamma(s)) = \lambda_t$.

Proof. Since g_t is the identity at $z = \infty$ to order z^{-1},

$$\lim_{s\to\infty} \mathrm{Re}(\Gamma(s)) = \lim_{s\to\infty} \mathrm{Re}(g_t(\Gamma(s))).$$

Note, however, that $g_t(\Gamma)$ is the hyperbolic geodesic in $\mathbb{H}$ from $g_t(\gamma(t)) = \lambda(t)$ to ∞, which is simply the vertical line $\{\mathrm{Re}(z) = \lambda(t)\}$. □

Our third viewpoint on the driving function is a stochastic interpretation paralleling (2.5). This is implicit in Lawler's work [17, Prop. 3.43], but we explicitly work out the details. We note that from the point of view of the conformal map $f_t := g_t^{-1} : \mathbb{H} \to \mathbb{H}\backslash\gamma([0,t])$, $\gamma = \gamma([0,t])$ has two sides, corresponding to the two adjacent intervals $[a(t), \lambda(t)], [\lambda(t), b(t)] \subset \mathbb{R}$ that the boundary extension of f_t maps onto γ. We call these the left- and right-hand sides of γ, respectively, and write them as $\gamma_-(t)$ and $\gamma_+(t)$.

Lemma 2.2. *The hitting probability of the set $\gamma_+(t) \cup [\gamma(0), \infty)$ of two-dimensional Brownian motion B_t started at iy, $y > 0$, and stopped upon leaving $\mathbb{H}\backslash\gamma([0,t])$ at time τ satisfies*

$$\mathbb{P}^{iy}\big(B_\tau \in \gamma_+(t) \cup [\gamma(0), \infty)\big) = \frac{1}{2} - \frac{\lambda(t)}{\pi y} + o(y^{-1}), \qquad y \to \infty. \tag{2.7}$$

In other words,

$$\lambda(t) = \lim_{y\to\infty} \pi y\Big(\frac{1}{2} - \mathbb{P}^{iy}(B_\tau \in \gamma_+(t) \cup [\gamma(0), \infty)\Big). \tag{2.8}$$

We thus see $\lambda(t) > 0$ if Brownian motion is more likely to hit the left side of $\gamma \cup \mathbb{R}$ than the right when started high up on the imaginary axis. Note also that the complementary event yields the equivalent limit

$$\lambda(t) = \lim_{y\to\infty} \pi y\Big(\mathbb{P}^{iy}(B_\tau \in (-\infty, \gamma(0)] \cup \gamma_-(t)) - \frac{1}{2}\Big).$$

Note also that the probability in (2.7) is precisely the harmonic measure

$$\omega\big(iy, \gamma_+(t) \cup [\gamma(0), \infty), \mathbb{H}\big)$$

of $\gamma_+(t) \cup [\gamma(0), \infty)$ in $\mathbb{H}$ as seen from iy. Compare these formulas with the parallel results for half-plane capacity in (2.4) and (2.5).

Proof. Let $\tau_{\mathbb{R}}$ be the hitting time of the real line. Using conformal invariance and the hydrodynamic normalization (2.2) of g_t, we have

$$\begin{aligned}
\mathbb{P}^{iy}(B_\tau \text{ is in the RHS of } \gamma \cup \mathbb{R}) &= \mathbb{P}^{g_t(iy)}(B_{\tau_{\mathbb{R}}} \in [\lambda(t), \infty)) \\
&= \mathbb{P}^{i\mathrm{Im}(g_t(iy))}(B_{\tau_{\mathbb{R}}} \in [\lambda(t) - \mathrm{Re}(g_t(iy)), \infty)) \\
&= \mathbb{P}^{i(y+O(1/y))}(B_{\tau_{\mathbb{R}}} \in [\lambda(t) + O(1/y^2), \infty)) \\
&= \mathbb{P}^{i}\big(B_{\tau_{\mathbb{R}}} \in \big[\frac{\lambda(t) + O(1/y^2)}{y + O(1/y)}, \infty\big)\big) \\
&= \frac{1}{2} - \frac{1}{\pi} \arctan\Big(\frac{\lambda(t) + O(1/y^2)}{y + O(1/y)}\Big).
\end{aligned}$$

We obtain (2.8) by multiplying and taking the limit. □

Example 2.3. The simplest example of a driving function is for the vertical line segment $\gamma_y = [0, iy]$, $y > 0$, where a map $\mathbb{H}\backslash\gamma_y \to \mathbb{H}$ which fixes infinity is

$$\sqrt{z^2 + y^2} = z + \frac{y^2/2}{z} + O(z^{-3}), \qquad z \to \infty.$$

Hence the capacity parametrization for the imaginary axis is $\gamma(t) = 2i\sqrt{t}$, and the driving function is $\lambda(t) \equiv 0$. Note that the vanishing of the driving function is clear without any calculation from both Lemmas 2.1 and 2.2.

See [17, §4.1] for some more elementary examples of driving functions. We discuss the driving function for an energy-minimizing curve family, circular arcs orthogonal to $\mathbb{R}$, and straight line segments in Chapter 5.

It is also helpful to consider how the driving function changes under the action of $\gamma \mapsto T(\gamma)$ for $T \in \mathrm{Aut}(\mathbb{H})$. Let g_t be the family of maps for the curve $\gamma : [0, T] \to \mathbb{H} \cup \{x\}$ with driver λ. If $b \in \mathbb{R}$, then the maps for $\gamma + b$ are $g_t(z - b) + b$, and so the driver for $\gamma + b$ is $\lambda + b$. If $a > 0$, the maps for $a\gamma$ are $a g_{a^2 t}(z/a)$, and so we have to re-scale time by $1/a^2$ to maintain capacity parametrization, yielding the driver

$$t \mapsto a\lambda(t/a^2). \tag{2.9}$$

Hence drivers exhibit *Brownian scaling*; this plays an important role when the driving function is 1-dimensional standard Brownian motion.

Lastly, it is not known how the driving function changes under inversion $\gamma \mapsto -1/\gamma$ (if $\gamma([0,T])$ is not an infinite curve, first make it so by attaching the hyperbolic geodesic from $\gamma(T)$ to ∞). The map $\gamma \mapsto \lambda$ is very non-linear, as is the reciprocation map, and it is not known how the original driver "spreads out" when the original curve is reciprocated. The only thing known is a result of Wang [42] that the L^2-norm of $\dot{\lambda}$ does not change under this inversion, see below in §2.2.4.

2.2.3 The Loewner equation and its variants

As mentioned above, the driver λ encodes its curve γ as a real-valued function. The mechanism for this is the *Loewner differential equation*, which says the time derivative $\dot{g}_t$ of the maps $g_t : \mathbb{H}\backslash\gamma([0,t]) \to \mathbb{H}$ in (2.2) satisfy

$$\dot{g}_t(z) = \frac{2}{g_t(z) - \lambda(t)}, \qquad g_0(z) = z. \tag{2.10}$$

An intuitive approach to (2.10) is to consider mapping down infinitesimal slits using maps similar to those in Example 2.3. Indeed, if our curve currently has its base at $\lambda(t)$, note that the hydrodynamically-normalized map which maps down the slit $[0, \lambda(t) + i\Delta t]$ is

$$\sqrt{(z-\lambda(t))^2 + 4\Delta t} + \lambda(t) = z + \frac{2\Delta t}{z - \lambda(t)} + O\Big(\frac{(\Delta t)^3}{(z-\lambda(t))^3}\Big), \qquad z \to \infty,$$

which shows the time derivative (2.10). Thus we can view the Loewner flow generated by (2.10) as the composition of mapping down many infinitesimal slits.* This is not a proof of the Loewner equation, but it is a helpful intuition. See [17, Ch.4] for an actual derivation.

Writing $g_t = x(t) + iy(t)$ in terms of its real and imaginary parts, we expand (2.10) to see

$$\dot{x}(t) = \frac{2(x(t) - \lambda(t))}{(x(t)-\lambda(t))^2 + y(t)^2} \qquad \text{and} \qquad \dot{y}(t) = \frac{-2y(t)}{(x(t)-\lambda(t))^2 + y(t)^2}, \tag{2.11}$$

*I am indebted to Tao, [40], for this point of view.

and so the flow of the image point $x(t)+iy(t)$ as we map more and more of the curve down is horizontally away from the line $\{\mathrm{Re}(z) = \lambda(t)\}$ and always vertically downwards. Far away from the singularity there is very little movement, as we expect from (2.2).

Reversing the direction of the flow is achieved by the h_t maps which satisfy

$$\dot{h}_t(z) = \frac{-2}{h_t(z) - \xi(t)}, \qquad h_0(z) = z, \tag{2.12}$$

where $\xi(t) := \lambda(T - t)$ is the reversed driving function. The following lemma makes precise what we mean by "reversing the flow" in the h_t maps.

Lemma 2.4. *Fix $T > 0$. Then for any $0 \leq t \leq T$,*

$$h_t^{-1} \circ g_{T-t} = g_T. \tag{2.13}$$

Proof. Note that (2.13) holds when $t = 0$. Differentiating the left-hand side with respect to t yields $\frac{\partial}{\partial t}(h_t^{-1} \circ g_{T-t}) = 0$, and so (2.13) actually holds for all t. □

So if we flow up with the h_t map, the resulting curve segment in $\mathbb{H}$ is the partially-mapped-down curve $g_{T-t}(\gamma([T-t, T])$. We will frequently re-center the reversed driver, and take $\xi(t)$ as $\lambda(T - t) - \lambda(T)$ so that $\xi(0) = 0$. If this shifting matters, which version we use will be clear from the context.

We will also need the centered versions of these flows. The centered downwards flow is defined by

$$G_t(z) := g_t(z) - \lambda(t) \tag{2.14}$$

while the centered upwards flow by

$$H_t(z) := h_t(z) - \xi(t). \tag{2.15}$$

Under g_t and h_t, infinity is fixed and there is local translation around the base of the curve given by the driving function. For G_t and H_t we subtract off that translation and hence fix the base of the curve and "translate infinity," meaning there is now a shift in the expansion

(2.2). At points of differentiability of λ and ξ these become differentiable, and we see from (2.10) and (2.12) that their differential equations are

$$\dot{G}_t(z) = \frac{2}{G_t(z)} - \dot{\lambda}(t) \tag{2.16}$$

and

$$\dot{H}_t(z) = \frac{-2}{H_t(z)} - \dot{\xi}(t) \tag{2.17}$$

When regularity is an issue, (2.10) and (2.12) are easier to work with because they do not assume any regularity. When we have differentiability, (2.16) and (2.17) can be convenient, especially as they mirror the zipper process of welding two points $x < 0 < y$ together at the origin.

The Loewner equation goes back to a 1923 paper of Carl Loewner (or Karl Löwner) [25], where a parallel to (2.10) was developed for the setting of the unit disk instead of $\mathbb{H}$. Löwner was working on Bieberbach's 1916 conjecture that if $f : \mathbb{D} \to \Omega$ is a normalized conformal map

$$f(z) = z + \sum_{n=2}^{\infty} a_n z^n,$$

then $|a_n| \leq n$ for all $n \geq 2$. He used the disk Loewner equation for prove this for the third coefficient, $|a_3| \leq 3$ (see the account in [9, §3.5]). The Loewner equation was also a crucial tool used by de Branges when he finally proved the conjecture in 1984. The chordal equation (2.10) took on new importance when Oded Schramm used it as the setting for *Stochastic Loewner Evolution* SLE, now usually called *Schramm Loewner Evolution* in his honor, which uses scaled Brownian motion $\sqrt{\kappa}B_t$ as the driver $\lambda(t)$ [35]. Among many other consequences, SLE theory led to the first rigorous proofs for the conformal invariance of scaling limits of several famous two-dimensional models in statistical physics [18].

2.2.4 Loewner energy

The Loewner energy is a measurement of the regularity of a curve γ, and curves with finite Loewner energy have "local curvature which is square integrable." We will not make that

statement precise, but refer the reader to [5] for geometric characterizations of finite-energy curves which give this statement justification.† The Loewner energy is the sup over all partitions of a certain difference quotient. A *partition* $\mathcal{P}$ *of* $[0,T]$ is a list $\mathcal{P} = (t_0, t_1, \ldots, t_n)$ such that

$$0 = t_0 < t_1 < \cdots < t_n = T.$$

Let $\Pi[0,T]$ be the collection of all partitions of $[0,T]$.

Definition 2.1. The *Loewner energy* $I(\gamma) = I_T(\gamma)$ of a curve γ on $[0,T]$ with upwards driving function ξ is

$$I(\gamma) := \sup_{\mathcal{P}\in\Pi[0,T]} \sum_{j=1}^{n} \frac{(\xi(t_j) - \xi(t_{j-1}))^2}{2(t_j - t_{j-1})}. \tag{2.18}$$

We may alternatively write $I(\xi)$ for $I(\gamma)$, or even $I(\lambda)$, as it is evident that the supremum in (2.18) is not changed if we replace the reversed driver ξ in the sum with the usual driver λ. The factor of 2 in the denominator in (2.18) is a normalization choice by Wang [42] in order to match the large deviations good-rate function for Brownian motion. We choose to follow this convention. Observe that the sum in (2.18) is monotonic in the partition: if $\mathcal{P}' \supset \mathcal{P}$ is a refinement of $\mathcal{P}$, then

$$\sum_{\mathcal{P}} \frac{(\xi(t_j) - \xi(t_{j-1}))^2}{2(t_j - t_{j-1})} \leq \sum_{\mathcal{P}'} \frac{(\xi(t'_j) - \xi(t'_{j-1}))^2}{2(t'_j - t'_{j-1})}. \tag{2.19}$$

It is also a fact from analysis that a driver ξ with $I_T(\xi) < \infty$ belongs to the *Dirichlet space* on $[0,T]$, which is to say ξ is absolutely continuous, $\dot{\xi} \in L^2([0,T])$ and

$$I_T(\xi) = \frac{1}{2}\int_0^T \dot{\xi}(t)^2 dt.$$

See, for instance, [29, §1.4].

Example 2.5. Let $\xi : [0,1] \to [0,1]$ be the Cantor function. We claim that $I(\xi) = \infty$, which is easy to see from the iterative construction ξ_n for ξ. At stage 1, divide $[0,1]$ into 3

†See also Chapter 9 where we discuss and extend one of these characterizations.

equal sub-intervals, and define ξ_1 to be linear on $[0, 1/3]$, constant on $[1/3, 2/3]$ and linear on $[1/3, 2/3]$, with

$$\xi_1(1/3) - \xi_1(0) = \xi_1(1) - \xi_1(2/3) = \frac{1}{2}.$$

For ξ_2, divide the two intervals on which ξ_1 was not constant into three equal sub-intervals, with ξ_2 constant on each of the middle of these sub-intervals and

$$\xi_2\Big(\frac{2k-1}{3^2}\Big) - \xi_2\Big(\frac{2k-2}{3^2}\Big) = \frac{1}{2^2}$$

for the k defining the four non-middle sub-intervals. Continuing with such subdivisions, at stage n with have 2^n intervals where ξ_n is not constant and where

$$\xi_n\Big(\frac{2k-1}{3^n}\Big) - \xi_n\Big(\frac{2k-2}{3^n}\Big) = \frac{1}{2^n} \tag{2.20}$$

for the appropriate k generating the 2^n new "non-middle" sub-intervals. Furthermore, all ξ_m for $m > n$ agree with ξ_n at the endpoints of these intervals, and hence we may get a lower bound for (2.18) with each ξ_n, choosing our partition $\mathcal{P}_n$ to be exactly the endpoints of these intervals where ξ_n is not constant. On each such interval the change (2.20) is the same, and so our sum is

$$\sum_{j=1}^{2^n} \frac{(\xi(t_j) - \xi(t_{j-1}))^2}{2(t_j - t_{j-1})} = 2^n \frac{((2^{-n})^2}{2 \cdot 3^{-n}} = \frac{1}{2}\Big(\frac{3}{2}\Big)^n \to \infty.$$

Let $\gamma \cup \mathbb{H} \cup \{0\}$ be a curve from 0 to ∞. It is a non-trivial fact that $I(T(\gamma)) = I(\gamma)$ for any $T \in \mathrm{Aut}(\mathbb{H})$ which fixes ∞ or exchanges 0 and ∞. Invariance under $\mathrm{Aut}_\infty(\mathbb{H})$ is, however, elementary: since shifting the curve $\gamma \mapsto \gamma + b$ shifts the driver, its derivative does not change and the energy is the same. We saw in (2.9) that the scaling $\gamma \mapsto a\gamma$ yields a new driver $a\lambda(t/a^2)$, and hence the new energy is

$$\frac{1}{2}\int_0^\infty \frac{1}{a^2}\dot{\lambda}(t/a^2)^2 dt = \frac{1}{2}\int_0^\infty \dot{\lambda}(t)^2 dt.$$

The non-trivial invariance is that $I(-1/\gamma) = I(\gamma)$, and Wang proved this using the reversibility of SLE and the fact that the Loewner energy is the large deviations rate function for

Brownian motion [42]. An open question is how to deterministically prove this "reversibility" using the driving function λ. Wang has subsequently given formulas for $I(\gamma)$ in terms of conformal maps which give purely deterministic proofs of reversibility [43] (but these do not use the driving function).

Aside from conformal invariance, another crux of the theory is lower semi-continuity: If $\xi_n \to \xi$ uniformly on $[0,T]$, then

$$\liminf_{n\to\infty} I_T(\xi_n) \geq I_T(\xi), \tag{2.21}$$

as follows from the difference quotient expression (2.18), see [42]. So the energy can decrease in the limit, but not increase. A surprising amount of the theory regarding minimizers is built upon the foundation of (2.21).

Another important property is that bounded-energy drivers are uniformly Hölder -1/2 continuous. Indeed, for a constant C, set

$$I_T(C) := \{\, \xi : [0,T] \to \mathbb{R} \ : \ I_T(\xi) \leq C \,\}.$$

Then for any $\xi \in I_T(C)$,

$$|\xi(t_2) - \xi(t_1)| \leq \int_{t_1}^{t_2} |\dot{\xi}(t)| dt \leq \left(\int_{t_1}^{t_2} dt \right)^{1/2} \left(\int_{t_1}^{t_2} \dot{\xi}(t)^2 dt \right)^{1/2} \leq \sqrt{2C}\sqrt{t_2 - t_1}.$$

In particular, the family $I_T(C)$ is bounded and equicontinuous on $[0,T]$, and so by Arzela-Ascoli is precompact in the uniform norm on $[0,T]$. However, by lower semi-continuity, any subsequential limit also belongs to $I_T(C)$, and so $I_T(C)$ is compact. This is another valuable property that we will use repeatedly.

The Loewner energy has been generalized to loops by Rohde and Wang [33].

2.3 Quasiconformal mappings

In this section recall a useful properties about planar quasiconformal mappings. For proofs and more details, we refer the reader to the accounts in [2], [19] and [20].

A *K-quasiconformal map* $f : \Omega_1 \to \Omega_2$ is an orientation-preserving homeomorphism which is absolutely continuous on a.e. line parallel to the axes and differentiable at Lebesgue-almost every $z \in \Omega_1$, and whose "complex directional derivatives"

$$\partial_\alpha f(z) := \lim_{r \to 0} \frac{f(z + re^{i\alpha}) - f(z)}{re^{i\alpha}}$$

satisfy

$$\max_\alpha |\partial_\alpha f(z)| \leq K \min_\alpha |\partial_\alpha f(z)| \tag{2.22}$$

at points z of differentiability. More succinctly, f is K-quasiconformal if $f \in W^{1,2}_{\text{loc}}(\Omega_1)$ with derivatives satisfying (2.22) almost everywhere. Conformal maps are K-quasiconformal with $K = 1$. Quasiconformal maps are a powerful generalization of conformal maps, however, because they are more flexible but still have enough structure for a robust theory. For example, we have the following useful normality property.

Proposition 2.6. *[19, Thm. 2.1] A family F of K-quasiconformal mappings of $\Omega_1 \subset \hat{\mathbb{C}}$ is normal in the spherical metric if for three distinct points $z_1, z_2, z_3 \in \Omega_1$, the spherical distances $d_{\hat{\mathbb{C}}}(z_j, z_k)$ are uniformly bounded away from zero, $j \neq k$, $j, k = 1, 2, 3$.*

Furthermore, the subsequential locally-uniform limits are also either K-quasiconformal or constant, a generalization of the Hurwitz theorem for conformal mapping.

Proposition 2.7. *[19, Thm. 2.2, 2.3] Let $f_n : \Omega_1 \to \Omega_2$ be a sequence of K-quasiconformal maps which converges locally uniformly to f. Then f is either K-quasiconformal or f maps all of Ω_1 to a single boundary point of Ω_2.*

Another helpful characterization of quasiconformal maps is in terms of infinitesimal circles and ellipses. From the derivative bound (2.22), the a.e.-defined differential Df of a quasiconformal maps takes circles in the tangent space to ellipses of bounded eccentricity (instead of circles, as for conformal maps). A nice framework for describing this is the *complex dilatation* $\mu(z)$. Write $\partial_z f := \frac{1}{2}(f_x - if_y)$ and $\partial_{\bar{z}} f := \frac{1}{2}(f_x + if_y)$ for the standard z and $\bar{z}$ derivatives. Then one can show $\max_\alpha |\partial_\alpha f(z)| = |\partial_z f(z)| + |\partial_{\bar{z}} f(z)|$ and

$\min_\alpha |\partial_\alpha f(z)| = |\partial_z f(z)| - |\partial_{\bar{z}} f(z)|$, and hence the ratio of the semi-major to semi-minor axis of an infinitesimal circle under f is

$$D_f(z) := \frac{\max_\alpha |\partial_\alpha f|}{\min_\alpha |\partial_\alpha f|} = \frac{|\partial_z f(z)| + |\partial_{\bar{z}} f(z)|}{|\partial_z f(z)| - |\partial_{\bar{z}} f(z)|} \leq K.$$

Re-arranging the inequality on the right-hand side yields

$$|\partial_{\bar{z}} f(z)| \leq \frac{K-1}{K+1} |\partial_z f(z)|. \tag{2.23}$$

Since f is orientation preserving, we further have $0 < J_f = |\partial_z f|^2 - |\partial_{\bar{z}} f|^2$, yielding $|\partial_z f(z)| > |\partial_{\bar{z}} f(z)|$. We may thus divide by $|\partial_z f|$ in (2.23) to obtain

$$|\mu(z)| := \frac{|\partial_{\bar{z}} f(z)|}{|\partial_z f(z)|} \leq \frac{K-1}{K+1} < 1,$$

where $\mu(z) := \partial_{\bar{z}} f / \partial_z f$ is the *complex dilatation* of f. Thus at points of differentiability, we see that a K-quasiconformal map satisfies the *Beltrami equation*

$$\partial_{\bar{z}} f(z) = \mu(z) \partial_z f(z) \tag{2.24}$$

where $\mu(z)$ is uniformly bounded by $(K-1)/(K+1) < 1$. Furthermore, (2.24) characterizes quasiconformal maps.

Proposition 2.8. *[19, Thm. 4.1] A homeomorphism $f : \Omega \to \Omega'$ is K-quasiconformal if and only if f is a $W^{1,2}_{loc}(\Omega)$ solution to* (2.24) *for some measurable map $\mu : \Omega \to \mathbb{C}$ with $\|\mu\|_\infty < 1$.*

Note from (2.24) that f is conformal iff $\mu(z) \equiv 0$; this is just the Cauchy-Riemann equations $\partial_{\bar{z}} f(z) \equiv 0$. Quasiconformal maps thus satisfy the "generalized Cauchy-Riemann equations" (2.24).

We will discuss other aspects of quasiconformal maps in the body of the thesis as the need arises.

2.4 Other notation

The length of an interval $I = [a, b]$ is $b - a =: |I|$. $B(z, r)$ is the open ball centered at z of radius r.

Let I an interval on $\mathbb{R}$ and $0 \leq \alpha \leq 1$. We say a function $\xi : I \to \mathbb{R}$ is *α-Hölder continuous* on I if

$$\sup_{\substack{t_1,t_2 \in I \\ t_1 \neq t_2}} \frac{|\xi(t_2) - \xi(t_1)|}{|t_2 - t_1|^\alpha} \leq M < \infty. \tag{2.25}$$

In this case we write $|\xi|_\alpha$ to be the infimum over all such M, and call this the *α-Hölder seminorm* of ξ, and we have $|\xi(t_1) - \xi(t_2)| \leq |\xi|_\alpha |t_2 - t_1|^\alpha$ for all $t_1, t_2 \in I$.

We say $\xi \in C^{n,\alpha}(I)$ if ξ and each of its first n derivatives are continuous on I and if $\xi^{(n)}$ is α-Hölder continuous on I. The $C^{n,\alpha}$-norm is

$$\|\xi\|_{C^{n,\alpha}} = \|\xi\|_{C^{n,\alpha}(I)} := \sum_{k=0}^{n} \sup_{t \in I} |\xi^{(k)}(t)| + |\xi^{(n)}|_\alpha.$$

For $1 < s \notin \mathbb{N}$, $C^s := C^{\lfloor s \rfloor, s - \lfloor s \rfloor}$, where $\lfloor x \rfloor$ is the greatest integer $n \leq x$. We write $C_0^{n,\alpha}$ for the subset of $\xi \in C^{n,\alpha}$ such that $\xi(0) = 0$.

Chapter 3

ESTIMATES AND TAYLOR EXPANSIONS

To prove Theorem 1.1 we need some machinery to control the distance between points that are welded at the same time by different drivers, in terms of the supremum distance between the drivers. This is the content of Lemmas 3.1 and 3.2. We do an explicit expansion for the points $x(t) < 0 < y(t)$ welded together by a linear driver as $t \to 0^+$ in Lemma 3.3, and then use the preceding estimates and the Taylor-error control of Lemma 3.4 to conclude the same expansion holds for any $C^{3/2+\epsilon}$ driver in Theorem 3.5, the main result of this section. This is the welding parallel of the expansion of the curve $\gamma(t)$ for small t in terms of the driver λ at $t = 0$ given in [22] and [24].

Lemma 3.1. *Let $I = [0, T]$ and let $\lambda : I \to \mathbb{R}$ and $\eta : I \to \mathbb{R}$ be driving functions for simple curves $\gamma^\lambda, \gamma^\eta \subset \mathbb{H} \cup \{0\}$ with $\lambda(0) = \eta(0) = 0$. Let g_t^λ and g_t^η be the associated mapping down functions for the un-centered downward Loewner flow generated by λ and η, respectively. Then for any $t \in [0, T]$ and $x \in \mathbb{R}\backslash\{0\}$,*

$$|g_t^\lambda(x) - g_t^\eta(x)| \leq \|\lambda - \eta\|_{L^\infty[0,T]}. \tag{3.1}$$

In particular,

$$|g_t^\lambda(0+) - g_t^\eta(0+)| \leq \|\lambda - \eta\|_{L^\infty[0,T]} \qquad \textit{and} \tag{3.2}$$

$$|g_t^\lambda(0-) - g_t^\eta(0-)| \leq \|\lambda - \eta\|_{L^\infty[0,T]}. \tag{3.3}$$

Proof. Suppose that $x < 0$; the positive case is similar. Set $s := \|\lambda - \eta\|_{L^\infty[0,T]}$. We first observe that if $\lambda \leq \eta$ are drivers for simple curves in $\mathbb{H}$ and $x < \lambda(0)$, then $g_t^\lambda(x) \leq g_t^\eta(x)$, as follows from the Loewner equation (2.10). Since the Loewner flow $g_t^\lambda(x)$ is monotonic in x, we therefore have

$$g_t^\lambda(x) \geq g_t^\lambda(x - s) \geq g_t^{\eta - s}(x - s) = g_t^\eta(x) - s,$$

and so $g_t^\eta(x) - g_t^\lambda(x) \leq s$. Exchanging the roles of λ and η yields the other direction, proving (3.1). (Note that the assumption on γ^λ and γ^η ensures $g_t^\lambda(x)$ and $g_t^\eta(x)$ are well defined.) Since γ^λ and γ^η are simple curves in $\mathbb{H} \cup \{0\}$, the the downward flow maps g_t extend to be continuous on either side of 0. Hence we may take one-sided limits in (3.1) to obtain (3.2) and (3.3). □

Now we switch viewpoints to consider the upward flow driven by some ξ with $\xi(0) = 0$. We say a point $x \in \mathbb{R}$ "hits the singularity at time t_0" if the image $x(t_0)$ of x under the uncentered upwards flow generated by ξ after t_0 units of time is identical to $\xi(t_0)$, $x(t_0) = \xi(t_0)$. We can use Lemma 3.1 to conclude that the map $(\xi, \tau) \mapsto x$, where x is a point whose hitting time under ξ's upward flow is τ, is Lipschitz continuous with respect to ξ, when we equip continuous functions ξ on $[0, \tau]$ with the supremum norm.

Lemma 3.2. *Suppose $x_1, x_2 < 0$ both hit the singularity at the same time τ under the upwards Loewner flow generated by drivers ξ_1 and ξ_2, respectively, where $\xi_1(0) = \xi_2(0) = 0$ and the ξ_j generate simple curves in $\mathbb{H} \cup \{\xi_j(\tau)\}$. Then*

$$|x_1 - x_2| \leq 3\|\xi_1 - \xi_2\|_{L^\infty[0,\tau]}. \tag{3.4}$$

This bound also holds for $0 < y_j$ with the same hitting time τ under ξ_j, $j = 1, 2$.

Proof. If $h_t^{\xi_j}$ are the upwards flow maps (2.12) for the ξ_j, then our assumption $h_\tau^{\xi_j}(x_j) = \xi_j(\tau)$, $j = 1, 2$, is the same as saying

$$g_\tau^{\lambda_j}(\xi_j(\tau)-) = x_j \tag{3.5}$$

for the downward flow maps g_t under the reversed drivers $\lambda_j(t) := \xi_j(\tau - t)$. If we recenter these via $\lambda_j(t) - \xi_j(\tau)$, Lemma 3.1 then yields

$$|g_\tau^{\lambda_1 - \xi_1(\tau)}(0-) - g_\tau^{\lambda_2 - \xi_2(\tau)}(0-)| \leq \|\lambda_1 - \lambda_2 + \xi_2(\tau) - \xi_1(\tau)\|_{L^\infty[0,\tau]} \leq 2\|\xi_1 - \xi_2\|_{L^\infty[0,\tau]}.$$

Noting by (3.5) that

$$x_j - \xi_j(\tau) = g_\tau^{\lambda_j}(\xi_j(\tau)-) - \xi_j(\tau) = g_\tau^{\lambda_j - \xi_j(\tau)}(0-),$$

we thus have

$$|x_1 - x_2| = |g_\tau^{\lambda_1 - \xi_1(\tau)}(0-) - g_\tau^{\lambda_2 - \xi_2(\tau)}(0-) + \xi_1(\tau) - \xi_2(\tau)| \le 3\|\xi_1 - \xi_2\|_{L^\infty[0,\tau]}. \qquad \square$$

Our next lemma gives Taylor expansions for the points $x_1 < 0 < y_1$ which the linear driver $\xi(t) = ct$ welds together. The expansions for a general $C^{3/2+\epsilon}$ driver $\tilde{\xi}(t) = ct + O(t^{3/2+\epsilon})$ must be similar by the Lipschitz property of Lemma 3.2.

Lemma 3.3. *The points $x(t) < 0 < y(t)$ welded together at time t by the upward Loewner flow generated by $\xi(t) = ct$, $c \in \mathbb{R}$, are real-analytic functions of $\sqrt{t}$ with expansions*

$$\begin{aligned} x(t) &= -2\sqrt{t} + \frac{2}{3}ct - \frac{1}{18}c^2t^{3/2} - \frac{1}{135}c^3t^2 + O(t^{5/2}), \\ y(t) &= 2\sqrt{t} + \frac{2}{3}ct + \frac{1}{18}c^2t^{3/2} - \frac{1}{135}c^3t^2 + O(t^{5/2}) \end{aligned} \tag{3.6}$$

at $t = 0+$. In particular, there exists $t_0 > 0$ such that for any $c \neq 0$ and $t < t_0/c^2$,

$$\max\left\{\left|x(t) - (-2\sqrt{t} + \frac{2}{3}ct - \frac{1}{18}c^2t^{3/2})\right|,\ \left|y(t) - (2\sqrt{t} + \frac{2}{3}ct + \frac{1}{18}c^2t^{3/2})\right|\right\} \le \frac{|c|^3}{100}t^2. \tag{3.7}$$

Proof. If $c = 0$, then (3.6) holds for all time t by explicit calculation. So we may assume $c \neq 0$.

Note that if $x(\tau)$ hits the singularity $\xi(\tau)$ at time τ, this is equivalent to saying the upward flow map h satisfies $h_\tau^\xi(x(\tau)) = \xi(\tau)$, or that the downward flow map g satisfies $g_\tau^\lambda(\xi_\tau -) = x(\tau)$, where $\lambda(t) := \xi(\tau - t)$ is the reversed driver. Thus

$$x(\tau) = g_\tau^\lambda(\xi_\tau -) - \xi(\tau) + \xi(\tau) = g_\tau^{\lambda - \xi(\tau)}(0-) + \xi(\tau).$$

If $\xi(t) = ct$, then $\lambda(t) - c\tau = -ct$, and so note that

$$g_\tau^{\lambda - \xi(\tau)}(0-) + \xi(\tau) = g_\tau^{\lambda - \xi(\tau)}(0-) - (\lambda - \xi(\tau))(\tau) = G_\tau^{\lambda - \xi(\tau)}(0-),$$

the downward centered Loewner map. So we begin by finding the image of $0\pm$ under the centered downward flow, first considering the case of $c = -1$ and $\lambda(t) - c\tau = t =: \eta(t)$. Explicit computations in [16, §3] show $G_\tau^\eta(x)$ satisfies

$$G_t^\eta(x) + 2\log(2 - G_t^\eta(x)) = x + 2\log(2 - x) - t,$$

and so sending $x \to 0\pm$ yields

$$u + 2\log(2-u) = 2\log(2) - t$$

for either $u = x(t)$ or $u = y(t)$. Hence, for t such that $|x(t)| < 2$ and $|y(t)| < 2$, both $u = x(t)$ and $u = y(t)$ are solutions to

$$t = \sum_{n=2}^{\infty} \frac{1}{2^{n-1}n} u^n = \left(\frac{1}{2}u + \frac{1}{12}u^2 + \frac{7}{288}u^3 + \cdots\right)^2 =: \varphi(u)^2,$$

where φ is real-analytic with $\varphi'(0) > 0$, and hence has inverse $\varphi^{-1}(u) = \sum_{k=1}^{\infty} a_k u^k$ in some neighborhood of zero. Therefore

$$x(t) = \varphi^{-1}(-\sqrt{t}) = -2\sqrt{t} - \frac{2}{3}t - \frac{1}{18}t^{3/2} + \frac{1}{135}t^2 + O(t^{5/2})$$

and

$$y(t) = \varphi^{-1}(\sqrt{t}) = 2\sqrt{t} - \frac{2}{3}t + \frac{1}{18}t^{3/2} + \frac{1}{135}t^2 + O(t^{5/2})$$

are real-analytic functions of $\sqrt{t}$ for small t. Writing $R_n^x := x(t) - \sum_{k=1}^{n} a_k(-\sqrt{t})^k$ and similarly for the error R_n^y for $y(t)$, we have, in particular, some $t_0 > 0$ such that $0 \le t \le t_0$ implies

$$\max\{|R_3^x|, |R_3^y|\} \le \frac{1}{100}t^2. \tag{3.8}$$

For the general driver $\xi(t) = ct$, we recall that scaling a curve $\gamma \mapsto r\gamma$ for $r > 0$ transforms the driver according to $\lambda(t) \mapsto r\lambda(t/r^2)$, and reflecting the curve over the imaginary axis $\gamma \mapsto -\overline{\gamma}$ reflects the driver $\lambda(t) \mapsto -\lambda(t)$. Thus to obtain $\lambda(t) = dt$, $d > 0$, we scale by $r = 1/d$, and our expressions become

$$\begin{aligned} x_d(t) &:= \frac{1}{d}x(d^2t) = -2\sqrt{t} - \frac{2}{3}dt - \frac{1}{18}d^2t^{3/2} + \frac{1}{135}d^3t^2 + O(t^{5/2}), \\ y_d(t) &:= \frac{1}{d}y(d^2t) = 2\sqrt{t} - \frac{2}{3}dt + \frac{1}{18}d^2t^{3/2} + \frac{1}{135}d^3t^2 + O(t^{5/2}). \end{aligned} \tag{3.9}$$

If d is negative, we reflect and our x-value becomes $-y_{-d}(t)$, and our y-value becomes $-x_{-d}(t)$, which give the same formulas as $x_d(t)$ and $y_d(t)$ above, respectively. So (3.9) holds for all $d \in \mathbb{R}$. Since $\xi(t) = ct$ corresponds to $\lambda(t) = -ct$, setting $d = -c$ in (3.9) gives (3.6). The error bound (3.7) follows from (3.8) by replacing $\varphi^{-1}(\pm\sqrt{t})$ with $\frac{1}{d}\varphi^{-1}(\pm\sqrt{d^2t})$. □

The following is a standard lemma about Taylor approximation for Hölder functions (see [22, Proposition 2.1], for instance). We include the elementary proof for completeness.

Lemma 3.4. *If $\xi \in C^{n,\alpha}(I)$ for some $n \in \mathbb{N}$ and $\alpha \in (0,1)$ with $\|\xi\|_{C^{n,\alpha}(I)} \leq M$, then the remainder in the nth Taylor approximation for ξ satisfies*

$$\left| \xi(t+h) - \sum_{k=0}^{n} \frac{\xi^{(k)}(t)}{k!} h^k \right| \leq C|h|^{n+\alpha} \tag{3.10}$$

whenever $t, t+h \in I$, where $C = C(n,\alpha,M) = \frac{M}{(n+\alpha)!}$ with $(n+\alpha)! := (n+\alpha)(n+\alpha-1)\cdots(\alpha+1)$.

Proof. For the base case of induction we have

$$|\xi(t+h) - \xi(t) - \dot{\xi}(t)h| \leq \int_t^{t+h} |\dot{\xi}(s) - \dot{\xi}(t)||ds| \leq M \int_t^{t+h} |s-t|^\alpha |ds| = \frac{M}{1+\alpha}|h|^{1+\alpha}.$$

Now suppose (3.10) holds for some $n \geq 1$, and let $h > 0$ (the case $h < 0$ is similar). The integral form of the Taylor error yields

$$\begin{aligned}
\left| \xi(t+h) - \sum_{k=0}^{n+1} \frac{\xi^{(k)}(t)}{k!} h^k \right| &= \left| \left(\xi(t+h) - \sum_{k=0}^{n} \frac{\xi^{(k)}(t)}{k!} h^k \right) - \frac{\xi^{(n+1)}(t)}{(n+1)!} h^{n+1} \right| \\
&= \left| \frac{1}{n!} \int_t^{t+h} (t+h-s)^n \xi^{(n+1)}(s) ds - \frac{1}{n!} \int_t^{t+h} \xi^{(n+1)}(t)(t+h-s)^n ds \right| \\
&\leq \frac{1}{n!} \int_t^{t+h} |\xi^{(n+1)}(s) - \xi^{(n+1)}(t)| (t+h-s)^n ds \\
&\leq \frac{M}{n!} \int_t^{t+h} (s-t)^\alpha (t+h-s)^n ds \\
&= \frac{M}{(n+\alpha)!} \int_t^{t+h} (s-t)^{n+\alpha} ds = \frac{M}{(n+1+\alpha)!} h^{n+1+\alpha},
\end{aligned}$$

where the second-to-last equality comes from integrating by parts n times. □

The previous three lemmas immediately give the following Taylor expansions for the points $x(t) < 0 < y(t)$ welded by a general driver $\xi \in C^{3/2+\epsilon}$. The expressions are identical to those in Lemma 3.3.

Theorem 3.5. *Let $\xi \in C^{3/2+\epsilon}([0,T])$ for some $\epsilon > 0$ and $T > 0$, with with $\|\xi\|_{C^{3/2+\epsilon}([0,T])} = M$. Then as $t \to 0$, the points $x(t) < 0 < y(t)$ welded together at time t by the upward Loewner flow generated by ξ have expansions*

$$x(t) = -2\sqrt{t} + \frac{2}{3}\dot{\xi}(0)t - \frac{1}{18}\dot{\xi}(0)^2 t^{3/2} + O(t^{3/2+\epsilon}), \tag{3.11}$$

$$y(t) = 2\sqrt{t} + \frac{2}{3}\dot{\xi}(0)t + \frac{1}{18}\dot{\xi}(0)^2 t^{3/2} + O(t^{3/2+\epsilon}), \tag{3.12}$$

where the $O(t^{3/2+\epsilon})$-term in either expansion has the same quantitative bound for all $t \le t_1 = t_1(M)$.

Note that by "quantitative bound," we mean that the version of the max in (3.7) which uses the coefficients in the above expansions is bounded by $C|t|^{3/2+\epsilon}$ whenever $t \le t_1$, where $C = C(M)$.

Proof. Let $\xi_1(t) = \dot{\xi}(0)t$ be the first-order Taylor approximation of ξ. Since the driving functions ξ_1 and ξ both have local Hölder-$1/2$ norm less than 4, they generate simple curves [27, 23]. By Lemma 3.2 and Lemma 3.4, the points $x(t) = x^{\xi}(t)$ and $x^{\xi_1}(t)$ which hit the singularity at time t under ξ and ξ_1, respectively, satisfy

$$|x^{\xi}(t) - x^{\xi_1}(t)| \le C_1 t^{3/2+\epsilon}$$

for any $t \in I$. Sending $t \to 0^+$ shows $x^{\xi}(t)$ must have the identical first three terms of Taylor expansion as $x^{\xi_1}(t)$ in Lemma 3.3, which gives (3.11) and (3.12). To quantify the error, we apply (3.7) to obtain

$$\begin{aligned}\Big|x^{\xi}(t) - \Big(-2\sqrt{t} + \frac{2}{3}\dot{\xi}(0)t - \frac{1}{18}\dot{\xi}(0)^2 t^{3/2}\Big)\Big| \\ &\le |x^{\xi}(t) - x^{\xi_2}(t)| + \Big|x^{\xi_2}(t) - \Big(-2\sqrt{t} + \frac{2}{3}\dot{\xi}(0)t - \frac{1}{18}\dot{\xi}(0)^2 t^{3/2}\Big)\Big| \\ &\le C_1 t^{3/2+\epsilon} + C_2 t^2 \le 1.5 C_1 t^{3/2+\epsilon}\end{aligned}$$

for all $t \le t_1 = t_1(M)$. The same argument, with the same constants, also holds for $y(t)$. □

Chapter 4

ON THE TOPOLOGY OF DRIVERS AND WELDINGS

In this section we prove that locally uniform convergence of drivers $\xi_n \to \xi$ implies locally uniform convergence of the corresponding welding homeomorphisms, given that the ξ_n and ξ all generate simple curves (and hence their weldings are all defined). The idea, inspired from [3], is to transfer the problem to the hitting times $\tau(x)$ of points $x \in \mathbb{R}$ under ξ. Combined with an estimate for the hitting times of nearby points under different drivers from [41], we obtain this result; see Theorem 4.5. We use Theorem 4.5 in §5.4 in our proof of the existence of a driver ξ which minimizes the Loewner energy among all drivers which weld given $x < 0 < y$. This chapter is joint work with Vlad Margarint and Yizheng Yuan.

Our setting is that $\xi : [0, \infty) \to \mathbb{R}$ is a (continuous) driving function with $\xi(0) = 0$. We consider the upward flow generated by $\xi(t)$, described by (2.12), and write $x(t) := h_t(x)$ for the image of a point $x \in \overline{\mathbb{H}}$ under this flow after t units of time.

Lemma 4.1. *Suppose the driving function ξ generates a simple curve γ in $\mathbb{H}$. Then the hitting time function $x \mapsto \tau(x)$ is continuous. It is strictly increasing for $x > 0$ and strictly decreasing for $x < 0$.*

Our notation for τ will be as follows. We write $\tau_- := \tau|_{x \le 0}$ and $\tau_+ := \tau|_{x \ge 0}$, and if there are multiple drivers ξ in consideration, $\tau(\cdot; \xi)$ specifies that the times come from ξ.

Lemma 4.1 is a simple consequence of the Loewner equation (2.12) and the fact that our conformal maps h_t have nice extensions to $\partial\mathbb{H}$.

Proof. By symmetry it suffices to consider points $x > 0$. Let $x_j(t)$ be the image of a point $x_j = x_j(0)$ after t units of time of the upwards Loewner flow (2.12) generated by ξ. Note

that if $0 < x_1 < x_2$ and $t < \tau(x_1)$,

$$\frac{\partial}{\partial t}\big(x_2(t) - x_1(t)\big) = \frac{2(x_2(t) - x_1(t))}{(x_2(t) - \xi(t))(x_1(t) - \xi(t))} > 0,$$

where $x_1(t)$ and $x_2(t)$ are the images of x_1 and x_2 under the un-centered upwards Loewner flow generated by ξ. Hence at $t = \tau(x_1)$, we have $x_1(\tau(x_1)) = \xi(\tau(x_1)) < x_2(\tau(x_1))$. Since ξ is continuous, $\tau(x_1) < \tau(x_2)$, and we see $x \mapsto \tau(x)$ is strictly increasing.

In particular, τ can only have jump discontinuities. To see this actually does not happen, pick $0 < x_1 < x_3$ arbitrarily and let $t_2 \in (\tau(x_1), \tau(x_3))$. We show there exists x_2 with $\tau(x_2) = t_2$. Indeed, map up with h_{t_2}. Since the curve γ_{t_2} generated by $\xi([0, t_2])$ is simple, the boundary point $\xi(t_2)$ of $\mathbb{H}\backslash\gamma_{t_2}$ corresponds to exactly two pre-images $y_2 < 0$ and $x_2 > 0$ under the extension of h_{t_2}. Since

$$h_{t_2}(x_2) = \xi(t_2), \tag{4.1}$$

$\tau(x_2) \leq t_2$.

Suppose that x_2's hitting time is actually earlier, i.e.

$$\tau(x_2) =: t_2' < t_2. \tag{4.2}$$

During the interval $[t_2', t_2]$, ξ generates the curve segment $\gamma_{t_2}([0, t_2 - t_2'])$ of half-plane capacity $2(t_2 - t_2') > 0$. In particular, $\Gamma := \gamma_{t_2}([0, t_2 - t_2'])$ is a non-degenerate continuum in $\mathbb{H} \cup \{\xi(t_2)\}$. The "right half" Γ^+ of this Jordan arc is homeomorphic under the boundary extension of h_{t_2} to an interval $[x_2', x_2] \subset \mathbb{R}_{>0}$, where the right end-point is x_2 by (4.1).

Now, starting at time t_2, flown *down* by $t_2 - t_2'$ units of time. This is equivalent to applying the map $h_{t_2'} \circ h_{t_2}^{-1}$. Then the curve segment Γ is completely mapped down to $\mathbb{R}$, and as $h_{t_2'} \circ h_{t_2}^{-1}$ has a homeomorphic extension to the "right side" γ^+ of γ, the image of Γ^+ is the non-degenerate interval $[\xi(t_2'), \xi(t_2') + c] \subset \mathbb{R}$. But note

$$[\xi(t_2'), \xi(t_2') + c] = h_{t_2'} \circ h_{t_2}^{-1}(\Gamma^+) = h_{t_2'}([x_2', x_2]),$$

and recall by (4.2) that $h_{t_2'}(x_2) = \xi(t_2')$. This says $c = 0$ and hence Γ is homeomorphic to a point, a contradiction. Therefore $\tau(x_2) = t_2$, and τ has no jump discontinuities. $\square$

We borrow the following lemma from [41, Lemma 5.1].

Lemma 4.2. *Given ξ and $\delta > 0$, we have that for all $\tilde{\xi}$ with $\|\xi - \tilde{\xi}\|_\infty \leq \delta$ and $x > 0$ that if $\tau(x;\xi) > T$, then $\tau(x+\delta;\tilde{\xi}) > T$.*

By sending $T \nearrow \tau(x;\xi)$, we note Lemma 4.2 gives

$$\tau(x;\xi) \leq \tau(x+\delta;\tilde{\xi}). \tag{4.3}$$

Lemma 4.3. *Suppose ξ generates a simple curve, and $\xi^n \to \xi$ uniformly. Then $\tau(x;\xi^n) \to \tau(x;\xi)$ for all x.*

Proof. By symmetry it suffices to consider $x > 0$. Fix $x > 0$ and let $\varepsilon > 0$. By the continuity of $\tau(\cdot;\xi)$ we can find $\delta > 0$ such that $|\tau(x';\xi) - \tau(x;\xi)| \leq \varepsilon$ for $|x' - x| \leq \delta$.

For large n, two applications of (4.3) yields

$$\tau(x-\delta;\xi) \leq \tau(x;\xi^n) \leq \tau(x+\delta;\xi),$$

and hence the claim. □

Lemma 4.4. *Let $f_n, f \colon \mathbb{R} \to \mathbb{R}$ be continuous and strictly increasing. Suppose $f_n \to f$ point-wise. Then $f_n^{-1} \to f^{-1}$ point-wise.*

Proof. Let $y \in \mathbb{R}$ and $x = f^{-1}(y)$. By the monotonicity of f we have $f(x-\varepsilon) < f(x) < f(x+\varepsilon)$. Let $\delta := |f(x) - f(x-\varepsilon)| \vee |f(x) - f(x+\varepsilon)|$. Let n be large enough such that $|f(x \pm \varepsilon) - f_n(x \pm \varepsilon)| < \delta$. Then $f_n(x-\varepsilon) < f(x) < f_n(x+\varepsilon)$, and consequently $f_n^{-1}(y) \in (x-\varepsilon, x+\varepsilon)$ by monotonicity of f_n. □

Theorem 4.5. *Suppose ξ^n and ξ generate simple curves, and $\xi^n \to \xi$ locally uniformly. Then the corresponding welding homeomorphisms converge locally uniformly.*

Proof. Note that the welding φ_λ associated to a driver λ can be defined as

$$\varphi_\lambda(x) := \tau_+^{-1}(\cdot;\lambda) \circ \tau_-(x;\lambda), \quad x \leq 0,$$

and so Lemmas 4.3 and 4.4 immediately give

$$\varphi_{\xi_n}(x) \to \varphi_{\xi}(x) \tag{4.4}$$

for each $x \leq 0$. In our setting, this is enough: recall Dini's Theorem states that point-wise convergence on a compact set of monotonic functions to a continuous limit implies uniform convergence. Hence the convergence (4.4) is actually locally uniform. □

Chapter 5

FAMILIES OF CURVES

5.1 Overview

Each step of the zipper algorithm welds the next two data points $x < 0 < y$ to the base of the constructed curve. Many different curve families can do this, as in Figure 5.1. For instance, we could always use straight slit segments, or hyperbolic geodesic segments (orthogonal circular arcs), or curves that minimize the Loewner energy in some way.

In this chapter we discuss six such curve families. Three of these - the straight slit family, the orthogonal circular arc family, and the Wang minimizer family - are already known. We shed some new light on the Wang minimizers, though, by giving a new deterministic proof for their existence, uniqueness, and energy formula, and we also explicitly compute their driving function. See Theorem 5.2.

We also introduce three new families. The *energy-minimizers for welding (EMW) family* minimizes the Loewner energy among all curves which weld given points $x < 0 < y$. We prove such a minimizer exists, is unique, is smooth, and we give a formula for the minimal energy to weld x to y. We also show that as $x < 0 < y$ vary, the minimizing curves can all be obtained from a single curve in $\mathbb{H}$ by truncating it at an appropriate point and re-scaling. See Theorem 5.5.

We also discuss the relationship between the Wang and EMW families, and show that the circular arc family, perhaps surprisingly, is always "nearby" both families in a precise energy sense. See Lemma 5.7(iv) and (v). We also show in Theorem 5.2(iv) and Theorem 5.5(v) that *all* curves driven by sufficiently-smooth drivers are asymptotically nearby the Wang and EMW families in exactly the same sense.

We close with a consideration of the *slow* and *fast drivers*, which give our two other new

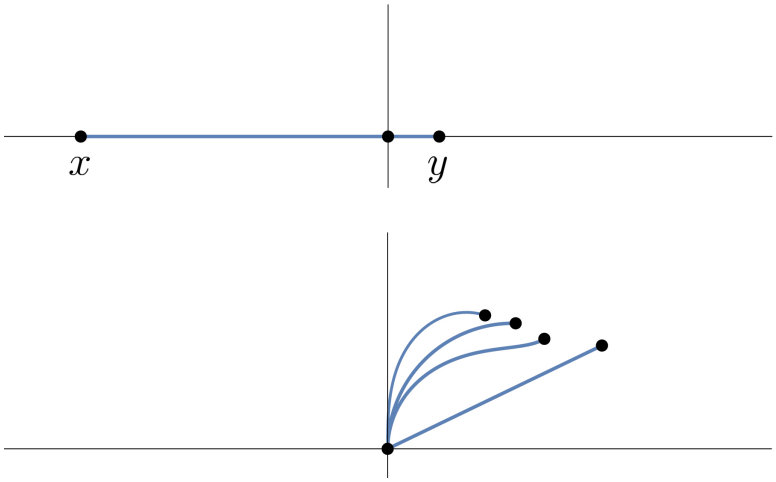

Figure 5.1: Welding the same points $x < 0 < y$ with the EMW family, the circular arc family, the Wang minimizers, and the straight slit family, from left to right in the lower picture. Compare the first column of Table 5.1.

families. These are only curve families in an extended sense, as they are extremal cases with respect to half-plane capacity and have discontinuous driving functions. We will see in Corollary 5.10 that they give us sharp lower and upper bounds for how long a monotone driver can take to weld given points $x < 0 < y$, and we will also see that the zipper algorithm numerically *diverges* when run with the fast driver, even when using smooth data. This appears to be the first known example of divergence for the zipper, although it is not a zipper in the sense of creating a simple curve. It suggests, however, that the family of all monotone drivers is too large to always guarantee a convergent zipper. See the example and discussion in §5.7.4.

Tables 5.1 and 5.2 summarize some of the properties of our families which are relevant for our zipper convergence arguments.* The chapter begins in §5.2 by setting out a framework for curve families which will be amenable for the zipper. Subsequent sections discuss the

*As an aside we remark that the tables also show elegant similarities for several functionals between the different curve families; the reason for these similarities is not understood.

Wang minimizers, the EMW family, the circular arc family, the straight slit family, and then lastly the slow and fast drivers.

5.2 Curve families and tractable curve families

For us, a *curve family* is a systematic procedure of welding $x < 0 < y$ to the base of a simple curve segment in $\mathbb{H}$. The following definition is based on the curve families we will use and provides a framework where we can apply our convergence arguments for the zipper. Intuitively, a *tractable curve family* is a collection of curves whose drivers are monotone and have controlled movement in terms of the starting points x and y.

Definition 5.1. A *tractable curve family* $\mathcal{C}$ is a collection of simple curves in $\mathbb{H}\cup\{0\}$ indexed by $x < 0 < y$ with upwards Loewner driving functions $\mathcal{D} = \mathcal{D}(\mathcal{C}) = \{\xi\}$ such that:

(*i*) For every $x < 0 < y$, there exists a unique curve $\gamma \in \mathcal{C}$ whose conformal map $h_t : \mathbb{H} \to \mathbb{H}\backslash\gamma$ welds $[x, 0]$ and $[0, y]$ to its two sides, taking x and y to the base of the curve and 0 to its tip. In terms of its driver $\xi = \xi(\mathcal{C}, x, y)$, $\xi(0) = 0$ and ξ welds x to y at some time $\tau = \tau(\mathcal{C}, x, y)$.

(*ii*) ξ is non-decreasing if $-x \leq y$ while non-increasing if $y \leq -x$.

(*iii*) The terminal value of the driver $\xi(\tau)$ is a continuous function of x and y and satisfies

$$\xi(\tau) = c(x + y) + O\Big(\frac{(x + y)^3}{(y - x)^2}\Big) \tag{5.1}$$

for some constant $c > 0$ as $\frac{y}{y-x} \to \frac{1}{2}$, with quantitative control on the error. That is, there exists constants $\delta = \delta(\mathcal{C})$ and $C = C(\mathcal{C})$ such that whenever $\big|\frac{y}{y-x} - \frac{1}{2}\big| < \delta$, the driver ξ for x and y satisfies

$$\big|\xi(\tau) - c(x + y)\big| \leq C\frac{|x + y|^3}{|y - x|^2}. \tag{5.2}$$

Note that it follows from (*ii*) that $\xi(\tau) = 0$ if and only if $y = -x$. Three of our four main curve families satisfy (5.1) with error of zero (see Table 5.1), but allowing a quantitative

error gives us more flexibility and does not dramatically affect our arguments. The error expression in (5.1) is admittedly ad-hoc, and is based on the behavior of the Wang minimizers, see Theorem 5.2(iii).

5.3 The Wang minimizer family

A natural question for Loewner energy is whether an energy minimizing curve from 0 to a given point $z_1 \in \mathbb{H}$ exists, and if so, whether it is unique. From scaling invariance, it suffices to consider $z_1 = e^{i\theta}$. Both questions were answered in the affirmative by Wang [42], who furthermore showed that the minimal energy is exactly $I(\gamma_\theta) = -8\log(\sin(\theta))$ [42, Proposition 3.1]. Although this is a deterministic statement, her argument uses an SLE formula from Schramm [36], thus invoking substantial probabilistic machinery.

In this section we give an entirely deterministic proof of Wang's result through Lemma 5.1 and Theorem 5.2, and we furthermore explicitly compute the associated driving function λ_θ and discuss several other of their properties. See Theorem 5.2. Our approach is elementary and similar to one we take for our other minimizing family, the "EMW" family, in §5.4 below (where Theorem 5.5 is the counterpart to Theorem 5.2). The EMW family is in some sense "dual" to this family; see the discussion in Remark 5.6 in §5.4.

Several analysis results help us obtain existence of minimizing curves both in this section and below in §5.4. First, recall that we have the continuous inclusion

$$W^{1,2}([0,T]) \hookrightarrow C^{1/2}([0,T]) \tag{5.3}$$

by Morrey's inequality [10, §4.5.3], in the sense that $f \in W^{1,2}([0,T])$ has a continuous equivalence-class representative $\tilde{f}$ in $C^{1/2}([0,T])$. Hence continuous driver families with controlled $W^{1,2}([0,T])$-norm are bounded and equicontinuous and therefore precompact in $C([0,T])$ by the Arzela-Ascoli theorem.

To state the same thing in more pedestrian language, if η is an absolutely-continuous driver with $\int_0^T \dot{\eta}(t)^2 dt = M < \infty$, then

$$|\eta_n(t_1) - \eta_n(t_2)| \leq \int_{t_1}^{t_2} |\dot{\eta}(t)| dt \leq \sqrt{M}\sqrt{|t_1 - t_2|} \tag{5.4}$$

by the Cauchy-Schwarz inequality. Hence a sequence of drivers $\{\eta_k\}$, all with $\eta_k(0) = 0$ and energy less than M on $[0,T]$, is bounded and equicontinuous on $[0,T]$, and so $\{\eta_k\}$ has uniform subsequential limits.

Our first lemma says that when mapping down a finite-energy curve, the tip tends to the imaginary axis.

Lemma 5.1. *Suppose λ is the driver for the simple curve $\gamma : [0,T] \to \mathbb{H} \cup \{0\}$ with $I(\gamma) < \infty$. Then under the centered downward Loewner flow generated by λ, the image $z_t := G_t(\gamma(T))$ of the tip of the curve satisfies*

$$\lim_{t \to T^-} \arg(z_t) = \frac{\pi}{2}. \tag{5.5}$$

The idea for the proof is simple: if $\int_0^T \dot{\lambda}(t)^2 dt < \infty$, then $\lim_{r \to T^-} \int_r^T \dot{\lambda}(t)^2 dt = 0$ and so $|\lambda(t_1) - \lambda(t_2)| \leq \epsilon \sqrt{|t_1 - t_2|}$ for all t_1, t_2 close to T by Cauchy-Schwarz, as in (5.4). Thus λ is close to the constant driver for t near T, which means it cannot "capture" points with argument bounded away from $\pi/2$. That is the idea; we carefully write out the details below.

Proof. Suppose there exists $\epsilon > 0$ and a sequence of times $t_n \to T^-$ such that

$$|\arg(z(t_n)) - \frac{\pi}{2}| > \epsilon$$

for all n. Take a subsequence which is always on one side of the imaginary axis; by symmetry we may suppose $\arg(z(t_n)) < \pi/2$, and we show that having $\pi/2 - \arg(z(t_n)) > \epsilon$ for all n requires infinite energy.

Consider first the case where

$$\arg(z(t_n)) < \arctan(1/2) \tag{5.6}$$

for all large n. Fix n such that $t_n \in [\tilde{T}, T)$, where $\tilde{T}$ is a time close to T to be specified below. Re-scale the picture by $r = \frac{1}{|z(t_n)|}$ to move the tip to $\partial\mathbb{D}$; for our new time parameter $s := t/r^2$ the corresponding time is now $s_0 := r^2 t_n \in [r^2\tilde{T}, r^2 T)$ and the tip of our curve is at

$$\tilde{z}(s_0) = \cos(\theta_0) + i \sin(\theta_0),$$

where $y(s_0) < \frac{1}{2}x(s_0)$ by (5.6). Choose $\tilde{T}$ large enough so that whenever $t_1, t_2 \geq \tilde{T}$,

$$|\lambda(t_1) - \lambda(t_2)| \leq \frac{\cos(\theta_0) - \sin(\theta_0)}{\sqrt{3}}\sqrt{|t_1 - t_2|}, \tag{5.7}$$

where $\cos(\theta_0) - \sin(\theta_0) \in (0, 1)$ by (5.6) again. By the invariance of the Hölder -1/2 semi-norm $|\lambda|_{1/2}$ under the scaling transformation $\lambda(\cdot) \mapsto r\lambda(\cdot/r^2)$, (5.7) also holds for our re-scaled driver $\tilde{\lambda}(s)$. We may assume $\tilde{\lambda}(s_0) = 0$, and we now let $\tilde{z}(s)$ be the image of $\tilde{z}(s_0)$ under the *uncentered* downward flow (2.10) generated by $\tilde{\lambda}$, with $x(s) := \mathrm{Re}(\tilde{z}(s))$ and $y(s) := \mathrm{Im}(\tilde{z}(s))$. We claim that for all $s \geq s_0$,

$$x(s) - \tilde{\lambda}(s) \geq \sin(\theta_0) > 0. \tag{5.8}$$

If true, then $\tilde{\lambda}$ is bounded away from $\tilde{z}(s)$ and so that point will never hit the singularity, a contradiction. We prove (5.8) by working in s-time intervals of length 3. For $s \in [s_0, s_0 + 3]$, (5.7) yields

$$|\tilde{\lambda}(s)| \leq \cos(\theta_0) - \sin(\theta_0) < \cos(\theta_0) = x(s_0) < x(s) \tag{5.9}$$

by the Loewner equation (2.11), yielding (5.8) for $s \in [s_0, s_0 + 3]$. We furthermore claim that

$$x(s_0 + 3) - \tilde{\lambda}(s_0 + 3) \geq \cos(\theta_0). \tag{5.10}$$

If so, then we may repeat the same analysis, obtaining (5.8) on $[s_0 + 3, s_0 + 6]$, and similarly by induction for all $s \geq s_0$. To see (5.10), we note from the Loewner equation (2.11) that

$$\frac{d}{d\lambda}\dot{x}(s) = \frac{2(x - \lambda)^2 - 2y^2}{((x - \lambda)^2 + y^2)^2},$$

and so $\frac{d}{d\lambda}\dot{x} > 0$ if $x - \lambda > y$. This holds in our case for $s \in [s_0, s_0 + 3]$, since

$$x(s) - \lambda \geq \sin(\theta_0) = y(s_0) \geq y(s)$$

by (2.11). Therefore, writing $m = m(\theta_0) := \cos(\theta_0) - \sin(\theta_0)$ and noting

$$y(s)^2 \leq x(s)^2 < (x(s) + m)^2$$

by (5.6) and (2.11), we have

$$\dot{x}(s) \geq \frac{2(x+m)}{(x+m)^2+y^2} \geq \frac{1}{x+m}$$

by (5.9). The equality case $\dot{u} = \frac{1}{u+m}$ has solution

$$u(s) = -m + \sqrt{2(s-s_0) + (u(s_0)+m)^2}, \tag{5.11}$$

and hence by comparison

$$x(s) \geq \sin(\theta_0) - \cos(\theta_0) + \sqrt{2(s-s_0) + (2\cos(\theta_0) - \sin(\theta_0))^2}. \tag{5.12}$$

In particular,

$$x(s_0+3) - \tilde{\lambda}(s_0+3) \geq 2\sin(\theta_0) - 2\cos(\theta_0) + \sqrt{6 + (2\cos(\theta_0) - \sin(\theta_0))^2} \geq \cos(\theta_0), \tag{5.13}$$

where the last inequality follows by calculus for $\theta_0 \in [0, \pi/4]$. Hence we have (5.10) as claimed. We may iterate this argument, since our lower bound (5.11) grows in the initial value $u(s_0)$, and so (5.12) will continue to hold by (5.10), yielding (5.13) at the end of subsequent intervals.

This contradiction shows (5.6) cannot hold, and so suppose $\arctan(1/2) < \arg(z(t_n)) < \pi/2 - \epsilon$. If for all $t \geq t_n$, $\lambda(t) \equiv \lambda(t_n)$ were constant, then the explicit mapping down function would be $\sqrt{z^2 - 4(t-t_n)}$, and it is not hard to see that the image of $z(t_n)$ under this map eventually has arbitrarily-small argument. By continuity of solutions to ODE's, drivers sufficiently close to constant and bounded away from $\mathrm{Re}(z(t_n))/2$, say, will map $z(t_n)$ to similarly-small argument eventually, putting us in the context of (5.6) again. We have this for λ for times sufficiently close to T^-, yielding a contradiction. □

Our main collection of results about the Wang minimizers are in the following theorem. The statement of (i) is from Wang but the remainder is original to our work. The point of including part (i), again, is because of our alternative deterministic proof.

Theorem 5.2. *Let $\theta \in (0, \pi)$.*

(*i*) *[42, Proposition 3.1] There exists a unique $\gamma_\theta \subset \mathbb{H}$ from 0 to $e^{i\theta}$ which minimizes the Loewner energy among all such curves. Furthermore,*

$$I(\gamma_\theta) = -8\log(\sin(\theta)). \tag{5.14}$$

(*ii*) *For $0 < \theta < \pi/2$, the downward Loewner driving function λ_θ for γ_θ is monotonic, $C^\infty([0,\tau_\theta))$ and is explicitly*

$$\lambda_\theta(t) = \frac{4}{3}\cos(\theta) - \frac{4}{3}\left(\sqrt[3]{f(\theta,t) + \sqrt{f(\theta,t)^2 + \frac{\sin^6(\theta)}{\cos^2(\theta)}}} + \sqrt[3]{f(\theta,t) - \sqrt{f(\theta,t)^2 + \frac{\sin^6(\theta)}{\cos^2(\theta)}}}\right)^{3/2},$$

where $f(\theta,t) = 1 - 6t - \frac{1}{2}\cos(2\theta)$ and $0 \le t \le \frac{1}{6}(1 - \frac{1}{2}\cos(2\theta)) =: \tau_\theta$. For $\pi/2 < \theta < \pi$, the driver is $-\lambda_{\pi-\theta}$.

(*iii*) *For any points $x < 0 < y$, there exists a unique Wang minimizer γ which welds x to y at the base of γ. The capacity time τ for γ and the terminal driving function value $\lambda(\tau)$ satisfy*

$$\tau = \frac{32 - 3\pi^2}{24\pi^2}\Big(x^2 - \frac{12\pi^2 - 64}{32 - 3\pi^2}xy + y^2\Big) + O\left(\frac{(x+y)^4}{(y-x)^2}\right),$$
$$\lambda(\tau) = -\frac{8}{3\pi}(x+y) + O\Big(\frac{(x+y)^3}{(y-x)^2}\Big)$$

as the ratio $\frac{y}{y-x} \to \frac{1}{2}$. The errors in both expressions have quantitative control.

(*iv*) *If γ is any curve driven by $\lambda \in C^2([0,T))$ with $\dot\lambda(0) \neq 0$, then as $t \to 0^+$, $\gamma([0,t])$ uses an asymptotic factor of 9/8 of the energy of the energy-minimizing curve from 0 to $\gamma(t)$.*

We call this family of curves the *Wang minimizers*.

Remark 5.3. When we map down an initial portion $\gamma_\theta([0,t])$ of a Wang minimizer, the remainder $G_t(\gamma_\theta([t,\tau_\theta]))$ is the Wang minimizer for the angle of $G_t(e^{i\theta})$, since if not, we could

replace $G_t(\gamma_\theta([t,\tau_\theta]))$ with the minimizer and lower the energy. We see below in (5.16) that if $\theta \neq 0$, $\dot{\lambda}_\theta \neq 0$, and so part (iv) in particular applies to the Wang minimizers themselves, and so the initial portion $\gamma_\theta([0,t])$ of a Wang minimizer is *not* also a Wang minimizer. Hence the symmetry of the Wang family is with respect to the "top," or the portion remaining after mapping down, not with respect to the "base" or the portion mapped down. This is the opposite of what we will see for the EMW family, where what we map down is an EMW curve, but what remains is not. Compare Theorem 5.2(iv) with Theorem 5.5(v) and see Remark 5.6.

Proof. For (i), we begin by giving a standard argument for the existence of minimizers based on the lower semi-continuity of energy (2.21). Afterwards we show that the driver of a minimizer must satisfy a given differential equation at all points of differentiability, which will give uniqueness and the formula (5.14).

The orthogonal circular arc segment from 0 to $e^{i\theta}$ has some energy $0 < C_\theta < \infty$ (which we explicitly compute to be $-9\log(\sin(\theta))$ in §5.5 below). Let Γ_θ be the collection of all Jordan arcs $\gamma_\theta \subset \mathbb{H} \cup \{0\}$ from 0 to $e^{i\theta}$ with $I(\gamma_\theta) \leq C_\theta$. By [42, Prop. 2.1], each $\gamma \in \Gamma_\theta$ is a K-quasislit halfplane for some fixed $K = K(C_\theta)$.[†] That is, there exists a K-quasiconformal self-map q of $\mathbb{H}$ fixing 0 and ∞ with $q([0,i]) = \gamma$. Now, let $\{\gamma_n\}$ be a sequence such that

$$I(\gamma_n) \to \inf_{\gamma \in \Gamma_\theta} I(\gamma) =: L$$

and let $\{q_n\}$ be corresponding K-quasiconformal maps. The family $\{q_n\}$ is normal in the spherical metric and any limiting function is either identically a point in $\partial_{\hat{\mathbb{C}}}\mathbb{H}$ or a K-quasiconformal self-map of $\mathbb{H}$ [19, §2.2f]. The former cannot happen because all q_n map i to $e^{i\theta}$, and hence, by moving to a subsequence, which we relabel as q_n again, we have a locally uniform limit $q_n \to q$ in $\mathbb{H}$ and a limiting curve $\gamma := q([0,i])$.[‡]

[†]While we are quoting Wang's paper, this result is independent of her proof of (5.14), and so our deterministic proof is still independent of her stochastic argument.

[‡]While the convergence is locally uniform in $\mathbb{H}$, and hence not on all of $[0,i]$, we may reflect over $\mathbb{R}$ and regard the family q_n as normal on $\hat{\mathbb{C}}$, as the three points $0, i$ and ∞ have images bounded away from each other (indeed, fixed). Thus $q_n([0,i]) \to q([0,i])$ uniformly.

In particular, γ and all the $\{\gamma_n\}$ are K-quasiarcs, and so by the 3-point condition of Ahlfors we have some $M = M(K)$ such that, for $\beta \in \{\gamma, \gamma_n\}$,

$$|\beta(0) - \beta(t)| = |\beta(t)| \leq M|\beta(0) - \beta(T_\beta)| = M$$

for each $0 < t < T_\beta$, the capacity time of β. By monotonicity of half-plane capacity, we thus have

$$\text{hcap}(\beta) \leq \text{hcap}(B_M(0) \cap \mathbb{H}) = M^2$$

for all β. It follows that we can consider all our curves to be defined on the same finite interval $[0, T]$ of capacity time, as we can extend β, if necessary, by an appropriate-length segment of the hyperbolic geodesic from $e^{i\theta}$ to ∞ in $\mathbb{H}\backslash\beta$. (This is the same as extending the driver η for β by the constant function $\eta(t) \equiv \eta(T_\beta)$ for $T_\beta < t \leq T$).

By the proof of Theorem 4.1 in [21], the modulus of continuity of a K-quasiarc in its capacity parametrization depends only upon K, and hence $\{\gamma_n, \gamma\}$ is a bounded and equicontinuous family, and so by moving to a further subsequence, if needed, we have $\gamma_n \to \gamma$ uniformly on $[0, T]$ by Arzela-Ascoli.

Since the associated drivers λ_n also satisfy the equicontinuity (5.4), by passing to another subsequence we have that $\lambda_n \to \lambda$ uniformly on $[0, T]$. A priori, λ has no relation to γ, but since both $\gamma_n \to \gamma$ and $\lambda_n \to \lambda$ uniformly on $[0, T]$, by [21, Lemma 4.2] we have that γ is driven by λ. The lower semicontinuity of energy then yields

$$I(\gamma) \leq \liminf_{n\to\infty} I(\gamma_n) = \inf_{\beta\in\Gamma_\theta} I(\beta),$$

and as $e^{i\theta} \in \gamma$, we have $I(\gamma)$ equals the infimum and thus minimizers exist.

Let λ be any minimizing driver, and let $z(t) = x(t) + iy(t) := G_t(e^{i\theta})$ be the image of $e^{i\theta}$ under the centered downwards flow generated by λ. Since $I(\lambda) < \infty$, λ is absolutely continuous and so differentiable for a.e. t. We claim that at for a.e. t,

$$\dot{\lambda}(t) = \frac{8x(t)}{|z(t)|^2}. \tag{5.15}$$

By scale invariance the energy depends only on the angle, and by Lemma 5.1 the angle $\theta(t) := \arg(z(t))$ must tend towards $\pi/2$ if λ minimizes energy. And indeed, it must move strictly monotonically: if the angle ever decreases and then returns to the same value, energy is wasted, while if the angle is constant over some interval, then λ cannot be constant and we have also wasted energy. Hence $z(t)$ should traverse through the angles as efficiently as possible; the change in angle to the change in energy, $d\theta/dI$, must be optimal. That is, $d\theta/dI$ must be maximized when $\theta < \pi/2$ and minimized when $\theta > \pi/2$.

Suppose first that λ is right-differentiable at $t = 0$ and that $t = 0$ is a Lebesgue point for $\dot{\lambda}^2$. Then the energy expelled on a small interval $[0, \Delta t]$ is $\frac{1}{2}\dot{\lambda}^2(0)\Delta t + o(\Delta t)$. Furthermore, θ is right-differentiable at $t = 0$, and

$$\Delta\theta = \dot{\theta}(0)\Delta t + o(\Delta t) = \operatorname{Im}\Big(\frac{\dot{z}(0)}{z(0)}\Big)\Delta t + o(\Delta t) = (-4x(0)y(0) + \dot{\lambda}(0)y(0))\Delta t + o(\Delta t)$$

by the Loewner equation (2.16) and the fact that $|z(0)| = 1$. We thus have

$$\frac{\Delta\theta}{\Delta I} = \frac{(-4xy + \dot{\lambda}y)\Delta t + o(\Delta t)}{\frac{1}{2}\dot{\lambda}^2\Delta t + o(\Delta t)} \to \frac{-8xy}{\dot{\lambda}^2} + \frac{2y}{\dot{\lambda}}$$

as $\Delta t \to 0$, where x, y and $\dot{\lambda}$ are evaluated at $t = 0$, and $\dot{\lambda}(0)$ is the right derivative of λ. This expression is optimized with respect to $\dot{\lambda}$ when $\dot{\lambda}(0) = 8x(0)$, which yields a local max when $x > 0$ and a local min when $x < 0$, as needed. Thus any minimizer for which $\dot{\lambda}(0)$ exists and where $t = 0$ is a Lebesgue point of $\dot{\lambda}^2$ must satisfy (5.15) at $t = 0$ (recall $|z(0)| = 1$).

More generally, let t_0 be a point of differentiability of λ and a Lebesgue point of $\dot{\lambda}^2$. Note that the remaining curve $\tilde{\gamma} := G_{t_0}(\gamma([t_0, \tau]))$ must be an energy minimizer through $z(t_0)$, as discussed above in Remark 5.3. Thus $\tilde{\gamma}/|z(t_0)|$ is a minimizer as in the previous paragraph, and so its driver $\tilde{\lambda}$ has initial right derivative $8\tilde{x}(0) = 8x(t_0)/|z(t_0)|$. Recalling the scaling relation (2.9), we therefore have

$$|z(t_0)|\dot{\lambda}(t_0) = \dot{\tilde{\lambda}}(0) = \frac{8x(t_0)}{|z(t_0)|},$$

as in (5.15). Since λ is differentiable at a.e. t and a.e. t is a Lebesgue point of the integrable function $\dot{\lambda}^2$, (5.15) holds as claimed. We note that we obtain the same answer if we immediately optimize $d\theta/dI$ with respect to $\dot{\lambda}$.

By (2.16) we thus obtain the system of differential equations

$$\dot{\lambda}(t) = \frac{8x}{x^2+y^2}, \qquad \dot{x}(t) = \frac{-6x}{x^2+y^2}, \qquad \dot{y}(t) = \frac{-2y}{x^2+y^2} \tag{5.16}$$

for which the triple (λ, x, y) generated by λ is an a.e.-t solution, and where each component is absolutely continuous. Since we can thus recover each of λ, x and y through integration and the three right-hand sides in (5.16) are continuous, we have that (5.16) actually holds for *all* t, and hence each of λ, x and y is C^1 on $[0, \tau_\theta)$. By bootstrapping in (5.16), then, they are all C^2, and continuing, they are all $C^\infty([0, \tau_\theta))$.

Classical solutions to (5.16) are also unique: starting at any point (x_0, y_0), both $x(t)$, $y(t)$ are bounded away from 0 on a small time interval, and so the function $f(t, \lambda, x, y) = \big(8x(x^2+y^2)^{-1}, -6x(x^2+y^2)^{-1}, -2y(x^2+y^2)^{-1}\big)$ is Lipschitz. Thus we have smoothness, uniqueness, as well as monotonicity of λ from (5.16).

For the energy formula (5.14), write $m(\theta)$ for energy of the curve through $e^{i\theta}$. If we flow down starting from a fixed $\theta = \theta(0)$, we know the remaining curve is always the minimizer for the angle

$$\theta(t) = \arg(z(t)), \tag{5.17}$$

the argument of the image of the tip (see the remark before the proof). Hence through the composition $m(\theta(t))$ we may regard m as a function of t, and we find

$$\frac{dm}{d\theta} = \frac{\dot{m}}{\dot{\theta}} = \frac{-\frac{1}{2}\dot{\lambda}^2}{\frac{-4xy}{(x^2+y^2)^2} + \frac{\dot{\lambda}y}{x^2+y^2}} = -8\frac{x}{y} = -8\cot(\theta),$$

and therefore

$$m(\pi/2) - m(\theta_0) = -m(\theta_0) = \int_{\theta_0}^{\pi/2} -8\cot(\theta)d\theta = 8\log(\sin(\theta_0)),$$

as claimed, completing the proof of (i).

Our formulas in (ii) for λ_θ and the capacity time now are exercises in ODE. We note from (5.16) that x is monotonically decreasing (recall we are assuming $0 < \theta < \pi/2$), and so we may reparametrize λ as a function of x and note $\frac{d\lambda}{dx} = -\frac{4}{3}$ from (5.16), and hence

$$\lambda(t) = \lambda(x(t)) - \lambda(x(0)) = \frac{4}{3}\cos(\theta) - \frac{4}{3}x(t). \tag{5.18}$$

To determine $x(t)$, we note from (5.16) that

$$\frac{dx}{dy} = 3\frac{x}{y}, \qquad \text{implying} \qquad x(t) = \frac{\cos(\theta)}{\sin^3(\theta)} y(t)^3 \tag{5.19}$$

since $(x(0), y(0)) = (\cos(\theta), \sin(\theta))$. Writing $a = a(\theta) := \frac{\cos(\theta)}{\sin^3(\theta)}$ and substituting back into the equation for $\dot{y}(t)$ yields

$$\dot{y}(t) = \frac{-2}{a^2 y^5 + y}$$

which has implicit solution

$$\frac{a^2}{6} y(t)^6 + \frac{1}{2} y(t)^2 = -2t + \frac{1}{6}\cos^2(\theta) + \frac{1}{2}\sin^2(\theta).$$

We thus see that $u(t) := y(t)^2$ satisfies the cubic

$$0 = u^3 + 3\frac{\sin^6(\theta)}{\cos^2(\theta)} u + 6\frac{\sin^6(\theta)}{\cos^2(\theta)}\big(2t - \frac{1}{6}\cos^2(\theta) - \frac{1}{2}\sin^2(\theta)\big) =: u^3 + pu + q.$$

As the discriminant $4p^3 + 27q^2$ is manifestly positive, by Cardano's cubic formula [7] the real root is

$$y(t)^2 = \sqrt[3]{\frac{\sin^6(\theta)}{\cos^2(\theta)} f(\theta,t) + \sqrt{\frac{\sin^{12}(\theta)}{\cos^4(\theta)} f(\theta,t)^2 + \frac{\sin^{18}(\theta)}{\cos^6(\theta)}}} + \sqrt[3]{\frac{\sin^6(\theta)}{\cos^2(\theta)} f(\theta,t) - \sqrt{\frac{\sin^{12}(\theta)}{\cos^4(\theta)} f(\theta,t)^2 + \frac{\sin^{18}(\theta)}{\cos^6(\theta)}}}.$$

The claimed formula then follows from pulling out the trig functions and substituting back into (5.19), and then into (5.18).

For the terminal Loewner-time formula

$$\tau_\theta = \frac{1}{6}(1 - \frac{1}{2}\cos(2\theta)), \tag{5.20}$$

note that we can regard τ_θ as a function of t through the composition $\tau_{\theta(t)} = \frac{1}{2}\,\mathrm{hcap}(\gamma_{\theta(t)})$, with $\theta(t)$ given by (5.17). That is, $\tau_{\theta(t)}$ is the capacity time of the minimizing segment $\gamma_{\theta(t)}$ from 0 to $e^{i\theta(t)}$ (not the capacity time of the remaining curve), where the 1/2-factor is because

the half-plane capacity is twice the Loewner time. We claim that $\tau_{\theta(t)}$ is differentiable in t and satisfies

$$\frac{d}{dt}\tau_{\theta(t)} = -1 + 4\tau_{\theta(t)}(1 + 2\cos^2(\theta)). \tag{5.21}$$

Indeed, if we map a small portion $\gamma_\theta([0, \Delta t])$ of γ_θ down, we have

$$\tau_{\theta(\Delta t)} = \frac{\tau_\theta - \Delta t}{|z(\Delta t)|^2} \tag{5.22}$$

because the remaining curve is the minimizer through $\theta(\Delta t)$; the denominator is because of the scaling property $\mathrm{hcap}(r\gamma) = r^2\,\mathrm{hcap}(\gamma)$. From (5.16),

$$\frac{d}{dt}|z(t)|^2 = \frac{-12x^2 - 4y^2}{x^2 + y^2} = -4(1 + 2\cos^2(\theta)),$$

and so $|z(\Delta t)|^2 = 1 - 4(1 + 2\cos^2(\theta))\Delta t + o(\Delta t)$ as $\Delta t \to 0$. Plugging this into (5.22) yields

$$\frac{\tau_{\theta(\Delta t)} - \tau_\theta}{\Delta t} = \frac{-\Delta t + 4\tau_\theta(1 + 2\cos^2(\theta))\Delta t + o(\Delta t)}{\Delta t\big(1 - (1 + 2\cos^2(\theta))\Delta t + o(\Delta t)\big)},$$

yielding (5.21) in the limit. Since $\theta(t)$ is differentiable with respect to t with

$$\dot\theta(t) = \frac{d}{dt}\,\mathrm{Im}(\log(z(t))) = \frac{4xy}{(x^2 + y^2)^2} = 4\cos(\theta)\sin(\theta) \tag{5.23}$$

at $t = 0$, we have

$$\frac{d\tau_\theta}{d\theta} = \frac{\dot\tau_\theta}{\dot\theta} = \frac{-1 + 4\tau_\theta(1 + 2\cos^2(\theta))}{4\cos(\theta)\sin(\theta)}.$$

This ODE has explicit solution

$$\tau_\theta = C\frac{\sin^3(\theta)}{\cos(\theta)} + \frac{1}{6}\big(1 - \frac{1}{2}\cos(2\theta)\big).$$

In order to have τ_θ bounded as $\theta \to \frac{\pi}{2}^-$, we must have $C = 0$, which yields (5.20). Note that this formula also extends to $\theta = 0$, where the minimizer $\gamma_{\pi/2} = [0, i]$ satisfies

$$\mathrm{hcap}([0, i]) = \frac{1}{2} = \frac{1}{3}\big(1 - \frac{1}{2}\cos(\pi)\big).$$

For (iii), we note that the welding $\varphi_\theta : [x_\theta, 0] \to [0, y_\theta]$ for γ_θ has been explicitly computed in [26], and when normalized to produce our γ_θ with tip at $e^{i\theta}$, the interval endpoints are explicitly

$$x_\theta = -\sqrt{\frac{\sin^3(\theta)}{\sin(\theta) - \theta\cos(\theta)}} \qquad \text{and} \qquad y_\theta = \sqrt{\frac{\sin^3(\theta)}{\sin(\theta) - \theta\cos(\theta) + \pi\cos(\theta)}}. \tag{5.24}$$

By inspection, the ratio $\frac{y_\theta}{y_\theta - x_\theta}$ monotonically increases from 0 to 1 as θ increases from 0 to $\pi/2$, which by symmetry gives a unique energy-minimizer for welding any two points $x < 0 < y$.

We begin by computing τ_θ and $\lambda_\theta(\tau_\theta)$ for θ close to $\pi/2$ where the welding interval has been normalized to have width 1; the formulas in (iii) then follow by appropriate scaling.

As $\theta \to \pi/2$, (5.24) yields

$$\alpha_\theta := \frac{y_\theta}{y_\theta - x_\theta} = \frac{1}{2} + \frac{\pi}{8}\left(\theta - \frac{\pi}{2}\right) + O\left(\theta - \frac{\pi}{2}\right)^3,$$

and inverting this expansion gives

$$\theta = \frac{\pi}{2} + \frac{8}{\pi}\left(\alpha - \frac{1}{2}\right) + O\left(\alpha - \frac{1}{2}\right)^3. \tag{5.25}$$

Feeding this into (5.20) along with the expansion

$$\frac{1}{(y_\theta - x_\theta)^2} = \frac{1}{4} + \frac{1}{64}\left(32 - 3\pi^2\right)\left(\theta - \frac{\pi}{2}\right)^2 + O\left(\left(\theta - \frac{\pi}{2}\right)^4\right) \tag{5.26}$$

yields that the capacity time of the minimizer which has welding interval width 1 and ratio α is

$$\left.\frac{\tau_\theta}{(y_\theta - x_\theta)^2}\right|_{\theta=\theta(\alpha)} = \frac{1}{16} + \left(\frac{16}{3\pi^2} - \frac{3}{4}\right)\left(\alpha - \frac{1}{2}\right)^2 + O\left(\alpha - \frac{1}{2}\right)^4.$$

Noting $\alpha - \frac{1}{2} = \frac{y+x}{2(y-x)}$, we scale up to interval width $y - x$ to obtain

$$\tau = (y-x)^2\frac{\tau_\theta(\alpha)}{(y_\theta - x_\theta)^2} = \frac{1}{16}(y-x)^2 + \left(\frac{4}{3\pi^2} - \frac{3}{16}\right)(x+y)^2 + O\left(\frac{(x+y)^4}{(y-x)^2}\right),$$

which is the same as the claimed expression.

The procedure is similar for the driver. We have explicitly $\lambda_\theta(\tau_\theta) = \frac{4}{3}\cos(\theta)$, and so by (5.25) and an expansion similar to (5.26), the terminal driver for the minimizer with welding interval of width 1 is

$$\frac{1}{y_\theta - x_\theta} \cdot \frac{4}{3}\cos\left(\frac{\pi}{2} + \frac{8}{\pi}\left(\alpha - \frac{1}{2}\right) + O\left(\alpha - \frac{1}{2}\right)^3\right) = -\frac{16}{3\pi}\left(\alpha - \frac{1}{2}\right) + O\Big(\alpha - \frac{1}{2}\Big)^3,$$

yielding the general terminal value

$$\lambda(\tau) = (y-x)\left(-\frac{16}{3\pi}\Big(\alpha - \frac{1}{2}\Big) + O\Big(\alpha - \frac{1}{2}\Big)^3\right) = -\frac{8}{3\pi}(x+y) + O\left(\frac{(x+y)^3}{(y-x)^2}\right).$$

Given these are expansions of smooth functions, we have quantitative control in both formulas in terms of the sizes of $\frac{(x+y)^4}{(y-x)^2}$ and $\frac{(x+y)^3}{(y-x)^2}$.

For (iv), the energy used by $\gamma([0,t])$ for small t is $\frac{1}{2}\dot\lambda(0)^2 t + o(t)$. To determine $\arg(\gamma(t))$, and hence the minimal energy possible for a curve through $\gamma(t)$, we recall the expansion

$$\gamma(t) = 2i\sqrt{t} + \frac{2}{3}\dot\lambda(0)t - \frac{i}{18}\dot\lambda(0)^2 t^{3/2} + \Big(\frac{4}{15}\ddot\lambda(0) + \frac{1}{135}\dot\lambda(0)^3\Big)t^2 + O(t^{5/2})$$

for the capacity parametrization of γ in terms of λ at $t = 0$ (see [24, Prop. 3.3] and [22, Prop. 6.2]). By symmetry we may assume $\dot\lambda(0) > 0$, and thus

$$\begin{aligned}\arg(\gamma(t)) &= \frac{\pi}{2} - \arctan\Big(\frac{\mathrm{Re}(\gamma_\theta(t))}{\mathrm{Im}(\gamma_\theta(t))}\Big)\\ &= \frac{\pi}{2} - \arctan\left(\frac{\frac{2}{3}\dot\lambda(0)t + O(t^2)}{2\sqrt{t} + O(t^{3/2})}\right) = \frac{\pi}{2} - \frac{1}{3}\dot\lambda(0)\sqrt{t} + O(t^{3/2}).\end{aligned}$$

The minimal-energy curve through this angle has energy

$$-8\log\left(\sin\Big(\frac{\pi}{2} - \frac{1}{3}\dot\lambda(0)\sqrt{t} + O(t^{3/2})\Big)\right) = \frac{4}{9}\dot\lambda(0)^2 t + O(t^{3/2}),$$

yielding the ratio

$$\frac{\frac{1}{2}\dot\lambda(0)^2 t + o(t)}{\frac{4}{9}\dot\lambda(0)^2 t + O(t^{3/2})} \to \frac{9}{8}.$$

□

5.4 The energy minimizer for weldings (EMW) family

From the welding point of view, the most natural energy minimizers are not those of Wang, but rather those that minimize the energy among all curves which weld a fixed $x < 0$ to

a fixed $0 < y$. In this section we establish the existence and uniqueness of this family and discuss some of its properties. We will see that these curves are "dual" to Wang's in some sense; if the latter are the energy minimizers for flowing *down* in the Loewner equation, these are the minimizers for flowing *up*. See Remark 5.6 below. We are thankful for the excellent idea from Steffen Rohde to investigate these curves.

Our approach and proof strategy runs parallel to §5.3; here Lemma 5.4 corresponds to Lemma 5.1 in §5.3, and our main results are collected in Theorem 5.5, this section's version of Theorem 5.2. We conclude the section with some numerical simulations and observations.

Lemma 5.4. *Suppose ξ has $\xi(0) = 0$ and $I(\xi) < \infty$. Let $x(t)$ and $y(t)$ be the positions of some $x_0 < 0 < y_0$ under the centered upwards flow (2.15) generated by ξ. If at time τ we have*

$$x(\tau) = 0 = y(\tau), \tag{5.27}$$

then $\frac{y(t)}{y(t)-x(t)} \to \frac{1}{2}$ as $t \to \tau^-$.

In words, if ξ welds x_0 to y_0 using finite energy, then $x(t)$ and $y(t)$ must "evenly" approach to the singularity. This is the upward flow parallel to the property in Lemma 5.1 for the downward flow. Put together, Lemmas 5.1 and 5.4 state that points welded by finite-energy ξ "evenly" approach ξ and then move up into $\mathbb{H}$ perpendicularly from the real line. Note that the conclusion of the lemma is equivalent to saying $r(t) := -x(t)/y(t) \to 1$.

Proof. We claim that there is a positive lower bound $m(r)$ for the energy to weld points with ratio $r = r(0) = -x_0/y_0 \neq 1$ that is strictly increasing in $|r - 1|$. Suppose momentarily that this holds. Then as $\frac{1}{2}\int_t^\tau \dot{\xi}(s)^2 ds \to 0$ as $t \to \tau^-$, we must have $m(r(t)) = m(-x(t)/y(t)) \to 0$ and so $r(t) \to 1$, as claimed.

We can give an explicit, albeit coarse, formula for $m(r)$. Switch to ξ's uncentered flow, writing $u(t)$ and $v(t)$ to be the images of x_0 and y_0, respectively, under this flow after t units of time. By (2.12), the average $A(t) := \frac{1}{2}(u(t) + v(t))$ satisfies

$$\dot{A}(t) = 2\frac{A(t) - \xi(t)}{(\xi(t) - u(t))(v(t) - \xi(t))},$$

and so $\dot{A}(t) > 0$ whenever $\xi(t) < A(t)$. Thus if $A(0) > 0$ and $\xi(\tau) < A(0)$, then $\xi(\tau) < A(\tau) < y(\tau)$, a contradiction. The case $A(0) < 0$ is similar, showing ξ travels at least to $A(0)$.

Suppose $r(0) < 1$ (as again, the other case follows). If ξ was instantaneously at A_0 and then remained stationary, $u(t)$ would hit A_0 at time

$$\frac{1}{4}(x_0 - A(0))^2 = \frac{(x_0 - y_0)^2}{16} =: \tau_0.$$

Therefore ξ must reach A_0 before this time, as otherwise we would have the collision $x(t) = \xi(t) < A(0) < A(t) < y(t)$. As Dirichlet energy is minimized by harmonic functions, the minimal-energy driver that reaches $A(0)$ in time τ_0 is the linear function $\eta(t) = \tau_0^{-1}A(0)t$, and $I(\eta) = \frac{1}{2\tau_0}A(0)^2$. We conclude

$$I(\xi) \geq I(\eta) = 2\frac{(x_0 + y_0)^2}{(x_0 - y_0)^2} = 2\left(\frac{1-r}{1+r}\right)^2 =: m(r) > 0 \tag{5.28}$$

when $r \neq 1$. By calculus, $m(r)$ is strictly increasing in $|r - 1|$ for $r \in (0, \infty)$. □

Again, our lower bound $m(r)$ in (5.28) is rather coarse. In the next theorem, we give a formula (5.30) for a sharp bound for each r that is attained by a unique, smooth driver. See Figure 5.2. We call the curves these minimizing drivers generate the *energy minimizer for welding (EMW) curves*. Similarly, the driving function is the *EMW driver*. As a way of welding any $x_0 < 0 < y_0$, they give us the *EMW curve family*.

Theorem 5.5. *For fixed $x_0 < 0 < y_0$, there exists a unique driving function ξ with $\xi(0) = 0$ and which welds x_0 to y_0 and minimizes the Loewner energy among all such drivers. Furthermore, ξ satisfies the following:*

(*i*) *For any $0 \leq t < \tau$, the hitting time of x_0 and y_0 under ξ,*

$$\dot{\xi}(t) = -4\left(\frac{1}{x(t)} + \frac{1}{y(t)}\right), \tag{5.29}$$

where $x(t)$ and $y(t)$ are the images of x_0 and y_0 under the centered upwards flow generated by ξ. Furthermore, $\xi \in C^\infty([0, \tau))$.

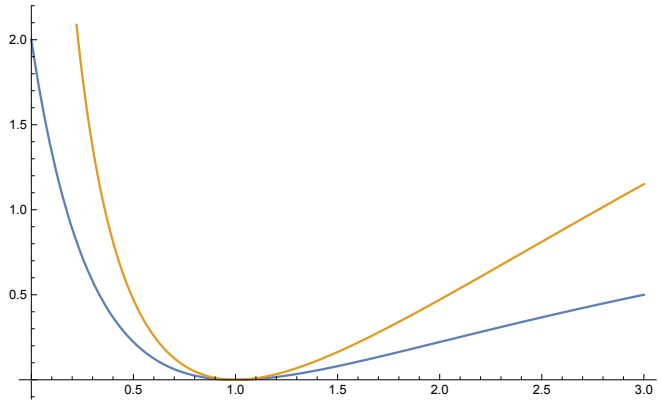

Figure 5.2: Lower bounds on the energy needed to weld $x_0 < 0 < y_0$ in terms of the ratio $r = -x_0/y_0 \in (0, \infty)$. The blue is the coarse bound $m(b)$ from Lemma 5.4, and the orange is the sharp formula (5.30). Near $r = 1$, the latter has expansion $(r-1)^2 + O(r-1)^3$.

(*ii*) *ξ is monotonic, $\tau = \frac{1}{24}(x_0^2 - 4x_0y_0 + y_0^2)$ and $\xi(\tau) = \frac{2}{3}(x_0 + y_0)$.*

(*iii*) *If $\alpha := \frac{y_0}{y_0 - x_0}$ is the "zipping angle" of x_0 and y_0, and $r := -x_0/y_0$ their ratio, the Loewner energy of ξ is*

$$I(\xi) = \frac{1}{2}\int_0^\tau \dot{\xi}(t)^2 dt = -4\log(4\alpha(1-\alpha)) = -4\log\left(\frac{4r}{(1+r)^2}\right). \tag{5.30}$$

(*iv*) *As $\alpha \to 1/2$, ξ uses an asymptotic factor of $\pi^2/16$ of the energy of the Wang minimizer which welds x_0 to y_0.*

(*v*) *Let $\eta \in C^{3/2+\epsilon}([0,T))$ be any driver with $\dot{\eta}(0) \neq 0$, and $\tilde{\gamma}_t$ the curve generated by η on $[0,t]$, and $u(t) < 0 < v(t)$ the points welded by η to the base of $\tilde{\gamma}$ at time t. As $t \to 0$, $\tilde{\gamma}_t$ uses asymptotically $9/8$ of the energy of the EMW curve which welds $u(t)$ to $v(t)$.*

(*vi*) *There exists a single curve $\Gamma : (1, \infty) \to \mathbb{H}$ such that for each ratio $r \in (1, \infty)$, the segment $\Gamma((1, r))$ is an EMW curve which welds points with ratio r to its base. We can reflect Γ across the imaginary axis to get the same statement for ratios $r \in (0, 1)$.*

Remark 5.6. Parts (ii) and (v) show that the EMW family is distinct from the Wang minimizers.

Note that the formula in part (iii) is invariant under scaling $z \mapsto cz$, reflection across the imaginary axis $z \mapsto -\overline{z}$, and inversion $z \mapsto -1/z$. Does this shed any light on reversibility of the Loewner energy? Part (vi) shows that, up to scaling and reflection in the imaginary axis, the entire EMW family comes from a single fixed curve Γ. The exact identity of Γ is not currently known, and although it bears similarities with the curve driven by $4\sqrt{t}$, it is distinct. See Figure 5.3.

Fix $x_0 < 0 < y_0$ with $-x_0 \neq y_0$, and flow up with the corresponding EMW driver ξ for some time $t < \tau$. Part (v) shows that this initial "Loewner portion" of the curve is not itself an EMW curve, as we may take $\eta = \xi$. However, the remaining curve that ξ generates on $[t, \tau]$ must be: if not, then we could replace ξ with the corresponding EMW driver for $x_0(t)$ and $y_0(t)$ and lower the energy. Hence the symmetry of the EMW family is with respect to the "base," or what remains to flow up, rather than with respect to the "top," or the curve segment already flown up in $\mathbb{H}$. This is the opposite of what we saw with the Wang minimizers, where the "base" did not correspond to another Wang minimizer, but the "top" always did, and it is in this sense that we say the EMW family is dual to the Wang family. Compare Theorem 5.2(iv).

Proof. Let $\mathcal{W}$ be the family of all drivers η which weld x_0 to y_0 and satisfy $\eta(0) = 0$. First note all hitting times τ_η for x_0 and y_0 under $\eta \in \mathcal{W}$ are bounded, as any curve γ^η generated by $\eta \in \mathcal{W}$ has $\operatorname{diam}(\gamma^\eta) \asymp y_0 - x_0$ [17, top of p.74], and so there exists $R > 0$ such that $\gamma^\eta \subset B_R(0) \cap \mathbb{H}$ for all η, implying

$$\operatorname{hcap}(\gamma^\eta) \leq \operatorname{hcap}(B_R(0) \cap \mathbb{H}) = R^2 \operatorname{hcap}(B_1(0) \cap \mathbb{H}) = R^2.$$

So if $\{\eta_n\}$ is a sequence such that

$$I(\eta_n) \to \inf_{\eta \in \mathcal{W}} I(\eta) =: L, \tag{5.31}$$

then by flowing upwards, if necessary, with the constant driver $\eta_n(\tau)$ from the moment that x and y are welded together, we may assume that each η_n is defined on the same interval $[0,T]$. Hence $\{\eta_n\}$ is a bounded subset of $W^{1,2}([0,T])$, and so by (5.3) and the subsequent discussion, is precompact in $C([0,T])$. If $\eta_{n_k} \to \xi$ is any uniform sub-sequential limit, by the lower semicontinuity of the Loewner energy

$$L = \liminf_{n\to\infty} I(\eta_{n_k}) \geq I(\xi),$$

and so $I(\xi) = L$ if $\xi \in \mathcal{W}$. We just have to ensure that ξ welds x_0 to y_0, and this follows from Theorem 4.5, as uniform convergence of the drivers $\eta_{n_k} \to \xi$ implies locally uniform convergence of the associated weldings $\varphi_{n_k} \to \varphi$. Hence $y_0 = \varphi_{n_k}(x_0) \to \varphi(x_0)$. We conclude ξ is an energy minimizer.

Since $I(\xi) = L < \infty$, ξ is absolutely continuous. We first show (5.29) holds at all times t where $\dot{\xi}$ exists and where t is a Lebesgue point of $\dot{\xi}^2$. By Lemma 5.4, $r(t) := -x(t)/y(t) \to 1$, and since ξ minimizes energy, r must (strictly) monotonically approach 1. Indeed, if $r(t_0) = 1$ for some $t_0 < \tau$, then we must have $r(t) \equiv 1$ for all $t_0 \leq t \leq \tau$. If $1 \neq r(t_1) = r(t_2)$ for some $t_1 < t_2$, then ξ cannot be constant on $[t_1, t_2]$, because a ratio distinct from 1 changes under the constant driver. So energy would be unnecessarily wasted on $[t_1, t_2]$, and we conclude that the claimed monotonicity holds.

To be a minimizer, ξ must expel as little energy as possible to move the ratio to 1. For $I(t) := \frac{1}{2}\int_0^t \dot{\xi}(s)^2 ds$, we thus need to optimize dr/dI, in the sense of maximizing it when $r < 1$ and minimizing it when $r > 1$.

Suppose first that ξ is right-differentiable at $t = 0$ and that $t = 0$ is a Lebesgue point for $\dot{\xi}^2$. Then the energy expelled on a small interval $[0, \Delta t]$ is $\frac{1}{2}\dot{\xi}^2(0)\Delta t + o(\Delta t)$. Furthermore, r is right-differentiable at $t = 0$, and

$$\Delta r = \dot{r}(0)\Delta t + o(\Delta t) = \Big(\frac{2(y^2 - x^2)}{xy^3} + \frac{\dot{\xi}}{y^2}(y - x)\Big)\Delta t + o(\Delta t)$$

by the Loewener equation (2.17), where x, y and $\dot{\xi}$ are all evaluated at $t = 0$, and $\dot{\xi}$ is the

right derivative of ξ. We thus have

$$\frac{\Delta r}{\Delta I} \to \frac{4(y^2 - x^2)}{\dot{\xi}^2 x y^3} + \frac{2(y - x)}{\dot{\xi} y^2}$$

as $\Delta t \to 0$. This expression is optimized with respect to $\dot{\xi}$ when $\dot{\xi}(0)$ satisfies (5.29) at $t = 0$, in the sense of yielding a local max if $r(0) < 1$ and a local min if $r(0) > 1$. Thus any minimizer for which $\dot{\xi}(0)$ exists and where $t = 0$ is a Lebesgue point of $\dot{\xi}^2$ must satisfy (5.29) at $t = 0$.

More generally, let t_0 be a point of differentiability of ξ and a Lebesgue point of $\dot{\xi}^2$. Note that the remaining driver $\xi|_{[t_0,\tau]}$ must be an energy minimizer for welding $x(t_0)$ to $y(t_0)$, as noted above in Remark 5.6. By the previous paragraph, we see $\dot{\xi}(t_0)$ satisfies (5.29). Since ξ is differentiable at a.e. t and a.e. t is a Lebesgue point of the integrable function $\dot{\xi}^2$, we have (5.29) at a.e. t.

Plugging this formula into (2.17) yields that $\xi(t), x(t)$ and $y(t)$ are absolutely continuous a.e. solutions to the system of differential equations

$$\dot{\xi}(t) = -\frac{4}{x(t)} - \frac{4}{y(t)}, \qquad \dot{x}(t) = \frac{2}{x(t)} + \frac{4}{y(t)}, \qquad \dot{y}(t) = \frac{4}{x(t)} + \frac{2}{y(t)} \tag{5.32}$$

with $\xi(0) = x(0) - x_0 = y(0) - y_0 = 0$, $0 \leq t < \tau$. Since each function is absolutely continuous, replacing the derivatives with these continuous expressions for all t does not change the values of the functions, and we see that each function is actually C^1. Then each of the right-hand sides in (5.32) is C^1, and so ξ, x and y are at least C^2. Continuing to bootstrap yields that each of these is C^∞ on $[0, \tau)$ (where we use one-sided derivatives at $t = 0$).

Note also that classical solutions to (5.32) are unique: by scale invariance we may assume $\min\{-x_0, y_0\} = 1$, and for small times $0 \leq t \leq t_0$, $|x(t)|$ and $|y(t)|$ are therefore both bounded below since ξ is $\sqrt{L}$-Hölder -1/2 continuous. Hence the map $f(t, \xi, x, y) = (-4(x^{-1} + y^{-1}), 2x^{-1} + 4y^{-1}, 4x^{-1} + 2y^{-1})$ is Lipschitz in (ξ, x, y) on $[0, t_0]$, giving uniqueness. Note that uniqueness also gives that if $r(0) \neq 1$, $r(t) \neq 1$ for all $t < \tau$, and so (5.29) also shows that ξ is strictly monotone.

For the formulas in (ii), observe from (5.32) that

$$\frac{d}{dt}\Big((y(t)-x(t))^2-2x(t)y(t)\Big)=-24,$$

and so integrating from 0 to $\tau-\epsilon$ and sending $\epsilon\to 0$ yields

$$0-(y_0-x_0)^2+2x_0y_0=-24\tau,$$

which yields the claimed expression. Also, if $A(t)=(x(t)+y(t))/2$, we find $\dot{A}(t)=-\frac{3}{4}\dot{\xi}(t)$ and hence

$$0-\frac{1}{2}(x_0+y_0)=-\frac{3}{4}\xi(\tau)-0,$$

as claimed.

For (iii), we see how energy is expelled as r approaches 1, and note we have the ODE

$$\frac{dI}{dr}=\frac{4y}{x}\cdot\frac{x+y}{x-y}=\frac{4}{r}\cdot\frac{1-r}{1+r}=\frac{4}{r}-\frac{8}{r+1},$$

and therefore

$$I(r(t))-0=4\log\Big(\frac{r(t)}{r}\Big)-8\log\Big(\frac{r(t)+1}{r+1}\Big).$$

Since $r(t)\to 1$, sending $t\to\tau^-$ yields (5.30).

For (iv), by explicit computations in [26], we have that the welding φ_θ of the Wang minimizer through $e^{i\theta}$ satisfies $\varphi_\theta:[x_\theta,0]\to[0,y_\theta]$, where

$$x_\theta=-\sqrt{\frac{\sin^3(\theta)}{\sin(\theta)-\theta\cos(\theta)}}\qquad\text{and}\qquad y_\theta=\sqrt{\frac{\sin^3(\theta)}{\sin(\theta)-\theta\cos(\theta)+\pi\cos(\theta)}}.$$

Using this, we can expand the angle $\alpha(\theta)=\frac{y_\theta}{y_\theta-x_\theta}$ in a series around $\theta=\pi/2$, which we can then locally invert to find

$$\theta(\alpha)=\frac{\pi}{2}+\frac{8}{\pi}\Big(\alpha-\frac{1}{2}\Big)+O\Big(\alpha-\frac{1}{2}\Big)^3$$

as $\alpha\to 1/2$. Plugging this into the energy formula $-8\log(\sin(\theta))$ yields that the energy $I_W(\alpha)$ for the Wang curve satisfies

$$I_W(\alpha)=\frac{256}{\pi^2}\Big(\alpha-\frac{1}{2}\Big)^2+O\Big(\alpha-\frac{1}{2}\Big)^4. \tag{5.33}$$

On the other hand,

$$-4\log(4\alpha(1-\alpha)) = 16\Big(\alpha - \frac{1}{2}\Big)^2 + O\Big(\alpha - \frac{1}{2}\Big)^4 \tag{5.34}$$

as $\alpha \to 1/2$, which gives the claimed ratio.

For (v), we use the expansions in Theorem 3.5 to see that the angle $\alpha(t) := \frac{v(t)}{v(t)-u(t)}$ is

$$\alpha(t) = \frac{1}{2} + \frac{1}{6}\dot{\eta}(0)\sqrt{t} + O(t^{1+\epsilon}).$$

Hence from (5.34), the minimal energy to weld $u(t)$ to $v(t)$ is

$$\frac{4}{9}\dot{\xi}(0)^2 t + O(t^{3/2+\epsilon}),$$

while the actual energy used is $\frac{1}{2}\dot{\xi}(0)^2 t + o(t)$, yielding the claimed ratio.

Lastly, for (vi), we note that if we have two ratios $1 < r_1 < r_2$ and we flow up with an energy-minimizing driver ξ_2 for r_2 (defined uniquely up to scaling), the ratio $-x(t)/y(t)$ of its welding endpoints will monotonically approach 1 and hence be r_1 at some time t_1. At this point, as argued in the paragraph preceding the proof, the remaining curve γ_{r_1} generated by ξ_2 on $[t_1, \tau_2]$ is the energy-minimizing curve for r_1 (again, defined uniquely up to scaling). Thus the curve γ_{r_2} for r_2 contains γ_{r_1} as a subcurve, and we similarly form a simple curve $\Gamma := \bigcup_{r>1} \gamma_r$ where γ_r is a curve generated by an EMW driver ξ which welding endpoints with ratio r, and where $\gamma_{r_1} \subset \gamma_{r_2}$ whenever $r_1 < r_2$. This Γ has the desired property. If $r < 1$, we reflect Γ over the imaginary axis. □

Figure 5.3 has several numerical simulations of both ξ and the resulting curves γ for different initial angles α. An interesting question is the nature of the limiting curve as $\alpha \to 1^-$ (or, equivalently, $\alpha \to 0^+$); that is, the identity of Γ in part (vi) above. The numerical simulations suggest that the "initial portion" of the driver converges to $4\sqrt{t}$, suggesting some connection to the curve created by $\lambda(t) = 4\sqrt{1-t} - 4$. The simulations also make it clear, however, that Γ is not identical to this curve. Informally speaking, the curve driven by $\lambda(t) = 4\sqrt{1-t} - 4$ moves horizontally too quickly and expends too much

energy in the process; the EMW curves expel less energy by moving higher in $\mathbb{H}$ to reach the same horizontal displacement. However, it may be the case that Γ also intersects $\mathbb{R}$ tangentially. Is Γ a variety, or the zero-set of a polynomial equation in x and y? What is Γ's driving function?

5.5 The circular arc family

Zipping up with segments of hyperbolic geodesics in $\mathbb{H}$, or circular arcs orthogonal to $\mathbb{R}$, is another nice option for the zipper algorithm. It was this curve family, in fact, that yielded the main convergence result thus far for the zipper: Marshall and Rohde proved the "opposite direction" of the algorithm converges when using the circular arc family, as the hyperbolic geometry yields control on the boundary of the constructed region via Jørgensen's Lemma, given mild assumptions on the input data [28]. The circular arc family is our nicest curve family, in the sense of giving the best approximation to smooth curves. Surprisingly, it is also a factor of 9/8 away from being an energy minimizer for both welding two given points $x < 0 < y$ together, and for reaching a given point $e^{i\theta} \in \mathbb{H}$; see parts (iv) and (v) of the following lemma.

Lemma 5.7. *For any $x < 0 < y$ there exists a unique driver $\xi : [0, \tau] \to \mathbb{R}$ with $\xi(0) = 0$ which welds x to y and generates a circular arc segment orthogonal to $\mathbb{R}$. Furthermore,*

(i) $\xi \in C^\infty([0, \tau])$ and is explicitly

$$\xi(t) = \frac{3}{4}(x+y) - \frac{3}{4}\frac{1}{x+y}\Big((y-x)^2 - \sqrt{16x^2y^2 + 32t(x+y)^2}\Big). \tag{5.35}$$

(ii) $\tau = \frac{1}{32}(x^2 - 6xy + y^2)$ and $\xi(\tau) = \frac{3}{4}(x+y)$.

(iii) If $\alpha := \frac{y_0}{y_0 - x_0}$ is the "zipping angle" of x_0 and y_0, and $r := -x_0/y_0$ their ratio, the Loewner energy of ξ is

$$I(\xi) = \frac{1}{2}\int_0^\tau \dot{\xi}(t)^2 dt = -\frac{9}{2}\log(4\alpha(1-\alpha)) = -\frac{9}{2}\log\Big(\frac{4r}{(1+r)^2}\Big). \tag{5.36}$$

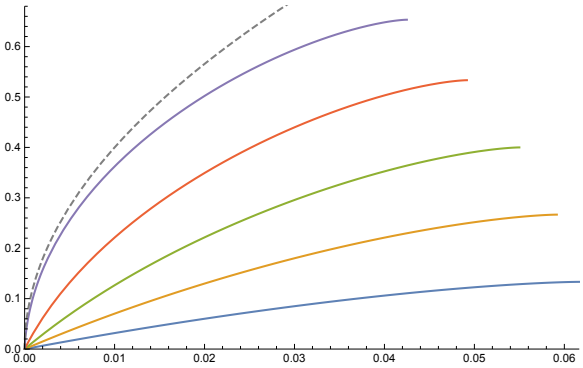

(a) The EMW driving functions for initial angles $\alpha = \frac{y_0}{y_0 - x_0} = \frac{k}{10}$, $k = 6, 7, 8, 9, 9.9$, with normalized welding interval $y_0 - x_0 = 1$. Higher k corresponds to a higher graph, and the dashed line is $y = 4\sqrt{x}$.

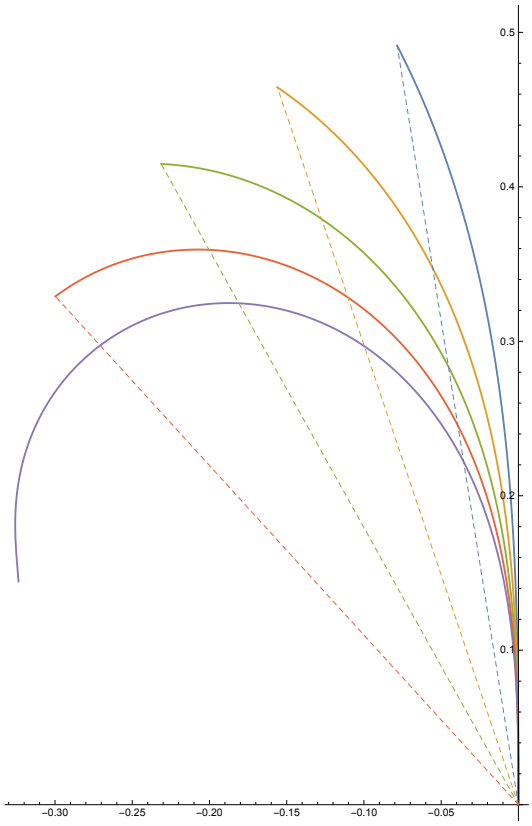

(b) The corresponding curves γ in $\mathbb{H}$. The dashed lines illustrate Theorem 5.5(vi): all of these curves, up to scaling, are initial portions of one fixed curve (in this case the purple curve for $\alpha = 0.99$).

Figure 5.3: Numerical simulations of the EMW drivers and their resulting curves.

(*iv*) *If $y \neq -x$, ξ uses exactly 9/8th the energy of the EMW curve which welds $x < 0 < y$.*

(*v*) *If $\theta \neq \pi/2$, the orthogonal circular arc to $z_0 := re^{i\theta}$ uses exactly 9/8th of the energy of the Wang minimizer to z_0.*

Note that when $\alpha = \frac{1}{2}$ or $\theta = \frac{\pi}{2}$, the circular arc is a segment of the imaginary axis and hence expends zero energy, thus coinciding with both the EMW and Wang curves.

Parts (*iv*) and (*v*) should be compared with Theorem 5.5(*v*) and Theorem 5.2(*iv*), respectively. In the latter two, we saw that sufficiently-smooth curves *asymptotically* use 9/8 of the energy of the minimizing families. Parts (*iv*) and (*v*) state that the 9/8 ratio *always* holds for the circular arc family.

Proof. For (*i*), we start with the downwards driving function λ_1 for the orthogonal circular arc from 0 to $x = 1$. This has already been computed by Lind [23, p.5] as

$$\lambda_1(t) = \frac{3}{2}(1 - \sqrt{1 - 8t}), \qquad 0 \leq t \leq \frac{1}{8}. \tag{5.37}$$

It is similarly possible ("although unpleasant," to quote Lind) to compute that the welding for the portion of the curve up to time $t \in (0, 1/8)$ is explicitly $\varphi_t : [x_t, 0] \to [0, y_t]$ for

$$\varphi_t(x) = -\frac{\sqrt{1 - 8t}\, x}{\sqrt{1 - 8t} - 2x}$$

with

$$x_t = -1 + \sqrt{1 - 8t} - \sqrt{1 - \sqrt{1 - 8t}} \quad \text{and} \quad y_t = -1 + \sqrt{1 - 8t} + \sqrt{1 - \sqrt{1 - 8t}}. \tag{5.38}$$

By inspection, the welding endpoint ratio $\alpha_t = \frac{y_t}{y_t - x_t}$ is monotonically decreasing from 1/2 to 0 as t ranges over $(0, 1/8)$, which shows there is a unique circular arc curve which welds a given ratio $\alpha = \frac{y}{y-x}$ (if $\alpha \in (1/2, 1)$, we use the circle reflected over the imaginary axis).

Suppose $y < -x$. We can then re-scale (5.37) to obtain the downwards driver λ for welding x to y. From (5.38) we can compute $\alpha_t = \frac{y_t}{y_t - x_t}$ and invert to find the time $t(\alpha)$ needed to obtain a given ratio α on the circular arc is

$$t(\alpha) = \frac{1}{8} - 2\alpha^2(1 - \alpha)^2 = \frac{1}{8} - \frac{2x^2y^2}{(y - x)^4}, \tag{5.39}$$

as we want $\alpha = \frac{y}{y-x}$. Our scaling factor is then $r = \frac{y-x}{y_t - x_t}$, and hence our desired driver is $\lambda(t) = r\lambda_1(t/r^2)$ for $0 \le t \le r^2 t(\alpha)$. Doing the computations yields

$$\lambda(t) = -\frac{3}{4}\frac{1}{x+y}\Big((y-x)^2 - \sqrt{(y-x)^4 - 32t(x+y)^2}\Big), \qquad r^2 t(\alpha) = \frac{1}{32}(x^2 - 6xy + y^2). \tag{5.40}$$

Noting that the desired ξ is thus $\xi(t) = \lambda(\tau - t) - \lambda(\tau)$ for $\tau = r^2 t(\alpha)$, we obtain the formula in (i).

If $-x_0 < y_0$, we just need to reflect the circular arc with ratio $1 - \alpha_0$ over the imaginary axis and take its driver; this is accomplished through replacing x and y with $-y_0$ and $-x_0$, respectively, and then taking $-\xi$ for our ξ in (5.35) for $-y_0$ and $-x_0$. This gives the same formula.

We have already shown the capacity time formula for τ in (5.40). Evaluating $\lambda(\tau)$ in (5.40) yields $\lambda(\tau) = -\frac{3}{4}(x+y)$, which gives the claimed formula for $\xi(\tau)$.

For (iii), by scaling invariance it suffices to work with λ_1 on $0 \le t \le t(\alpha)$, and we compute

$$\frac{1}{2}\int_0^{t(\alpha)} \dot{\lambda}_1^2(t)dt = -\frac{9}{4}\log(1 - 8t(\alpha)) = -\frac{9}{2}\log(4\alpha(1-\alpha)) \tag{5.41}$$

by (5.39).

Part (iv) immediately follows, then, by (5.30).

For (v) we can explicitly compute ("although unpleasant") that the parametrization of the circular arc from 0 to 1 is

$$\gamma_1(t) = 1 - \sqrt{1-8t} + i\sqrt[4]{1-8t}\sqrt{1-\sqrt{1-8t}}, \qquad 0 \le t \le \frac{1}{8},$$

and so the angle at time t is

$$\theta(t) = \arctan\Big(\frac{\sqrt[4]{1-8t}\sqrt{1-\sqrt{1-8t}}}{1-\sqrt{1-8t}}\Big) \quad \Rightarrow \quad t(\theta) = \frac{1}{8}\big(2\cos^2(\theta)\sin^2(\theta) + \cos^4(\theta)\big).$$

We then see from (5.41) that the energy expelled to attain an angle θ is

$$-\frac{9}{4}\log\big((1-\cos^2(\theta))^2\big) = -9\log(\sin(\theta)),$$

in contrast to (5.14). □

Curve family	$\xi(\tau)$	τ
Slow driver*	$\frac{1}{2}(x+y)$	$\frac{1}{16}(x^2-2xy+y^2)$
EMW	$\frac{2}{3}(x+y)$	$\frac{1}{24}(x^2-4xy+y^2)$
Circular arc	$\frac{3}{4}(x+y)$	$\frac{1}{32}(x^2-6xy+y^2)$
Wang minimizer	$\frac{8}{3\pi}(x+y)+O\big(\frac{(x+y)^3}{(y-x)^2}\big)$	$\frac{32-3\pi^2}{24\pi^2}\big(x^2-\frac{12\pi^2-64}{32-3\pi^2}xy+y^2\big)+O\left(\frac{(x+y)^4}{(y-x)^2}\right)$
Straight slit	$x+y$	$-\frac{1}{4}xy$

Table 5.1: Terminal values of the driving function and capacity times for welding $x<0<y$ under our various curve families. Compare Figure 5.1. Note that the slow zipper does not represent an actual curve family because its driving function ξ_s is not continuous, and so it does not generate simple curves in $\mathbb{H}$. However, we can closely approximate it with a continuous driver generating a simple curve. See §5.7.2.

5.6 The straight-slit family

The straight-slit family welds $x<0<y$ to the base of a straight line segment. The angle of the slit from the positive reals is $\pi\alpha$, where

$$\alpha := \frac{y}{y-x},$$

and this is the reason we informally speak of this ratio as the welding "angle" (this turns out to be a useful concept and is related to the Loewner energy; see §8 below).

The straight-slit family is the poorest-behaved family among our zipper options (although it is still a "tractable family" in the sense of definition 5.1). If $-x \neq y$, the Loewner energy of the zip is infinite, and the driving function is not smooth at one of the endpoints.

We proceed to derive properties of this family, akin to what we saw for the previous families in Theorems 5.2, 5.5 and Lemma 5.7. Nothing here rises even to the level of lemma;

Curve family	*Energy to weld* $x < 0 < y$ *with ratio* $\alpha = \frac{y}{y-x}$
Slow zipper	∞
EMW	$-4\log(4\alpha(1-\alpha))$
Circular arc	$-\frac{9}{2}\log(4\alpha(1-\alpha))$
Wang minimizer	$-\frac{64}{\pi^2}\log(4\alpha(1-\alpha)) + O\big(\alpha - \frac{1}{2}\big)^4$
Straight slit	∞

Table 5.2: The energy used by our curve families to weld two given points together. See Theorem 5.5 and Lemma 5.7 for the EMW and circular arc formulas, respectively. The formula for the Wang minimizers is from Theorem 5.5(iv) and (5.33), and holds as $\alpha \to 1/2$. The straight slit uses infinite energy whenever $\alpha \neq 1/2$. When $\alpha = 1/2$, all the families coincide and use zero energy. Note $64/\pi^2 \approx 6.48$.

we simply use known formulas to justify the expressions in Table 5.1.

Fix $x < 0 < y$, and set

$$\delta := \frac{1}{2} - \alpha = -\frac{1}{2} \cdot \frac{x+y}{y-x}.$$

A conformal map for welding $x < 0 < y$ to the base of a straight slit, sending zero to the tip of the slit, is

$$\begin{aligned} F(z) &= \Big(z - (y-x)\Big(\frac{1}{2} - \delta\Big)\Big)^{\frac{1}{2}-\delta}\Big(z + (y-x)\Big(\frac{1}{2} + \delta\Big)\Big)^{\frac{1}{2}+\delta} \\ &= (z-y)^{\frac{y}{y-x}}(z-x)^{\frac{-x}{y-x}} \\ &= z - (x+y) + \frac{xy}{2}\frac{1}{z} + O\Big(\frac{1}{z^2}\Big), \qquad z \to \infty. \end{aligned}$$

See [28, "The Slit Algorithm"] for a derivation. It follows that the hydrodynamically-normalized centered mapping down function for the slit is

$$G(z) = F^{-1}(z) = z + (x+y) - \frac{xy}{2}\frac{1}{z} + O\Big(\frac{1}{z^2}\Big), \qquad z \to \infty,$$

from which we can read off that $\tau = \frac{-xy}{4}$ and $\lambda(\tau) = x + y$. The driving function is

$$\lambda(t) = \frac{4\delta}{\sqrt{(\frac{1}{2} - \delta)(\frac{1}{2} + \delta)}}\sqrt{t} = -2\frac{x+y}{\sqrt{-xy}}\sqrt{t}$$

[17], or, in terms of the upwards flow, $\xi(t) = \lambda(\tau - t) - \lambda(\tau)$,

$$\xi(t) = (x+y)\Big(1 - \sqrt{1 + \frac{4t}{xy}}\Big), \qquad 0 \le t \le -\frac{xy}{4}.$$

5.7 The slow and fast drivers

One commonality of the preceding four curve families is that their driving functions are monotonic: given any $x < 0 < y$, any of the drivers is strictly increasing if $-x < y$ and strictly decreasing if $y < -x$. A naïve idea for proving zipper convergence is then the following: show that the algorithm converges for the worst-possible monotonic cases, the slowest and the fastest, and then conclude that it therefore works for all the others. Unfortunately this approach fails, but for a noteworthy reason that appears to be a new observation: it appears not all families with monotonic drivers produce a convergent algorithm. We provide numerical evidence along these lines in §5.7.4, but we do not give any proofs of divergence; we hope to further investigate this phenomenon in future work.

5.7.1 Overview

In this section we define the *slow driver* and *fast driver*. These discontinuous driving functions represent limiting cases of very slow and very fast ways to weld $x < 0 < y$ with a continuous monotonic driver ξ. The slow driver is actually the *universally* slowest way, even if non-monotonic continuous drivers are allowed, as we show in Lemma 5.8. In contrast, Lemma 5.9 says that there is no fastest way to weld $x < 0 < y$ among *all* continuous drivers. Together the two lemmas give sharp upper and lower bounds on the welding time for $x < 0 < y$ under a monotone continuous driver; see Corollary 5.10.

We close with a numerical example where we run the slow and fast drivers on actual welding data, as in the zipper algorithm. Neither driver creates a simple curve, however,

owing to their discontinuities, and so this is not a zipper algorithm in the standard sense. The results, nonetheless, are surprising: the slow zipper generates a driving function which rapidly converges to the true driver, while the fast zipper's constructed driving function diverges. We hope to investigate this phenomenon further in future work.

5.7.2 The slow driver

To weld $x < 0 < y$, the slow driver ξ_s starts with $\xi_s(0) = 0$ and immediately jumps to $\frac{x+y}{2}$, where it waits (patiently) for x and y to flow to itself.

Lemma 5.8. *Let ξ_s be the "slow driving function" given by*

$$\xi_s(t) := \begin{cases} 0 & t = 0 \\ \frac{x_1+y_1}{2} & 0 < t \leq \frac{(x_1-y_1)^2}{16}. \end{cases} \tag{5.42}$$

Then the upward flow generated by ξ_s welds x_1 to y_1 at time $\tau_s := (x_1 - y_1)^2/16$. If ξ is any continuous driving function with $\xi(0) = 0$ which welds $x_1 < 0 < y_1$ at time τ, then

$$\tau \leq \frac{(x_1 - y_1)^2}{16}, \tag{5.43}$$

with equality possible iff $y_1 = -x_1$. Furthermore, for any $\epsilon > 0$, there exists a driver ξ_ϵ that welds x_1 to y_1 at time τ_ϵ, where

$$\frac{(x_1 - y_1)^2}{16} - \epsilon < \tau_\epsilon. \tag{5.44}$$

Put another way, the lemma says

$$\sup\{\, \tau \;:\; \exists \text{ cont. driver } \xi \text{ such that } \xi(0) = 0, \xi \text{ welds } x_1 \text{ to } y_1 \text{ at time } \tau \,\} = \frac{(x_1 - y_1)^2}{16},$$

and that this supremum is attained if and only if $y_1 = -x_1$. We also see from (5.42) that the curve segment constructed by ξ_s is a vertical line segment with base at $(x_1 + y_1)/2$ and tip at $\frac{|y_1-x_1|}{2}i$.

Proof. First note that the hitting time under ξ_s is as claimed: the explicit solution to the Loewner equation

$$\dot{h}_t(z) = \frac{-2}{h_t(z) - (x_1 + y_1)/2}, \quad t > 0, \qquad h_0(z) = z \tag{5.45}$$

is $h_t(z) = \sqrt{(z - \frac{x_1+y_1}{2})^2 - 4t} + \frac{x_1+y_1}{2}$ for $z \in \mathbb{H} \cup \mathbb{R}_{\geq 0}$ and $h_t(x) = -\sqrt{(x - \frac{x_1+y_1}{2})^2 - 4t} + \frac{x_1+y_1}{2}$ for $x < 0$. Under this flow, both x_1 and y_1 hit the singularity $\frac{x_1+y_1}{2}$ at the same time $\tau_s = (x_1 - y_1)^2/16$.

Now suppose ξ is a driver starting from 0 that welds x_1 to y_1 at time τ. Let $x(t), y(t)$ be the flow of x_1, y_1 under ξ, and $x_s(t), y_s(t)$ the flow of x_1, y_1 under ξ_s. Let $\ell(t) := y(t) - x(t)$ and $\ell_s(t) := y_s(t) - x_s(t)$ be the interval lengths between these points. Note that the hitting times τ, τ_s are the first times that ℓ and ℓ_s vanish, respectively.

The (non-centered) Loewner equation (2.12) gives

$$\dot{\ell}(t) = \frac{-2\ell(t)}{(y(t) - \xi(t))(\xi(t) - x(t))} \leq \frac{-8}{\ell(t)}, \tag{5.46}$$

$0 \leq t < \tau$, with equality if and only if $\xi(t) = \frac{x(t)+y(t)}{2}$, as follows from maximizing $z \mapsto (y(t) - z)(z - x(t))$. We also have

$$\dot{\ell}_s(t) = \frac{-8}{\ell_s(t)} \tag{5.47}$$

for $0 < t < (x_1 - y_1)^2/16$.

Suppose first that $y_1 \neq -x_1$. By continuity, there is a small time ϵ where $|\xi(t)| < |(x(t) + y(t)|/2$ for $0 < t < \epsilon$, and so by (5.46) and (5.47) we have

$$0 < \ell(\epsilon) \leq \ell_s(\epsilon) - \delta < \ell_s(\epsilon)$$

for some $\delta = \delta(\epsilon, \xi) > 0$. It follows that there is some $\delta' > 0$ such that

$$\dot{\ell}(t) \leq \dot{\ell}_s(t) - \delta' < \dot{\ell}_s(t) < 0$$

for all subsequent time t (until the hitting times). In words, ℓ is monotonically decreasing faster than ℓ_s. Therefore ℓ reaches 0 first, which says $\tau < \tau_s$, and hence gives strict inequality in (5.43).

Suppose that $y_1 = -x_1$. We attain the bound $(x_1 - y_1)^2/16 = y_1^2/4$ in (5.43) with the driver $\xi(t) \equiv 0$. If $\xi(t) \not\equiv 0$, once ξ leaves 0 we can apply essentially the same argument as above: if $\xi(t) \neq 0$, the interval length $\ell(t)$ begins contracting faster compared to $\ell_s(t)$, and then continues that way for all subsequent time by (5.46) and (5.47). Hence $\tau < \tau_s$ in this case too. This proves (5.43) and the characterization of when equality is possible.

For (5.44), take the driver $\xi \equiv 0$ when $y_1 = -x_1$. If $y_1 \neq -x_1$, start ξ by moving extremely fast, say in some small time δ, to the average $(x_1(\delta) + y_1(\delta))/2$, and then remain at that point. From the smoothness of $\ell(t) = (y(t) - x(t))/2$ given by (5.46),

$$\ell_s(\delta) - \epsilon' \leq \ell(\delta) < \ell_s(\delta) \tag{5.48}$$

if δ is small enough. Subsequently, ℓ satisfies $\dot{\ell}(t) = -8/\ell(t)$, which one may solve explicitly to find that the hitting time τ for ξ is $\tau = \ell(\delta)^2/16 + \delta$. The hitting time for ξ_s is similarly $\tau_s = \ell_s(\delta)^2/16 + \delta$. Hence, for small enough ϵ' in (5.48),

$$\tau_s - \epsilon \leq \tau,$$

giving (5.44). □

5.7.3 The fast driver

While the slow driver immediately jumps to the average $\frac{x+y}{2}$, the fast driver waits at the origin until the nearer of x and y hits, and then immediately jumps to "capture" the other point.

Lemma 5.9. *Fix $x_1 < 0 < y_1$ and let ξ_f be the "fast driving function" given by*

$$\xi_f(t) := \begin{cases} 0 & 0 \leq t < \frac{y_1^2}{4} \\ -\sqrt{x_1^2 - y_1^2} & t = \frac{y_1^2}{4} \end{cases} \tag{5.49}$$

if $y_1 \leq -x_1$ and

$$\xi_f(t) := \begin{cases} 0 & 0 \leq t < \frac{x_1^2}{4} \\ \sqrt{y_1^2 - x_1^2} & t = \frac{x_1^2}{4} \end{cases}$$

if $-x_1 < y_1$. *If* ξ *is any continuous monotonic driving function with* $\xi(0) = 0$ *which welds* $x_1 < 0 < y_1$ *at time* τ, *then*

$$\frac{\min\{x_1^2, y_1^2\}}{4} \leq \tau$$

with equality iff $-x_1 = y_1$. *Furthermore, for any* $\epsilon > 0$, *there exist continuous drivers* ξ_1 *and* ξ_2 *that weld* x_1 *to* y_1 *at times* τ_1 *and* τ_2, *respectively, where* ξ_1 *is monotonic and*

$$\tau_1 - \epsilon < \frac{\min\{x_1^2, y_1^2\}}{4},$$

and where $\tau_2 < \epsilon$.

Put another way, the lemma says

$$\inf\{\,\tau \;:\; \exists \text{ cont. monotonic driver } \xi \text{ such that } \xi(0) = 0,\ \xi \text{ welds } x_1 \text{ to } y_1 \text{ at time } \tau\,\} = \frac{\min\{x_1^2, y_1^2\}}{4},$$

and that this infimum is attained if and only if $y_1 = -x_1$, and that furthermore

$$\inf\{\,\tau \;:\; \exists \text{ cont. driver } \xi \text{ such that } \xi(0) = 0,\ \xi \text{ welds } x_1 \text{ to } y_1 \text{ at time } \tau\,\} = 0.$$

We also see from (5.49) that the curve segment constructed by ξ_f is a vertical line segment with base at 0 and tip at $\min\{|x_1|, y_1\}i$.

Proof. We prove $0 < y < -x$; the argument in the other case is similar. Note that under ξ_f, y_1 moves according to $\dot{y}_1(t) = -\frac{2}{y_1(t)}$, whose explicit solution is $y_1(t) = \sqrt{y_1(0)^2 - 4t}$. This gives the claimed hitting time $\tau_f = y_1(0)^2/4$, and solving the same ODE for x_1 yields $x_1(\tau_f) = -\sqrt{x_1(0)^2 - y_1(0)^2}$, as claimed.

Now let ξ be any monotonic driver welding x_1 to y_1 at time τ. To accomplish this welding, ξ must move monotonically towards the average $A(t) = \frac{x_1(t)+y_1(t)}{2}$, where $x_1(t)$ and $y_1(t)$ are the images of x_1 and y_1 under the *uncentered* upwards flow generated by ξ. Hence ξ is non-increasing, and so

$$\dot{y}_1(t) = \frac{-2}{y_1(t) - \xi(t)} \geq -\frac{2}{y_1(t)} = \dot{y}_{1,f}(t),$$

the speed of y_1 under the fast zipper. Thus y_1 has further to travel and moves slower (less negatively) under ξ compared to ξ_f, yielding $\tau \geq \frac{y_1^2}{4}$. Equality cannot occur, however, because ξ is continuous. Drivers ξ do exist, though, which come arbitrarily close: the idea is to wait at the origin for a time τ_- very close to $y_1^2/4$. Then $y_1(\tau_-)$ is very close to the origin with large negative derivative, and so by moving very fast to capture x_1 we can weld both points at time $y_1^2/4 + \epsilon/2$.

If we relax the monotonicity requirement and admit any driver ξ, then our time may be arbitrarily close to 0: start by moving in a very small time δ to very close to y_1. Then $\dot{y_1}(\delta)$ is very large negatively, and so both ξ and y_1 can proceed to move very rapidly towards x_1. Stop ξ when it reaches the average $\frac{x_1(t)+y_1(t)}{2}$, and let both points weld. Moving sufficiently fast yields $\tau < \epsilon$. □

Lemmas 5.8 and 5.9 combine to yield the following.

Corollary 5.10. *If ξ is a continuous, monotonic driver welding $x_1 < 0 < y_1$ at time τ, then*

$$\frac{\min\{x_1^2, y_1^2\}}{4} \leq \tau \leq \frac{(x_1 - y_1)^2}{16}.$$

Both inequalities are strict and sharp if $-x_1 \neq y_1$, and both become equality if $-x_1 = y_1$.

5.7.4 A numerical example

For an example, we run a slow driver and fast driver "zipper algorithm" on welding data from the orthogonal circular arc segment illustrated in Figure 5.4. That is, we start with a discretization of welding in Figure 5.4b, and flow up step-by-step with the uncentered Loewner flow generated by the slow driver ξ_s and the fast driver ξ_f. In either case the idea is simple. For ξ_s, we always begin a new "zip" by jumping to the average of the next two data points and waiting there until they both weld together. For ξ_f, we start by waiting for the nearest of the next two data points to hit the driver, and then move immediately to the position of the other data point. The scare quotes in "zipper algorithm" and "zip" reflect

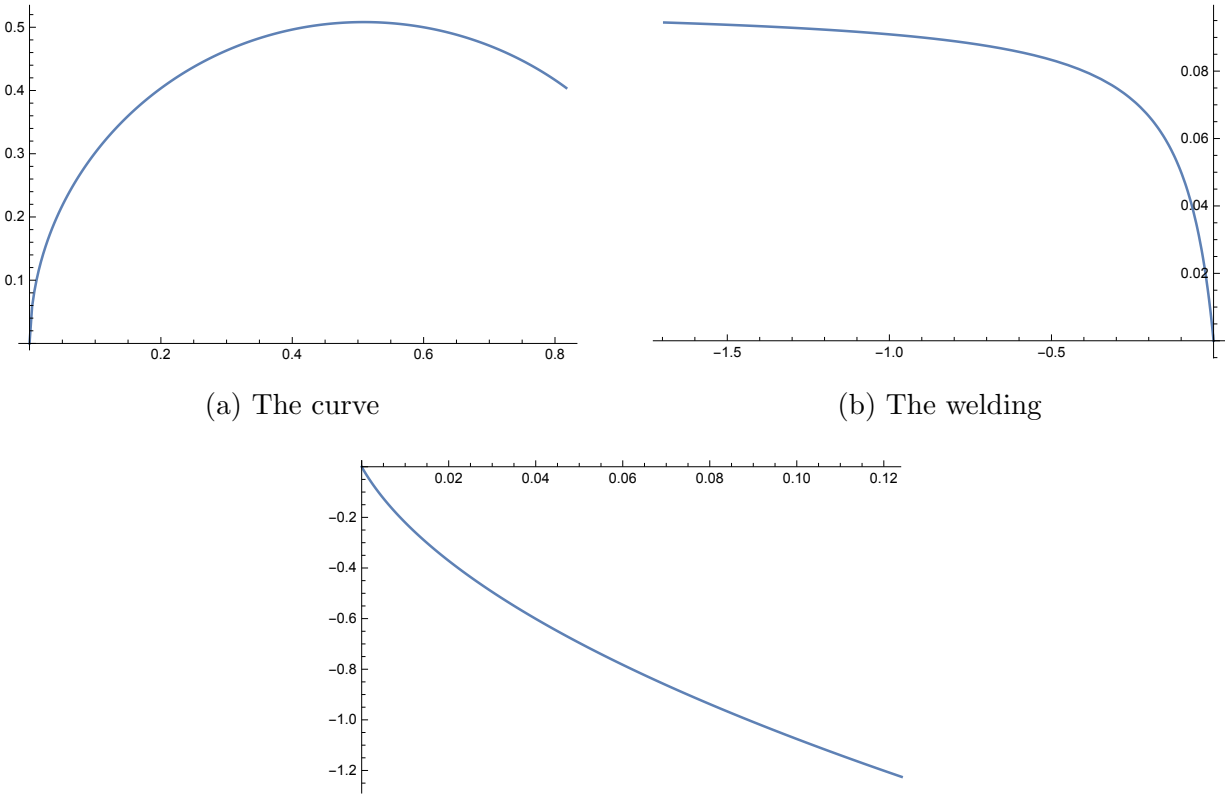

(a) The curve

(b) The welding

(c) The reversed driver $\xi(t) = \lambda(\tau - t) - \lambda(\tau)$

Figure 5.4: The true curve, welding and driving function for a numerical test for "zipper algorithms" generated by the slow and fast drivers.

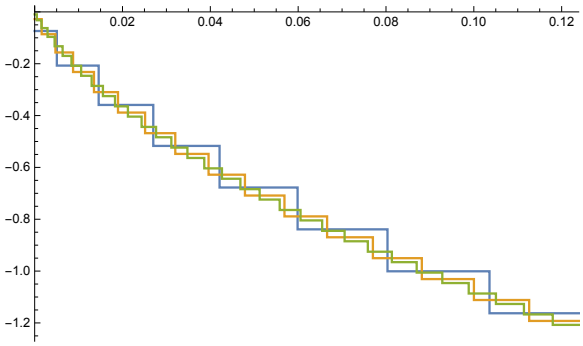

(a) Driving functions constructed by the slow driver "zipper"

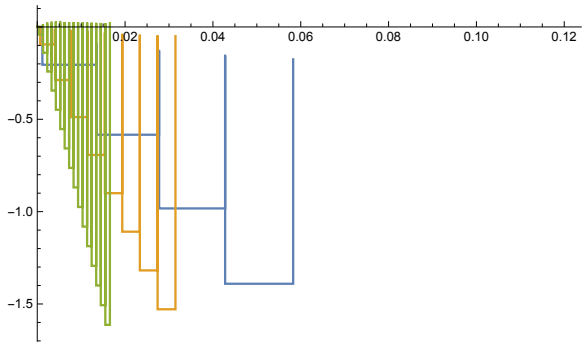

(b) Driving functions constructed by the fast driver "zipper"

Figure 5.5: Running the slow and fast driver "zipper algorithms" on partitions of the welding in Figure 5.4b consisting of 8, 16 and 32 data points.

the fact that these drivers do not produce simple curves, as they are discontinuous, and so do not yield a zipper algorithm in the standard sense of the term.

For our numerical experiment we consider the behavior of the constructed driving functions (not directly the constructed curves themselves). In Figure 5.5 we see the constructed drivers for partitioning the welding interval $[-a, 0]$ into 8, 16 and 32 equal segments, with corresponding plots in blue, orange and green, respectively. We plot the (horizontal) t-axis with the same range of values as for the true driver in Figure 5.4c. It is apparent that the slow driver quickly gives a good approximation to the true driver ξ, while this is far from the case for the fast driver, which uses much less time and has much larger jump discontinuities (the vertical lines). As we add in finer meshes with 64 and 128 data points in Figure 5.6, we see the same pattern continue: the slow driver yields even better approximations to the true driver (cf. Figure 5.7), while the fast driver has slightly larger jumps and takes even less time. This suggests that the entire (not-pictured) curve constructed by the fast driver stays very close to the real line, as its capacity time is very small, and that in the limit, the fast driver "zipper" diverges. We note that since this is not an actual zipper algorithm that

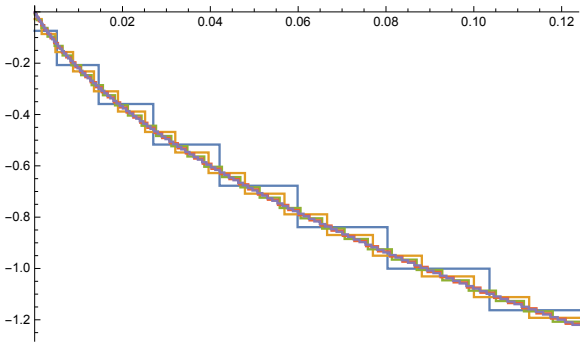

(a) Driving functions constructed by the slow driver "zipper"

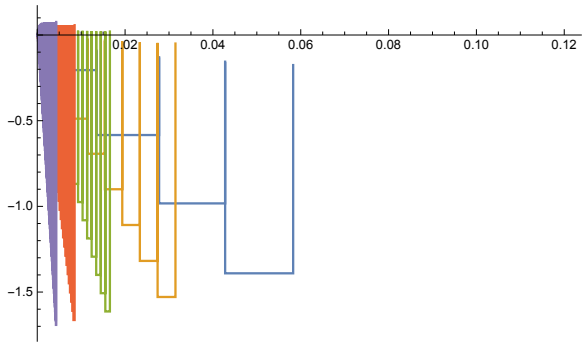

(b) Driving functions constructed by the fast driver "zipper"

Figure 5.6: Adding in two finer meshes.

welds the data with a simple curve, this is not a (numerical) example of zipper divergence. However, it may be possible to closely approximate the fast-driver "zipper" with an actual zipper which produces simple curves and also diverges. We hope to further investigate this in future work. Note that we will prove that the slow driver "zipper" produces a convergent driving function when run from the "equilibria points" in the following chapter, see Corollary 6.3.

A natural question that the fast driver generates is the location of the cutoff between monotonic drivers that yield a convergent algorithm and those that do not. This may be related to how far the driving function moves in welding x to y, the values in the first column in Table 5.1. Note that the fast zipper moves as far as possible for a monotonic driver: while waiting at the origin for the closer of x,y, the further point is moving as slow as possible for a monotonic driver, and it moves for the shortest amount of time possible (Lemma 5.9). If we consider the true points $x(t), y(t)$ given by the expansions in Theorem 3.5, then $\xi_f(\tau_f) = O(t^{3/4}) = O(x(t) + y(t))^{3/4}$ as $t \to 0$, whereas all our other curves families have $\xi^c(\tau^c) = O(t) = O(x(t) + y(t))$. Does any curve family with $\xi^c(\tau^c) = O(t^{1-\epsilon})$ yield a divergent zipper?

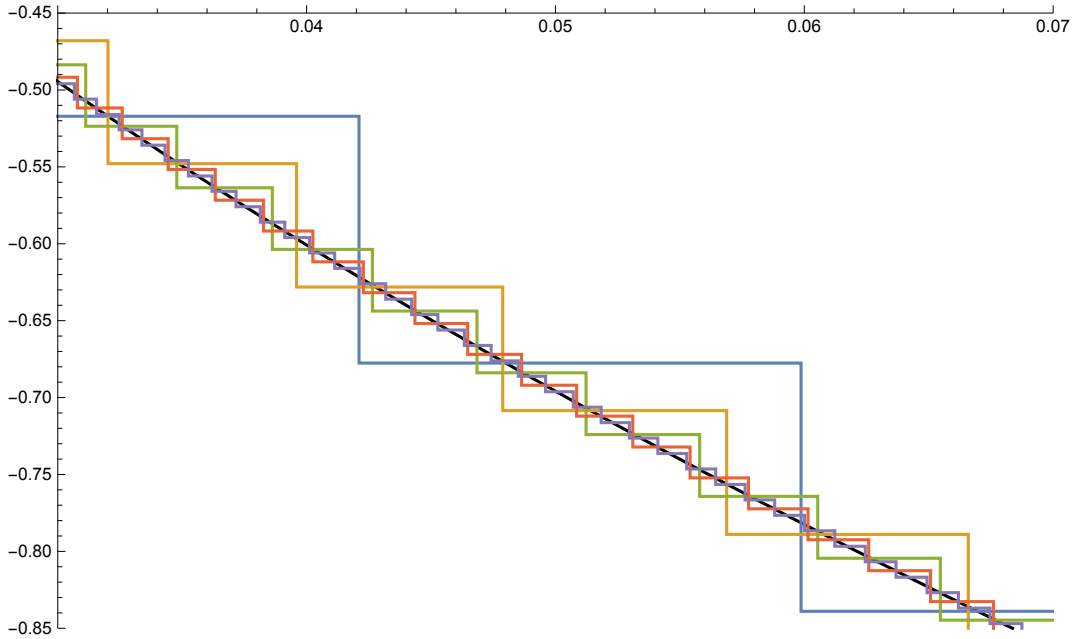

Figure 5.7: Zooming in on Figure 5.6a. The true driver is in black.

Problem 5.11. Determine the threshold for when a monotonic curve family no longer yields a convergent welding zipper algorithm.

Chapter 6

EQUILIBRIA POINTS AND CONVERGENCE OF THE CONSTRUCTED DRIVERS

6.1 Introduction

One step of the zipper algorithm welds the next two data points to the origin. The images of the remaining data points under this conformal map become the updated data points, and the subsequent step takes the next pair of these and welds them together at the origin.

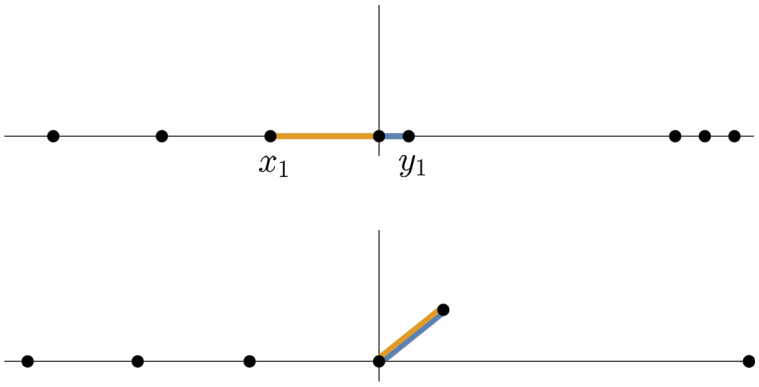

Figure 6.1: One zipper step with the straight slit family. The two intervals surrounding the origin are welded to either side of a single line segment, with the data points x_1, y_1 joined together at the origin. (Note that in the bottom picture a new data point is visible on the left and two of the right data points are pushed out of the frame.)

From the point of view of the Loewner equation, this is the centered upwards flow (2.15). One could also consider a single zip in two sub-steps, however, by first flowing up with the *uncentered flow* of (2.12). Then the next data points are welded together at the location of the terminal value of the upwards driving function for this increment, rather than at zero.

The overall zip is then completed by re-centering the entire picture back at the origin by subtracting off this driving function value. See Figure 6.2.

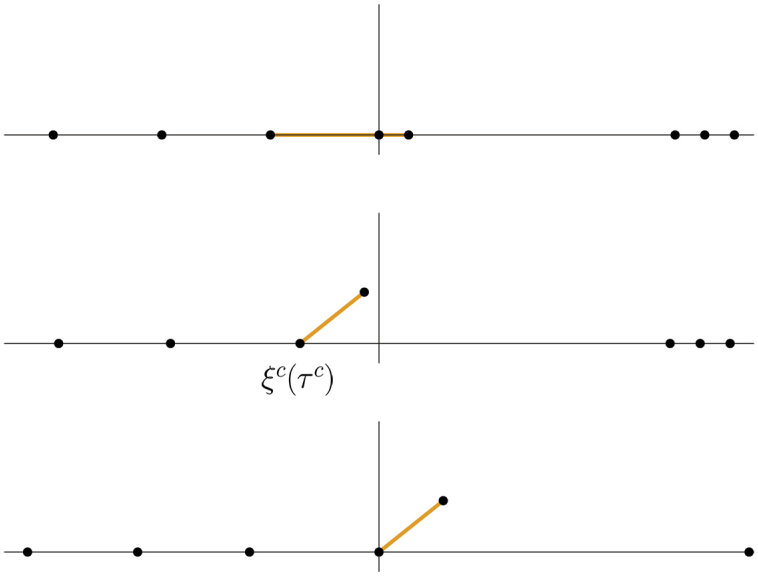

Figure 6.2: One zipper step viewed in two sub-steps: first, an un-centered upwards flow from the constructed driver ξ^c to weld the data points at $\xi^c(\tau^c)$, and then a translation back to the origin.

While this difference in viewpoint may seem cumbersome or irrelevant at best, it is actually insightful for analyzing the accumulation of errors in the remaining data points. That is, after one full zip, how far are the remaining data points from where they would be if we had zipped up with the true curve? Numerical simulations suggest that most of the error comes from the shifting in the second sub-step described above. That is, the error between the true and constructed drivers during the *uncentered* upwards flow is not "communicated" very much to the remaining points because of the local nature of the Loewner equation. However, when we finish the zip by re-centering around zero, the difference between the terminal values of the true and constructed drivers is transferred to the remaining data points, greatly accentuating the error. See Figure 6.3.

Our variation of the zipper algorithm eliminates the error when shifting back to zero. We achieve this by perturbing the initial data points so that the terminal values of the con-

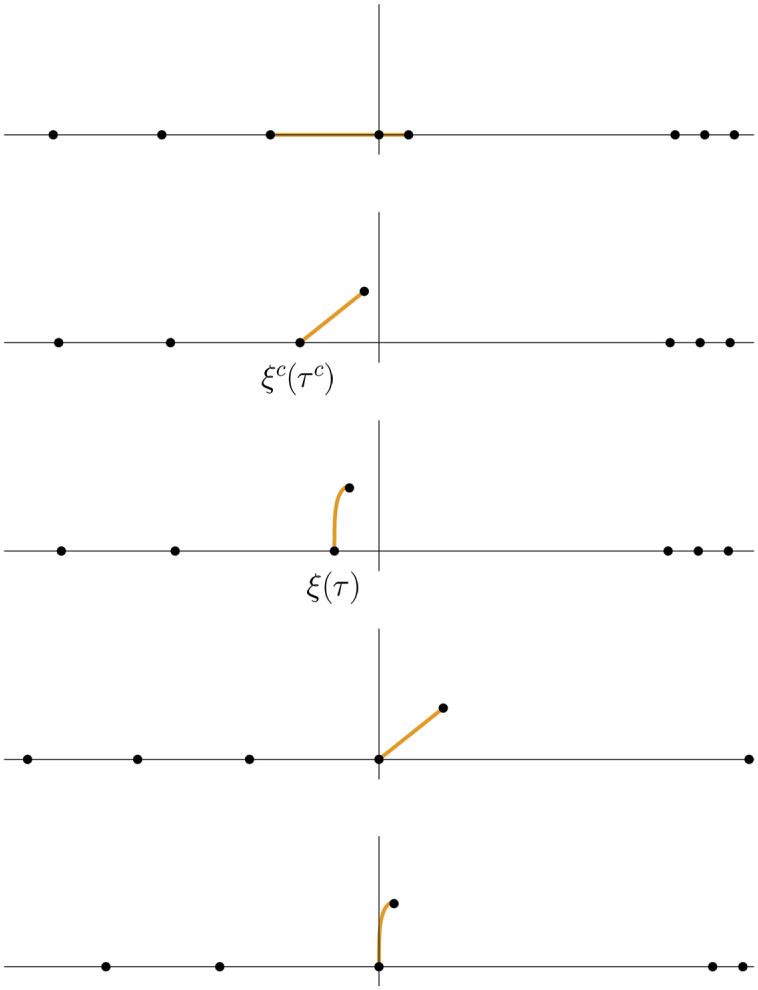

Figure 6.3: Welding the same segment together with both a zipper step and the true curve. We see in the second and third images that although the terminal values of the constructed and true drivers substantially differ, the remaining data points are still close. However, when we re-center and shift back to zero, this error $\xi(\tau) - \xi^c(\tau^c)$ is conferred to all the remaining data points.

structed and true drivers always agree. In this chapter we describe this in detail and explain the consequences for the constructed driving function. We begin in §6.2 by constructing these perturbations to form the *equilibria points*. We give the local expansion of the perturbations in §6.3, and then show in §6.4 that when we run the zipper from the equilibria points, the constructed driving function ξ_n^c converges to the true driver ξ. (We will show

later in Chapter 7 that the actual constructed curves γ_n^c also converge to the true curve γ, as claimed in Theorem 1.1.)

6.2 The equilibria points and our variation of the zipper algorithm

We define the *equilibria points* as a perturbation $\{(x_{nk} + \tilde{\delta}_{nk}^x, y_{nk} + \tilde{\delta}_{nk}^y)\}_{k=1}^{N(n)}$of the true data points $\{(x_{nk}, y_{nk})\}_{k=1}^{N(n)}$ such that the terminal value of the constructed driver on each segment is identical to the value of the true driver for that segment. That is, we shift our initial data points so that

$$\xi_n^c(\tau_{nk}^c) = \xi(\tau_{nk}) \tag{6.1}$$

for all n and k. In this section we describe how we generate these *equilibria shifts* $\tilde{\delta}_{nk}^x, \tilde{\delta}_{nk}^y$. For ease of reading, we subsequently drop the subscript n in most of the notation in sections 6.2 and 6.3. The n refers to the current partition $\mathcal{P}_n$, and hence we focus on a single mesh $\{(x_k, y_k)\}_{k=1}^N$.

The construction of the equilibria points is inductive. Suppose the true upwards driving function ξ welds the first two data points $x_1 < 0 < y_1$ together under its uncentered flow at $\xi(\tau_1)$ in time τ_1. To construct the first equilibria points, shift both x_1 and y_1 by the same amount δ_1 so that, for one zipper step from the tractable curve family $\mathcal{C}$ on the points $x_1 + \delta_1 < 0 < y_1 + \delta_1$, the constructed driver ξ^c has terminal value $\xi^c(\tau_1^c) = \xi(\tau_1)$.* See Figure 6.4. This shift δ_1 is determined by the curve family $\mathcal{C}$. This is obvious for the curve families in Table 5.1 where there is no error term in the expansion of $\xi(\tau)$, and we handle the general case below in Lemma 6.1. Note that while the driver values are the same, the constructed time τ_1^c will in general not be identical to τ_1.

So after one uncentered step both the true driver and the constructed drivers have welded x_1 and y_1 together at $\xi(\tau_1) = \xi^c(\tau_1^c)$. Re-center the remaining true data points around zero

*Recall from Definition 5.1(i) that given any $x < 0 < y$, there exists a unique member of our tractable curve family which welds these together.

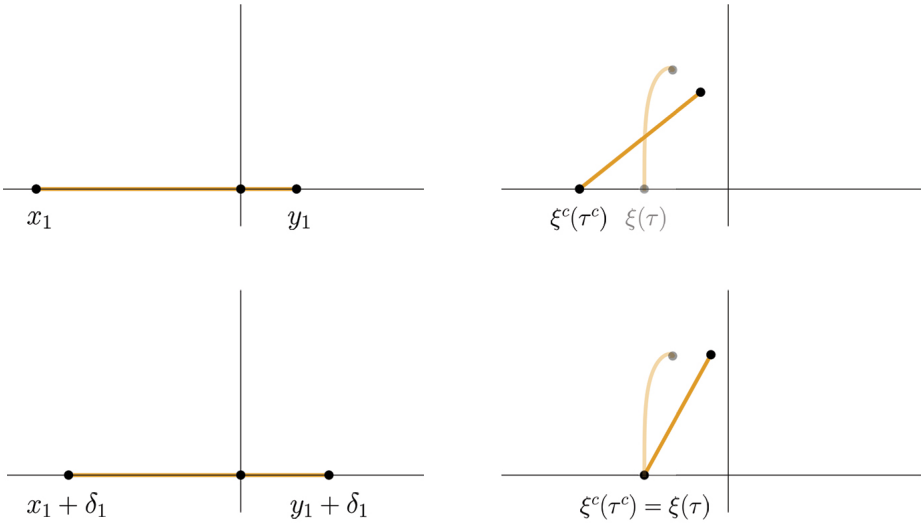

Figure 6.4: Constructing the equilibria points. In the top row, we take one uncentered zipper step, displaying the true curve in the background for reference. To construct the equilibria points, we shift both x_1 and y_1 by the same amount δ_1 so that our constructed driver ends the zipper step with the same value as the true driver, as shown in the second row.

by subtracting $\xi(\tau_1)$, and consider the next two true data points $x_2(\tau_1)$ and $y_2(\tau_1)$.[†] We again shift both $x_2(\tau_1)$ and $y_2(\tau_1)$ by the same amount $\tilde{\delta}_2$ so that our next zip from the curve family $\mathcal{C}$ run from $x_2(\tau_1) + \tilde{\delta}_2 < 0 < y_2(\tau_1) + \tilde{\delta}_2$ has identical driver increment as the true driver,

$$\xi^c(T_2^c) - \xi^c(\tau_1^c) = \xi(T_2) - \xi(\tau_1),$$

where $T_2^c = \tau_1^c + \tau_2^c$ and $T_2 = \tau_1 + \tau_2$. In this way we continue to construct the equilibria points $x_k(T_{k-1}) + \tilde{\delta}_k, y_k(T_{k-1}) + \tilde{\delta}_k$ in each zip stage k. After we have done this N times for our zipper partition $\mathcal{P}$, we flow down the *constructed* driver ξ^c. The images of the points $x_k(T_{k-1}) + \tilde{\delta}_k, y_k(T_{k-1}) + \tilde{\delta}_k$ we used to zip up the curve become some perturbations $\{(x_k + \delta_k^x, y_k + \delta_k^y)\}_{k=1}^N$ of the original data points, and these are the *equilibria points*. Note

[†]These are hence the images of the original data points x_2 and y_2 under the centered upwards Loewner flow (2.15) generated by the *true* driver ξ for τ_1 units of time.

that while we shifted both $x_k(T_{k-1})$ and $y_k(T_{k-1})$ by the same amount $\tilde{\delta}_k$, when we flow back down with ξ^c there is no reason the shift for x_k and y_k will be the same, and hence we have both δ_k^x and δ_k^y.

Our variation of the zipper algorithm is thus to use the data $\{(x_k+\delta_k^x, y_k+\delta_k^y)\}_{k=1}^N$ instead of $\{(x_k, y_k)\}_{k=1}^N$. That is, we make this shift to each of the data points, and then proceed with the algorithm exactly as usual, using our curve family $\mathcal{C}$ to zip up at each step. We again recall that the key property of the equilibria points is that they yield (6.1) *by construction* for all n and all k.

Definition 6.1. The *equilibria points* for zipper data $\{(x_k, y_k)\}_{k=1}^N$ are the points $\{(x_k + \delta_k^x, y_k + \delta_k^y)\}_{k=1}^N$ constructed above. Sometimes we will also refer to the images of these perturbed data points under the upwards centered flow generated by the constructed driver as the equilibria points, particularly when they are the next points $x_k(T_{k-1}) + \tilde{\delta}_k < 0 < y_k(T_{k-1}) + \tilde{\delta}_k$ to be zipped together. The meaning we have in mind should be clear from the context. We refer to the zipper run on the equilibria points as the *equilibria zipper algorithm* or the $\mathcal{C}$*-equilibria zipper algorithm* if we wish to emphasize what tractable curve family we are using. We refer to both the δ_k^x, δ_k^y and the $\tilde{\delta}_k$ as the *equilibria shifts.*

6.3 Properties of the equilibria points

We need some basic properties of the equilibria points in order to prove driver convergence. For instance, it is not at the outset obvious that

$$x_k(T_{k-1}) + \tilde{\delta}_k < 0 < y_k(T_{k-1}) + \tilde{\delta}_k,$$

as we have previously asserted. Lemma 6.1 addresses this, explicitly solving for the shifts $\tilde{\delta}_k$ under a curve family $\mathcal{C}$. Lemma 6.2 and Corollary 6.3 show that when we run the algorithm from the equilibria points, the constructed drivers converge to the true driver.

For calculating the $\tilde{\delta}_{nk}$, we lose no generality in assuming that the next points to be zipped up are, in fact, the first, that the current time is $t = 0$, and that the true driver ξ

begins at zero. We will always build our constructed curve with zips from tractable curve families in the sense of Definition 5.1, which we recall satisfy

$$\xi^c(\tau^c) = c(x+y) + O\Big(\frac{(x+y)^3}{(y-x)^2}\Big) \tag{6.2}$$

when zipping $x < 0 < y$. The error is as $\frac{y}{y-x} \to \frac{1}{2}$ and is quantitative in the sense of (5.2).

Lemma 6.1. *If $\xi \in C_0^{3/2+\epsilon}$ welds points $x_1 < 0 < y_1$ together at time τ, the corresponding equilibria points for the constructed curve with family $\mathcal{C}$ are $x_1 + \tilde{\delta}$ and $y_1 + \tilde{\delta}$, where*

$$\tilde{\delta} = \Big(\frac{1}{2c} - \frac{2}{3}\Big)\dot{\xi}(0)\tau + O(\tau^{3/2+\epsilon}) \tag{6.3}$$

as $\tau \to 0^+$. The constant is the c determined by the curve family in (6.2)*, and there exists a constant $\tau_1 = \tau_1(\mathcal{C}, \|\xi\|_{C^{3/2+\epsilon}})$ such that whenever $\tau \le \tau_1$,*

$$x_1 + \tilde{\delta} < 0 < y_1 + \tilde{\delta} \tag{6.4}$$

and furthermore we have the quantitative control

$$\Big|\tilde{\delta} - \Big(\frac{1}{2c} - \frac{2}{3}\Big)\dot{\xi}(0)\tau\Big| \le C\tau^{3/2+\epsilon} \tag{6.5}$$

in the error for (6.3)*, where $C = C(\mathcal{C}, \|\xi\|_{C^{3/2+\epsilon}})$ is a constant.*

Our expansions in Theorem 3.5 show that $x_1 = O(\sqrt{\tau}) = y_1$, whereas (6.3) says $\tilde{\delta} = O(\tau)$. That is, the equilibria points are extremely close to x_1 and y_1 when τ is small. This is the crux of why the equilibria points have any value: they are a useful perturbation because they dispense with the thorny problem of dealing with the accumulation of errors in the algorithm, but they are small enough that they still yield an algorithm whose constructed curves γ_n^c converge to the true curve (as we finish arguing below in Chapter 7).

Proof. Suppose first that there is no error-term in (6.2) for our curve family (as is the case for three of the four of our families in Chapter 5). Then we want some shift $\tilde{\delta}$ so that

$$\xi^c(\tau^c) = c(x_1 + y_1 + 2\tilde{\delta}) = \xi(\tau) = \dot{\xi}(0)\tau + O(\tau^{3/2+\epsilon}) \tag{6.6}$$

by Lemma 3.4. Noting from Theorem 3.5 that $x_1 = x_1(\tau)$ and $y_1 = y_1(\tau)$ satisfy

$$x_1 + y_1 + 2\tilde{\delta} = \frac{4}{3}\dot{\xi}(0)\tau + 2\tilde{\delta} + O(\tau^{3/2+\epsilon}), \tag{6.7}$$

solving for $\tilde{\delta}$ in (6.6) yields

$$\tilde{\delta} = \Big(\frac{1}{2c} - \frac{2}{3}\Big)\dot{\xi}(0)\tau + O(\tau^{3/2+\epsilon}). \tag{6.8}$$

Given the control on the $O(\tau^{3/2+\epsilon})$-terms in (6.6) and (6.7) from Lemma 3.4 and Theorem 3.5, respectively, we have the claimed control in (6.5).

In the presence of the error term in (6.2), we begin by dropping that and solving as above, obtaining the expression in (6.8) as our initial guess $\tilde{\delta}'$ for $\tilde{\delta}$. We claim that we only have to add a term which is quantitatively $O(\tau^{3/2+\epsilon})$ to obtain the true equilibria point $\tilde{\delta}$. Indeed, first note that, from the expansions in Theorem 3.5 again,

$$\frac{y_1 + \tilde{\delta}'}{y_1 + \tilde{\delta}' - (x_1 + \tilde{\delta}')} - \frac{1}{2} = \frac{2\sqrt{\tau} + \frac{1}{2c}\dot{\xi}(0)\tau + O(\tau^{3/2})}{4\sqrt{\tau} + O(\tau^{3/2})} - \frac{1}{2} = \frac{1}{8c}\dot{\xi}(0)\sqrt{\tau} + O(\tau) \leq \delta(\mathcal{C})$$

for all τ sufficiently small, where $\delta(\mathcal{C})$ is from part (iii) of Definition 5.1. Note that if we replace $\tilde{\delta}'$ by the translate $\tilde{\delta}' + r\tau^{3/2+\epsilon} =: \tilde{\delta} = \tilde{\delta}(r)$ where $r \leq C_2$ for some constant C_2, this inequality remains true provided $\tau \leq \tau_2 = \tau_2(C_2, \|\xi\|_{C^{3/2+\epsilon}})$. Thus for any such $\tilde{\delta}$ and τ, we have by (5.2) that the terminal driver value $\xi^c(\tilde{\delta}, \tau^c)$ for welding the points $x_1 + \tilde{\delta}$ and $y_1 + \tilde{\delta}$ with the family $\mathcal{C}$ satisfies

$$|\xi^c(\tilde{\delta}, \tau^c) - c(x_1 + y_1 + 2\tilde{\delta})| \leq C_3\frac{|x_1 + y_1 + 2\tilde{\delta}|^3}{|y_1 - x_1|^2} = C_3\frac{\big|\frac{\dot{\xi}(0)}{c}\tau + O(\tau^{3/2+\epsilon})\big|^3}{\big|4\sqrt{\tau} + O(\tau^{3/2})\big|^2} \leq C_4\tau^2, \tag{6.9}$$

where $C_4 = C_4(\mathcal{C}, C_2, \|\xi\|_{C^{3/2+\epsilon}})$, and the inequality holds for all $\tau \leq \tau_4 = \tau_4(\mathcal{C}, C_2, \|\xi\|_{C^{3/2+\epsilon}})$. By making τ_4 even smaller, if necessary, we also have

$$C_4\tau^2 < \frac{1}{2}C_2\tau^{3/2+\epsilon}$$

when $\tau \leq \tau_4$. When $r = 0$, we have $\tilde{\delta} = \tilde{\delta}'$, and recall that by construction, $c(x_1 + y_1 + 2\tilde{\delta}') = \xi(\tau)$, and so (6.9) says

$$\xi(\tau) - C_5\tau^2 \leq \xi^c(\tilde{\delta}', \tau^c) \leq \xi(\tau) + C_5\tau^2 \tag{6.10}$$

for $C_5 = C_5(\mathcal{C}, \|\xi\|_{C^{3/2+\epsilon}})$ and for all $\tau \leq \tau_5 = \tau_5(\mathcal{C}, \|\xi\|_{C^{3/2+\epsilon}})$. Note that there is no dependence upon C_2 now because we are not using any shift of $\tilde{\delta}'$. Inequality (6.10) says that $\xi^c(\tilde{\delta}', \tau^c)$ is in a very narrow window around $\xi(\tau)$, while (6.9) says that as we vary $\tilde{\delta}'$ by replacing it with the translates $\tilde{\delta} = \tilde{\delta}' + r\tau^{3/2+\epsilon}$, the resulting driver $\xi^c(\tilde{\delta}, \tau^c)$ stays very close to $c(x_1 + y_1 + 2\tilde{\delta})$. Since the magnitude of change in $c(x_1 + y_1 + 2\tilde{\delta})$ as we translate is of order $\tau^{3/2+\epsilon}$, while the magnitude of proximity in both (6.9) and (6.10) is order τ^2, by choosing large enough r and restricting to small enough time we can "drag" $\xi^c(\tilde{\delta}, \tau^c)$ outside of being within distance $C_5\tau^2$ of $\xi(\tau)$. For instance, we explicitly show we can make

$$\xi(\tau) + C_5\tau^2 < \xi^c(\tilde{\delta}, \tau^c) \tag{6.11}$$

by translating enough in $\tilde{\delta} = \tilde{\delta}' + r\tau^{3/2+\epsilon}$ and restricting to small-enough times. Indeed, set $C_2 = 1$. Inequality (6.10) yields

$$\xi^c(\tilde{\delta}, \tau^c) \geq -C_4\tau^2 + c(x_1 + y_1 + 2\tilde{\delta}' + 2r\tau^{3/2+\epsilon}) = -C_4\tau^2 + \xi(\tau) + 2cr\tau^{3/2+\epsilon}$$

by construction of $\tilde{\delta}'$, for $r \leq 1$. So combined with (6.11) we see it suffices to show

$$C_5\tau^2 < -C_4\tau^2 + 2cr\tau^{3/2+\epsilon} \qquad \Leftrightarrow \qquad \frac{1}{2c}(C_4 + C_5)\tau^{1/2-\epsilon} < r,$$

which is true for small τ.

As we translate by r, $\xi^c(\tilde{\delta}, \tau^c)$ varies continuously by assumption (iii) in Definition 5.1, and so there is a value of r we can choose so that $\xi^c(\tilde{\delta}, \tau^c) = \xi(\tau)$. This selection yields (6.3) and (6.5) again for new constants τ_1 and C.

Lastly, (6.4) follows immediately from the expansions for $x_1 = x_1(\tau)$ and $y_1 = y_1(\tau)$ in Theorem 3.5 and the expression we now have for $\tilde{\delta}$ in (6.3), where we shrink τ_1, if necessary.

□

Table 6.1 gives the shifts $\tilde{\delta}$ and corresponding capacity times for our several curve families. As an example, we work out the straight slit family computations in detail. We have from Table 5.1 that the driver $\xi^c(\tau^c)$ for welding together $x < 0 < y$ satisfies

$$\xi^c(\tau^c) = x + y, \qquad \tau^c = -\frac{1}{4}xy.$$

Curve family	*Equilibria shift* $\tilde{\delta}_k$	τ_k^c *for equilibria pts*
Slow driver*	$\frac{1}{3}\dot{\xi}(T_{k-1})\tau_k + O(\tau_k^{3/2+\epsilon})$	$\tau_k + \frac{\dot{\xi}(T_{k-1})^2}{18}\tau_k^2 + O(\tau_k^{2+\epsilon})$
EMW	$\frac{1}{12}\dot{\xi}(T_{k-1})\tau_k + O(\tau_k^{3/2+\epsilon})$	$\tau_k + \frac{5\dot{\xi}(T_{k-1})^2}{576}\tau_k^2 + O(\tau_k^{2+\epsilon})$
Circular arc	$O(\tau_k^{3/2+\epsilon})$	$\tau_k + O(\tau_k^{2+\epsilon})$
Wang minimizer	$\big(\frac{3\pi}{16} - \frac{2}{3}\big)\dot{\xi}(T_{k-1})\tau_k + O(\tau_k^{3/2+\epsilon})$	$\tau_k + \big(\frac{35}{144} - \frac{27\pi^2}{1024}\big)\dot{\xi}(T_{k-1})^2\tau_k^2 + O(\tau_k^{2+\epsilon})$
Straight slit	$-\frac{1}{6}\dot{\xi}(T_{k-1})\tau_k + O(\tau_k^{3/2+\epsilon})$	$\tau_k - \frac{\dot{\xi}(T_{k-1})^2}{144}\tau_k^2 + O(\tau_k^{2+\epsilon})$

Table 6.1: Equilibria shifts and welding times for our curve families. Here T_{k-1} is the time elapsed for the true curve through $(k-1)$ true zips; τ_k is the true time for the next increment, and τ_k^c is the time for the constructed zipper segment. The $\tilde{\delta}_k$'s are calculated from Lemma 6.1, and the τ_k^c from Table 5.1, $\tilde{\delta}_k$ and Theorem 3.5. All errors are quantitative. Note that running the zipper with the slow driver ξ_s does not yield a simple curve, as ξ_s is discontinuous.

Hence $c = 1$ in (6.2) with no error term, and so

$$\tilde{\delta} = -\frac{1}{6}\dot{\xi}(t_0)\tau + O(\tau^{3/2+\epsilon}),$$

with the quantitative control $|\tilde{\delta} + \frac{1}{6}\dot{\xi}(t_0)\tau| \leq C_2\tau^{3/2+\epsilon}$ for all $\tau \leq t_1$, for the t_1 of Theorem 3.5. The welding time τ^c for these equilibria points $x + \tilde{\delta} < 0 < y + \tilde{\delta}$ is therefore

$$-\frac{1}{4}\big(-2\sqrt{\tau} + \frac{1}{2}\dot{\xi}(t_0)\tau - \frac{1}{18}\dot{\xi}(t_0)^2\tau^{3/2} + O(\tau^{3/2+\epsilon})\big)\big(2\sqrt{\tau} + \frac{1}{2}\dot{\xi}(t_0)\tau + \frac{1}{18}\dot{\xi}(t_0)^2\tau^{3/2} + O(\tau^{3/2+\epsilon})\big)$$
$$= \tau - \frac{1}{144}\dot{\xi}(t_0)^2\tau^2 + O(\tau^{2+\epsilon}),$$

with quantitative control on the $O(\tau^{2+\epsilon})$-term for small τ in terms of $\dot{\xi}(t_0)$.

6.4 Convergence of the constructed drivers

We give broad conditions on curve families for when their zipper curves, constructed from their equilibria points, have drivers which converge to the true driving function.

Lemma 6.2 (Convergence of the constructed drivers)**.** *Let $\mathcal{C}$ be a curve family satisfying:*

(*i*) *For any $x < 0 < y$, the curve in $\mathcal{C}$ which welds x to y has monotonic driving function.*

(*ii*) *For a curve γ driven by a $C^{3/2+\epsilon}$ driver ξ, there exists $\delta > 0$ such that the welding time τ^c for the equilibria points $u < 0 < v$ corresponding to the true data points $x < 0 < y$ welded by ξ at time τ satisfies*

$$|\tau^c - \tau| \leq C\tau^{1+\delta} \tag{6.12}$$

whenever $\tau \leq \tau_1 = \tau_1(\mathcal{C}, \|\xi\|_{C^{3/2+\epsilon}})$, for some constant $C = C(\mathcal{C}, \|\xi\|_{C^{3/2+\epsilon}})$.

Then, in the setting of Theorem 1.1, the $\mathcal{C}$-zipper algorithm run from the equilibria points on the data $\mathcal{P}_n$ has driving function ξ_n^c which converge locally uniformly to ξ on $[0, T)$ as $n \to \infty$.

Note that we cannot guarantee convergence on all of $[0, T]$, since if T_n^c is the time of the constructed curve in the nth stage, we might have $T_n^c < T$ for all n. Our proof below shows, though, that $T_n^c \to T$.

The proof is an elementary consequence of Lemma 3.4: since the values $\xi^c(\tau_{nk}^c)$ and $\xi(\tau_{nk})$ are identical, ξ^c and ξ are well-behaved, and τ_{nk}^c is uniformly close to τ_{nk}, we have that ξ^c and ξ are always close. We proceed with the details.

Proof. The kth zip for the constructed curve has capacity time τ_{nk}^c which is close to the time τ_{nk} for the kth interval on the actual curve. We define α_n as the increasing, piece-wise linear perturbation of time which corrects this discrepancy. That is, if $T_{nk}^c = \sum_{j=1}^k \tau_{nj}^c$ is the total elapsed time after k zips of the constructed curve, and $T_{nk} = \sum_{j=1}^k \tau_{nj}$ that for the true curve, then

$$\alpha_n(t) = T_{nk} + \frac{\tau_{n,k+1}}{\tau_{n,k+1}^c}(t - T_{nk}^c) \tag{6.13}$$

for $t \in I_{nk}^c := [T_{nk}^c, T_{nk}^c + \tau_{n,k+1}^c]$. We first observe $\xi_n^c \circ \alpha_n^{-1}$ converges uniformly to ξ on $[0,T]$. Indeed, at a time t in an arbitrary interval $t = T_{nk} + h \in I_{nk} := [T_{nk}, T_{nk} + \tau_{n,k+1}]$, Lemma 3.4 yields

$$\begin{aligned}|\xi(t) - \xi_n^c \circ \alpha_n^{-1}(t)| &\le |\xi(t) - \xi(T_{nk}) - \dot\xi(T_{nk})h| + |\xi(T_{nk}) + \dot\xi(T_{nk})h - \xi_n^c \circ \alpha_n^{-1}(t)| \\ &\le Ch^{3/2+\epsilon} + \max\left\{|\dot\xi(T_{nk})|h,\ |\xi(T_{nk}) + \dot\xi(T_{nk})h - \xi(T_{n,k+1})|\right\}\end{aligned}$$

by monotonicity of $\xi_n^c \circ \alpha^{-1}$. Furthermore,

$$\begin{aligned}|\xi(T_{nk}) + \dot\xi(T_{nk})h - \xi(T_{n,k+1})| &\le |\xi(T_{nk}) + \dot\xi(T_{nk})\tau_{n,k+1} - \xi(T_{n,k+1})| + |\dot\xi(T_{nk})|(\tau_{n,k+1} - h) \\ &\le C\tau_{n,k+1}^{3/2+\epsilon} + |\dot\xi(T_{nk})|\tau_{n,k+1},\end{aligned}$$

by Lemma 3.4 again, and so we obtain

$$|\xi(t) - \xi_n^c \circ \alpha_n^{-1}(t)| \le 2C\tau_{n,k+1}^{3/2+\epsilon} + \max_{[0,T]} |\dot\xi(t)|\tau_{n,k+1} \to 0$$

uniformly by assumption (1.1) on the partitions $\mathcal{P}_n$.

Next, we note that α_n converges uniformly to the identity on $[0, T_n^c]$, where $T_n^c := T_{n,N(n)}^c$ is the total time of the constructed curve at stage n. Indeed, the slopes of linear segments of α_n are of the form

$$\frac{\tau_{n,k+1}}{\tau_{n,k+1}^c} = \frac{1}{1 + O(\tau_{n,k+1}^\delta)} \to 1$$

uniformly as $n \to \infty$ by assumption on the curve family $\mathcal{C}$, the true driver ξ, and the partitions $\mathcal{P}_n$. Thus

$$(1 - \epsilon_n)t \le \alpha_n(t) \le (1 + \epsilon_n)t, \tag{6.14}$$

for some sequence $\epsilon_n \to 0$ as $n \to \infty$. For large n, T_n^c is close to the true time T, as

$$|T_n^c - T| \le \sum_{k=1}^{N(n)} |\tau_{nk}^c - \tau_{nk}| \le C \sum_{k=1}^{N(n)} \tau_{nk}^{1+\delta} \le C\big(\max_k \tau_{nk}^\delta\big) \sum_{k=1}^{N(n)} \tau_{nk} = C\big(\max_k \tau_{nk}^\delta\big)T \to 0, \tag{6.15}$$

and so (6.14) yields that $\alpha_n(t) \to t$ uniformly on $[0, T_n^c]$, and hence that $\alpha_n^{-1}(t) \to t$ uniformly on $[0, T]$. Therefore, writing $\|\cdot\| = \|\cdot\|_{L^\infty[0,T]\cap[0,T_n^c]}$, we have

$$\|\xi_n^c - \xi\| \leq \|\xi_n^c - \xi_n^c \circ \alpha_n^{-1}\| + \|\xi_n^c \circ \alpha_n^{-1} - \xi\|.$$

We know $\|\xi_n^c \circ \alpha_n^{-1} - \xi\|$ is small when n is large, and we note

$$\|\xi_n^c - \xi_n^c \circ \alpha_n^{-1}\| = \|(\xi_n^c \circ \alpha_n^{-1}) \circ \alpha_n - \xi_n^c \circ \alpha_n^{-1}\|. \tag{6.16}$$

The uniformly-convergent sequence $\{\xi_n^c \circ \alpha_n^{-1}\}$ is uniformly equicontinuous on compact sets, and since α_n converges uniformly to the identity, we conclude (6.16) is likewise small. □

Since the errors in the constructed times τ^c in Table 6.1 are controlled by $\dot{\xi}(t)$, Lemma 6.2 immediately yields that these families produce convergent drivers. The lemma also applies if we switch between our four families as we zip up, "mixing and matching" between different curve families for different zips, as both conditions are still satisfied: (i) holds since all the families are tractable, and hence monotonic on each zip, and (ii) holds since we can take as C the maximum of the four C's for the four families, and τ_1 the minimum of the four τ_1's.

Corollary 6.3. *For driver ξ and partitions $\mathcal{P}_n$ as in the statement of Theorem 1.1, the equilibria-point zipper algorithm for any of the curve families in Table 6.1, or any combination of these families on individual zips, constructs drivers ξ_n^c which converge uniformly to ξ on compact subsets of $[0, T)$.*

Chapter 7

FROM DRIVER CONVERGENCE TO CURVE CONVERGENCE

7.1 Introduction

We have that when we run the zipper from the equilibria points, the constructed drivers ξ_n^c converge to the true driver ξ. Driving function convergence is weaker than convergence of actual curves, as a counter-example of Lawler shows [17, E.g.4.49]. Using the nature of our curve families and more refined information about our driver convergence, however, allows us to conclude that the actual curves γ_n^c converge. And not only to *some* curve $\tilde{\gamma}$, but to the true curve γ. Our preceding work already nearly proves this; we only lack compactness for the constructed curves γ_n^c and a link between driver convergence and curve convergence. Lind, Marshall and Rohde [21] have furnished all the necessary tools to complete the argument; we show in this chapter how the pieces fit together.

We begin by reproducing, for the convenience of the reader, the key results we will use from [21].

Proposition 7.1 (Lemma 4.1 [21])**.** *Let $\xi_j : [0,1] \to \mathbb{R}$ be continuous. For every $\epsilon > 0$, $C < 4$ and $D < 0$ there is $\delta > 0$ such that if*

$$\|\xi_1 - \xi_2\|_{L^\infty[0,1]} < \delta$$

and if

$$|\xi_j(t) - \xi_j(t')| \leq C|t - t'|^{1/2} \quad \text{whenever} \quad |t - t'| < D, \quad j = 1, 2, \tag{7.1}$$

then the hulls γ_1, γ_2 generated by ξ_1, ξ_2 are Jordan arcs with

$$\|\gamma_1 - \gamma_2\|_{L^\infty[0,1]} < \epsilon.$$

Proposition 7.2 (Lemma 4.2 [21]). *Suppose λ_n, λ are drivers on $[0,T]$ with λ_n generating Jordan arcs γ_n. If $\lambda_n \to \lambda$ uniformly on $[0,T]$ and there exists a Jordan arc γ such that $\gamma_n \to \gamma$ uniformly on $[0,T]$, then γ is the curve generated by λ.*

We will also use conclusions from the proof of Proposition 7.1 in [21]. Recall that a *K-quasislit half-plane* $\mathbb{H}\backslash\gamma$ is the image of $\mathbb{H}\backslash[0,i]$ under a K-quasiconformal map $f : \mathbb{H} \to \mathbb{H}$ that fixes ∞, and hence, in its boundary extension, takes $\mathbb{R}$ to $\mathbb{R}$ [23]. The proof of Lemma 4.1 in [21] shows that curves generated by drivers satisfying the local Hölder condition (7.1) are uniformly K-quasislit half planes.

Proposition 7.3 (From the proof of Lemma 4.1, [21]). *The hull γ generated by any continuous function λ satisfying* (7.1) *on $[0,T]$ is a K-quasislit halfplane, for some K depending only on C, D and T, and its half-plane capacity parametrization has modulus of continuity which depends only upon K.*

This is very valuable for us, because it affords subsequential limiting curves that are uniform limits in their capacity parametrizations. Since we know $\xi_n^c \to \xi$ from Corollary 6.3, Proposition 7.2 will show that the limiting curve is the true curve. We simply need to establish the local Hölder condition (7.1). Lemma 7.4 does this for the case of the straight-slit zipper, and Lemma 7.5 handles our other three families. Neither are difficult, but merely require some careful accounting and an ϵ of patience.

7.2 Hölder estimates

Recall our somewhat non-standard notation for the Hölder-1/2 seminorm: $|g|_{1/2}$ is the infimum of all M such that

$$|g(x_1) - g(x_2)| \leq M|x_1 - x_2|^{1/2}$$

for all x_1, x_2.

Lemma 7.4. *Let f be continuous on an interval I and linear on the subintervals $I_j = [x_j, x_{j+1}]$, $I = \bigcup_{j=1}^n I_j$, having slope m_j on the interior of each I_j. Let g be the piecewise square root interpolation of f on the I_j's,*

$$g(x) = f(x_j) + \frac{f(x_{j+1}) - f(x_j)}{\sqrt{x_{j+1} - x_j}} \sqrt{x - x_j}, \qquad x \in I_j. \tag{7.2}$$

Then g is Hölder-$1/2$ continuous on I with Hölder seminorm $|g|_{1/2}$ on I satisfying

$$|g|_{1/2} \leq \max_j |m_j| \sqrt{|I|}. \tag{7.3}$$

We note that while the estimate (7.3) is coarse, it will suffice for our purpose.

Proof. The elementary argument proceeds in two steps.

(*i*) Suppose first that $f(x) = x$ and $\bigcup_{j=1}^n I_j = [0, 1]$. We claim

$$|g|_{1/2} \leq 1, \tag{7.4}$$

as can be seen by induction. If there are just two subintervals, we have

$$g(x) = \begin{cases} \sqrt{a}\sqrt{x} & 0 \leq x \leq a \\ \sqrt{1-a}\sqrt{x-a} + a & a \leq x \leq 1 \end{cases}$$

for some $0 < a < 1$. Noting that $g(x) - g(0) \leq \sqrt{x - 0}$ for all $0 \leq x \leq 1$, we have that starting from any x_1, $g(x) - g(x_1)$ is always contained in the "envelope" formed by $\sqrt{|x - x_1|}$, yielding the claim for two intervals. (We leave the calculus details to the interested reader.) Note that if we had two intervals on $[0, b]$ instead of $[0, 1]$, still interpolating $f(x) = x$, then re-scaling yields $|g|_{1/2} \leq \sqrt{b}$ on $[0, b]$.

Suppose (7.4) holds when there are n intervals, and consider a square-root interpolation g of $f(x) = x$ on $n + 1$ subintervals of $[0, 1]$. Choose $x_1 < x_2 \in [0, 1]$. If they land in the same interval I_j, then as the square-root coefficient for g on this interval is $\sqrt{|I_j|}$,

$$g(x_2) - g(x_1) \leq \sqrt{|I_j|}\sqrt{x_2 - x_1} \leq \sqrt{x_2 - x_1}.$$

If they lie in adjacent intervals I_j, I_{j+1}, then by the base case

$$g(x_2) - g(x_1) \leq \sqrt{|I_j \cup I_{j+1}|}\sqrt{x_2 - x_1} \leq \sqrt{x_2 - x_1}.$$

If $x_1 \in I_j$ and $x_2 \in I_k$ where I_j and I_k have at least one other interval in-between themselves, replace g with $\tilde{g}$, where $\tilde{g} = g$ on $[0,1]\backslash(I_{k-1} \cup I_k)$, but where $\tilde{g}$ is a single square-root function on $I_{k-1} \cup I_k$ instead of the two for g. Then by the inductive hypothesis,

$$g(x_2) - g(x_1) = g(x_2) - \tilde{g}(x_1) \leq \tilde{g}(x_2) - \tilde{g}(x_1) \leq \sqrt{x_2 - x_1}$$

again yielding (7.4), and hence proving the claim for n subintervals of $[0,1]$.

If g is a piecewise square-root interpolation of $f(x) = mx + b$ on n sub-intervals of $I = [c,d]$, applying the above to the function

$$\tilde{g}(x) := \frac{1}{m(d-c)}\Big(g\big((d-c)x + c\big) - (mc + b)\Big)$$

shows

$$|g|_{1/2} \leq m\sqrt{|I|}. \tag{7.5}$$

(*ii*) Suppose now that f is piecewise linear with slopes $m_1, \ldots, m_n$. If we replace f with a linear function $\tilde{f}$ having constant slope $\max_j |m_j|$ on all of I, and g with the square-root interpolation $\tilde{g}$ of $\tilde{f}$ on the I_j, then

$$|g(x_2) - g(x_1)| \leq |\tilde{g}(x_2) - \tilde{g}(x_1)| \leq \max_j |m_j|\sqrt{|I|}\sqrt{|x_2 - x_1|}$$

by (7.5).

□

For our three smooth curve families, i.e. those with $\xi \in C^1$, we show (7.1) holds by uniformly bounding the driver derivatives, yielding a Lipschitz constant. The argument for each of the three families is essentially the same: for welding ratios α close to $1/2$, we can use convexity to control the derivative on an entire zipping interval with the initial derivative. Without loss of generality we are at time $t = 0$.

Lemma 7.5. *Suppose $x_1 < 0 < y_1$ are the next points to be welded at time τ by $\xi \in C^{3/2+\epsilon}$. Let ξ^c be the constructed driver for any of our three smooth curve families on the increment $[0, \tau^c]$ for the equilibria points $u_1 = x_1 + \delta, v_1 = y_1 + \delta$. Then there exists positive constants C and T such that*

$$\max_{t\in[0,\tau^c]} |\dot{\xi}^c(t)| \le C|\dot{\xi}(0)| \tag{7.6}$$

whenever $\tau^c < T$ (where derivatives are one-sided where needed). Here the same C and T work for all three curve families.

Proof. We show (7.6) holds individually for each curve family; take the maximum of the C's and the minimum of the T's to obtain the claimed result.

The Wang minimizers. It suffices to work with the downwards driver $\lambda^c = \lambda^c_\theta$ instead of the reversed ξ^c, as $\max|\dot{\xi}^c(t)| = \max|\dot{\lambda}^c(t)|$. By symmetry we may assume $0 < v_1 < -u_1$, yielding that the tip of the constructed curve has argument $\theta \in (0, \pi/2)$.

We claim that whenever $\alpha(0) := \frac{v_1}{v_1 - u_1}$ is sufficiently close to $1/2$, λ^c is concave down, and hence we can control the max in (7.6) by $|\dot{\lambda}^c(0)|$. Indeed, by (5.16) we have

$$\ddot{\lambda}^c(t) = \frac{16x}{(x^2+y^2)^3}(3x^2 - y^2),$$

where $x = x(t) = \mathrm{Re}(G_t(e^{i\theta}))$ and $y = y(t) = \mathrm{Im}(G_t(e^{i\theta}))$ are the real and imaginary parts of the image of the tip of the constructed curve under the centered downwards Loewner flow (2.16). This expression is negative whenever $3x^2 < y^2$ or $\sqrt{3} < \tan(\theta)$, and since the angle $\theta(t)$ of the tip is monotonically increasing as we map down by (5.23), λ^c is concave down as claimed: a ratio $\alpha(0)$ close to $1/2$ will yield $\theta = \theta(0)$ close to $\pi/2$ by (5.25).

Suppose that $u_1 < 0 < v_1$ are exactly the welding interval endpoints $x_\theta < 0 < y_\theta$ in (5.24) that generate the minimizing segment from 0 to $e^{i\theta}$. Then

$$\dot{\lambda}^c(0) = \dot{\lambda}_\theta(0) = 4\cos(\theta) = 4\cos(\theta(\alpha)) = -\frac{32}{\pi}\Big(\alpha(0) - \frac{1}{2}\Big) + O\Big(\alpha(0) - \frac{1}{2}\Big)^3 \tag{7.7}$$

by (5.25). We use Table 6.1 and Theorem 3.5 to compute

$$\alpha(0) = \frac{y_1 + \delta}{y_1 - x_1} = \frac{2\sqrt{\tau} + \frac{3\pi}{16}\dot{\xi}(0)\tau + \frac{1}{18}\dot{\xi}(0)^2\tau^{3/2} + O(\tau^{3/2+\epsilon})}{4\sqrt{\tau} + \frac{1}{9}\dot{\xi}(0)^2\tau^{3/2} + O(\tau^{3/2+\epsilon})}$$

$$= \frac{1}{2} + \frac{3\pi}{64}\dot{\xi}(0)\sqrt{\tau} + O\left(\tau^{1+\epsilon}\right), \tag{7.8}$$

and thus

$$\dot{\lambda}^c(0) = -\frac{3}{2}\dot{\xi}(0)\sqrt{\tau} + O(\tau^{3/2}) \tag{7.9}$$

by (7.7). For the general case, we need to scale by $r = \frac{v_1-u_1}{y_\theta - x_\theta} = \frac{y_1-x_1}{y_\theta-x_\theta}$ to obtain the correct welding interval, which transforms $\dot{\lambda}$ according to $\dot{\lambda} \mapsto \frac{1}{r}\dot{\lambda}(\cdot/r^2)$. Expanding $\frac{1}{r}$ using (5.24), (5.25), Theorem 3.5 and (7.8), we have

$$\begin{aligned}\frac{y_{\theta(\alpha)} - x_{\theta(\alpha)}}{y_1 - x_1} &= \frac{2 + \left(12 - \frac{128}{\pi^2}\right)\left(\alpha - \frac{1}{2}\right)^2 + O\left(\alpha - \frac{1}{2}\right)^3}{4\sqrt{\tau} + \frac{1}{9}\dot{\xi}(0)^2\tau^{3/2} + O(\tau^{3/2+\epsilon})} \\ &= \frac{1}{2\sqrt{\tau}} + \Big(\frac{27\pi^2}{4096} - \frac{97}{1152}\Big)\dot{\xi}(0)^2\sqrt{\tau} + O(\tau^{1/2+\epsilon}),\end{aligned}$$

and thus combining with (7.9) we have

$$\dot{\lambda}^c(0) = -\frac{3}{4}\dot{\xi}(0) + O(\tau),$$

and we conclude

$$\max_{t\in[0,\tau^c]} |\dot{\xi}^c(t)| \le |\dot{\lambda}^c(0)| \le |\dot{\xi}(0)|$$

whenever $\tau < T_W$.*

The EMW family. We again claim that the max in (7.6) is bounded by $|\dot{\xi}^c(0)|$ owing to the concavity of ξ^c. Suppose first that $0 < -u_1 < v_1$. Theorem 5.5 then yields that $-u_1(t) < v_1(t)$ and $\dot{\xi}^c(t) > 0$ for all $t \in [0, \tau^c)$, where $u_1(t)$ and $v_1(t)$ are the images of u_1 and v_1 after t units of time in the un-centered upwards flow under ξ^c. From (5.29) we see

$$\ddot{\xi}^c(t) = \frac{8}{u^2v^2}\left(\frac{u^3+v^3}{uv} + 2(u+v)\right),$$

where we have suppressed subscripts and the t. Hence the inequality $\ddot{\xi}^c(t) > 0$ is equivalent to

$$0 < u^3 + 2u^2v + 2uv^2 + v^3 = (u+v)^3 - uv(u+v). \tag{7.10}$$

*Note that this condition is in terms of τ, not τ^c, since our expansions are in terms of the actual time τ.

or $uv < (u+v)^2$, which is immediate because the left-hand side is negative. The argument for $0 < v_1 < -u_1$ is nearly identical; here we find $\dot{\xi}^c(t) < 0$ and $\ddot{\xi}^c(t) > 0$. In either case, then, $\max_{t\in[0,\tau^c]} |\dot{\xi}^c(t)| \le |\dot{\xi}^c(0)|$.

Using our expressions in Theorem 3.5 for x_1 and y_1 and our shift δ in Table 6.1 for the EMW family and (5.29), we have

$$\dot{\xi}^c(0) = \frac{-4}{-2\sqrt{\tau} + \frac{3}{4}\dot{\xi}(0)\tau - \frac{1}{18}\dot{\xi}(0)^2\tau^{3/2} + O(\tau^{3/2+\epsilon})} + \frac{-4}{2\sqrt{\tau} + \frac{3}{4}\dot{\xi}(0)\tau + \frac{1}{18}\dot{\xi}(0)^2\tau^{3/2} + O(\tau^{3/2+\epsilon})} = \frac{3}{2}\dot{\xi}(0) + O(\tau^{1/2+\epsilon}),$$

with quantitative control on the $O(\tau^{1/2+\epsilon})$ term for all sufficiently small τ. Hence

$$\max_{t\in[0,\tau^c]} |\dot{\xi}^c(t)| \le 2|\dot{\xi}(0)|$$

whenever $\tau < T_{EMW}$.

Circular arc family. As with the Wang and EMW families, it is not hard to see that ξ is concave down, and so it suffices to control $|\dot{\xi}^c(0)|$. Using the explicit formula (5.35), we compute

$$\dot{\xi}^c(0) = -3\Big(\frac{1}{x} + \frac{1}{y}\Big).$$

Since our equilibria shift is $\tilde{\delta} = O(\tau^{3/2+\epsilon})$, our equilibria points are the true points $x(\tau), y(\tau)$ in (3.5) through order $\tau^{3/2}$, and hence we compute

$$-3\Big(\frac{1}{u_1} + \frac{1}{v_1}\Big) = \dot{\xi}(0) + O(\tau^{1/2+\epsilon}),$$

with quantitative control. Hence $|\dot{\xi}^c(0)| \le \frac{3}{2}|\dot{\xi}(0)|$ for $\tau < T_{CA}$. □

7.3 Proof of Theorem 1.1

Families of K-quasiconformal mappings $f : \mathbb{H} \to \mathbb{H}$ are precompact with respect to uniform convergence in the spherical metric on compact sets, but limit points may be constant functions. The following lemma will help us avoid the degenerate case when working with collections of uniformly K-quasislit halfplanes.

Lemma 7.6. *If $\mathbb{H}\backslash\gamma$ is a K-quasislit halfplane, then there exists $\alpha \in (0, \pi/2]$ such that γ is contained in the cone*

$$C_\alpha := \{\, z \in \mathbb{H} \;:\; |\arg(z) - \pi/2| \le \pi/2 - \alpha \,\}. \tag{7.11}$$

Note that the cone C_α has angle α from the positive and negative real axis.

Proof. The associated K-quasiconformal map $f : \mathbb{H} \to \mathbb{H}$ fixes $\mathbb{R}$ and 0, and so $\eta := f([0, i] \cup \mathbb{R}_{\ge 0}) = \gamma \cup \mathbb{R}_{\ge 0}$ is a quasiarc and satisfies Ahlfors' three-point condition. Namely, there exists M such that

$$|\eta_a - \eta_b| \le M|\eta_a - \eta_c| \tag{7.12}$$

for any three successive points $\eta_a, \eta_b, \eta_c \in \eta$ (in either orientation). If there is no such cone, $\arg(\gamma_j) \to 0$ for some sequence $\{\gamma_j\} \subset \gamma$. Considering the triple $0 < \mathrm{Re}(\gamma_j), 0, \gamma_j$ on η, (7.12) becomes $\mathrm{Re}(\gamma_j) \le M\,\mathrm{Im}(\gamma_j)$, or $1 \le M\tan(\arg(\gamma_j)) \to 0$, a contradiction. □

We now have all the pieces in place to prove our main theorem about zipper convergence, Theorem 1.1.

Proof of Theorem 1.1. We establish the equicontinuity (7.1) for each of our curve families. For the Wang, EMW and circular arc family, we have that the constructed driver ξ_n^c has derivative uniformly close to $\dot\xi(t_n)$ on each zipping interval by Lemma 7.5. Hence the ξ_n^c are continuous, piecewise smooth with bounded derivative on their intervals of differentiability, and so in particular are absolutely continuous and Lipschitz, yielding (7.1).

For the straight-slit family, we view the constructed driver ξ_n^c as a piecewise square-root interpolation. It is nearly this for the true driver ξ, but is not exactly because the constructed time increments τ_{nk}^c are generally not identical with the true ones τ_{nk}. The times τ_{nk}^c and τ_{nk} are quantitatively close, however, and so pre-composing the true driver ξ with a small time dilation on each zipper increment (say, a piecewise affine function where the slopes are all close to one) yields a function $\tilde\xi_n$ for which ξ_n^c is a square root interpolation. Let $\ell_n(x)$ be the corresponding linear interpolation of $\tilde\xi_n$; that is, ℓ_n is linear on exactly the same intervals

on which ξ_n^c is a single square-root function. Since ξ is close to linear with controlled error on small intervals by Lemma 3.4, all the slopes of ℓ_n are bounded by some constant $2M$ for large-enough n. Hence for $t_1 < t_2$ we have

$$\begin{aligned}|\xi_n^c(t_2) - \xi_n^c(t_1)| &\le |\xi_n^c(t_2) - \ell_n(t_2)| + |\ell_n(t_2) - \ell_n(t_1)| + |\ell_n(t_1) - \xi_n^c(t_1)| \\ &\le |\xi_n^c(t_2) - \ell_n(t_2)| + 2\sqrt{t_2 - t_1} + |\ell_n(t_1) - \xi_n^c(t_1)| \end{aligned} \tag{7.13}$$

for sufficiently small $|t_2 - t_1|$. If $f(x) = mx + b$ is linear and g is the square-root interpolation (7.2) of f between some $x_1 < x_2$, then by calculus we see

$$\max_{x_1 \le x \le x_2} |f(x) - g(x)| = \frac{m}{4}(x_2 - x_1),$$

and so, writing τ_{nj}^c as the length of the interval containing t_j, (7.13) is bounded by

$$\frac{M}{2}\tau_{nk_2}^c + 2\sqrt{t_2 - t_1} + \frac{M}{2}\tau_{nk_1}^c \;\le\; M \max_j \tau_{nj}^c + 2\sqrt{t_2 - t_1} \;\le\; 3\sqrt{t_2 - t_1}$$

whenever $M^2(\max_j \tau_{nj}^c)^2 \le t_2 - t_1$. For $t_2 - t_1 < M^2(\max_j \tau_{nj}^c)^2$, we have by (7.3) that the Hölder seminorm $|\xi_n^c|_{1/2}$ of ξ_n^c restricted to $[t_1, t_2]$ satisfies

$$|\xi_n^c|_{1/2} \le 2M\sqrt{t_2 - t_1} < 2M^2 \max_j \tau_{nj}^c < 3$$

for all sufficiently large n. We thus have (7.1) for the straight-slit family too.

Note that the times T_n^c of the constructed curves converge to the true time T, as we saw in (6.15) in the proof of Lemma 6.2

In any of these cases, then, Proposition 7.3 yields that our constructed curves γ_n^c are thus uniformly K-quasislit halfplanes. Since the capacity times T_n of the constructed curves are close to T, the cone condition in Lemma 7.6 yields that $\operatorname{diam}(\gamma_n^c) \le D$ for all n. Thus $\{\gamma_n^c\}$ is bounded and further equicontinuous by Proposition 7.3, and hence precompact on compact subintervals of $[0, T)$ by Arzela-Ascoli. Fix such an interval $[0, T_0]$ and take a uniformly-converging subsequence $\gamma_{n_k}^c \to \tilde{\gamma}$ on $[0, T_0]$. To complete the proof it suffices to show that $\tilde{\gamma}$ is identical to γ on $[0, T_0]$. Note that the time interval $[0, T_0]$ for γ_n^c, the beginning of the curve, corresponds to concluding time interval $[T_n^c - T_0, T_n^c]$ for ξ_n^c.

First, we claim that this limit is actually a simple curve, i.e. $\tilde{\gamma}$ is injective. Let f_n be the associated K-quasiconformal self-maps of $\mathbb{H}$ which fix ∞ and satisfy $f_n([0,i]) = \gamma_n^c$. The family $\{f_n\}$ is normal in $\mathbb{H}$ with respect to the spherical metric [19, §2.2f]; after extracting a convergent subsequence and relabelling, we may assume $f_n \to f$ locally uniformly in $\mathbb{H}$, where f is either a constant in $\partial_{\hat{\mathbb{C}}}\mathbb{H}$ or is a K-quasiconformal self-map of $\mathbb{H}$. Since the capacity times T_n are near T, $f_n([0,i])$ cannot degenerate to 0 or ∞, the only options by the cone condition, showing that $f : \mathbb{H} \to \mathbb{H}$ is K-quasiconformal. Hence $\tilde{\gamma} \subset f([0,i])$ is, indeed, a Jordan arc.

By construction of the equilibria points, $\xi_n^c(T_n) = \xi(T)$ for all n. When we reverse ξ_n^c and ξ to obtain the downwards drivers $\lambda_n^c(t) = \xi_n^c(T_n - t) - \xi_n^c(T_n)$ and $\lambda(t) = \xi(T-t) - \xi(T)$, therefore, we still have the uniform convergence $\lambda_n^c \to \lambda$ on $[0, T_0]$. By Proposition 7.2, then, we have that the driver for $\tilde{\gamma}$ is $\lambda|_{[0,T_0]}$, and hence that $\tilde{\gamma}$ is γ on $[0, T_0]$, completing the proof.

In this argument we zipped up each time with a fixed curve family, but selecting different curve families from zip to zip also poses no difficulty. The argument is identical once we establish the equicontinuity (7.1) for the constructed drivers ξ_n^c with constants C and D independent of the curve family. When we alternate between different families on different zips, we end up with an "interpolation" of the piecewise linear function ℓ_n defined above which is a square-root function on some intervals and consists of uniformly-Lipschitz, monotonic functions on the others.[†] Its Hölder constant is comparable to switching everywhere to the square-root interpolation, which satisfies (7.1) by the above, and thus we still obtain the correct limiting curve through the quasiconformal mapping argument, as above. □

[†]Recall that the equilibria-point construction does not depend on what we have previously zipped up with the constructed curve, but only on the true location of the next data points. So switching between various curve families does not interfere with the analysis. For instance, if we zip up only with one of the three smooth families, we end up with a globally Lipschitz driver. That same Lipschitz constant thus works on all the intervals we use that driver for as we "mix and match."

Chapter 8

ZIPPER ENERGIES

8.1 Introduction and overview

What is the connection between the Loewner energy

$$\frac{1}{2}\int_{-\infty}^{\infty} \dot{\xi}(t)^2 dt$$

of a Jordan curve $\gamma \subset \hat{\mathbb{C}}$ and its conformal welding $\varphi : \partial\mathbb{D} \to \partial\mathbb{D}$? The problem of characterizing the weldings of finite-energy loops, i.e. those belonging to the Weil-Petersson class $T_0(1)$, was posed by Takjatan-Teo [39] and solved by Shen [38], who showed that $\gamma \in T_0(1)$ iff φ is absolutely continuous with $\log(\varphi') \in H^{1/2}$. Bishop [5] has recently given other characterizations of φ. It remains to be shown, however, how to *compute* the Loewner energy from the welding: while $I_L(\gamma) < \infty$ iff φ is absolutely continuous with $\|\log(\varphi')\|_{H^{1/2}} < \infty$, it is not known whether $\|\log(\varphi')\|_{H^{1/2}}$ or any of Bishop's quantities are a function of $I_L(\gamma)$.

In this section we show that one can compute the Loewner energy directly from the welding via the zipper algorithm. The simple idea is based off of the expansions for the welding points in Theorem 3.5, but uses a quantity that does not assume any regularity, namely the "zipping angle" $\alpha = \frac{y}{y-x}$ of the next data points $x < 0 < y$. We show that the ℓ^2-sum of the deviations of the angles from $1/2$, the *zipper welding energy*, converges to a multiple of the Loewner energy when the zipper is run from the equilibria points. We conjecture a similar identity holds when using the actual welding data. See Theorems 8.2 and 8.8. We also offer several instances of numerically computing the welding energy for the actual data points (not the equilibria points). These suggest a close connection between the flow of the equilibria points and the actual data points as the algorithm proceeds, and also suggest the welding energy diverges when the Loewner energy does. Hence the finiteness

of the welding energy may characterize finite-energy curves, as we hope to settle in future work. See Examples 8.4, 8.5 and 8.7.

We step back in §8.2.1 and ask if the idea behind the welding energy would be able to classify the various familiar subclasses of Teichmüller space: quasislit half planes, asymptotically smooth curves, and elements of p-summable Teichmüller space. This may be the real significance of the welding energy: it may offer new "zipper-characterizations" of classes of regularity which conceptually parallel the existing characterizations.

Lastly, in §8.3 we discuss a "dual" notion of energy, the *zipper angle energy*, that would have similar properties as the welding energy, and which we hope to investigate in future work. This energy may likewise offer new characterizations of familiar sub-classes of the universal Teichmüller space, including finite-energy curves. Furthermore, it appears to offer a purely geometric way to compute the Loewner energy, where "geometric" is interpreted in the context of the intermediate zipper curves.

8.2 The zipper welding energy

When using the straight-slit curve family, a natural quantity is the angle β_k of the kth zip from $\mathbb{R}_{\geq 0}$. Figure 8.1 plots $\alpha_k = \beta_k/\pi$ for a run of the zipper on smooth data φ with one point x_0 where $\varphi'(x_0) = 0$. When the welding φ is C^1 with slope bounded away from zero, numerical experiments show that these angles α_k tend to $1/2$ as the mesh size decreases, as we see for the zips "away from" where $\varphi'(x_0) = 0$ in Figure 8.1a. For the straight-slit zipper, one has the simple formula

$$\beta_k = \frac{\pi s}{s - r},$$

where $s < 0 < r$ are the next data points to be zipped up. Since this expression makes sense for any curve family, we define the *(normalized) zipping angle* α_k of the kth zip by

$$\alpha_k := \frac{s_k}{s_k - r_k} \in (0, 1), \tag{8.1}$$

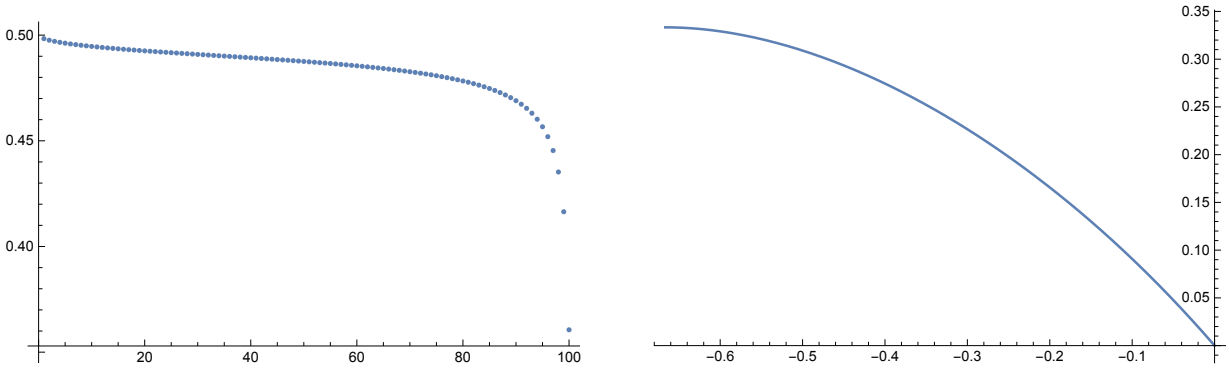

(a) The x-axis is the zip number and the y-axis is α_k.

(b) The curve welding φ for a line segment from 0 to $e^{i\pi/3}$.

Figure 8.1: A plot (a) of the "angles" α_k for a run of the zipper on data drawn from the welding φ in (b), which welds to a line segment. The zero slope of φ at $x = -2/3$ corresponds to where the α_k have their pronounced deviation from 1/2.

when $r_k < 0 < s_k$ are the next data points to be zipped up. The quantity $|\alpha_k - \frac{1}{2}|$ is then a measurement of how "rough" the current zip is; if this is zero for all k, for instance, we have the most regular-possible curve in terms of $\dot{\xi}$ and φ, a segment of the imaginary axis.

It is easy to give an explicit expansion for the α_k when our data ξ is regular and we are using the equilibria points of a tractable curve family (recall Definition 5.1). Without loss of generality we are on the first zip with $\xi^c(0) = \xi(0) = 0$.

Lemma 8.1. *Fix a tractable curve family $\mathcal{C}$ with constant c in* (5.1)*. If $\xi \in C_0^{3/2+\epsilon}$ welds points $x_1 < 0 < y_1$ together at time τ, the angle α_1 for the equilibria points $x_1 + \delta$ and $y_1 + \delta$ for $\mathcal{C}$ is*

$$\alpha_1 = \frac{1}{2} + \frac{1}{8c}\dot{\xi}(0)\sqrt{\tau} + O(\tau^{1+\epsilon}) \tag{8.2}$$

as $\tau \to 0^+$, with quantitative control on the error.

Proof. Using the formulas in lemmas 3.5 and 6.1, and writing $d = \frac{1}{2}\left(\frac{1}{c} - \frac{4}{3}\right)$, we compute

$$\begin{aligned}\alpha_1 = \frac{y_1 + \delta}{y_1 + \delta - (x_1 + \delta)} &= \frac{1}{2} \cdot \frac{1 + \left(\frac{1}{3} + \frac{d}{2}\right)\dot{\xi}(0)\sqrt{\tau} + \frac{1}{36}\dot{\xi}(0)^2\tau + O(\tau^{1+\epsilon})}{1 + \frac{1}{36}\dot{\xi}(0)^2\tau + O(\tau^{1+\epsilon})} \\ &= \frac{1}{2} + \frac{1}{8c}\dot{\xi}(0)\sqrt{\tau} + O(\tau^{1+\epsilon}).\end{aligned}$$

As we have quantitative control on the errors in expansions of x_1 and y_1 (Theorem 3.5), control on $O((x+y)^3/(y-x)^2)$ in (5.1) gives control on the $O(\tau^{1+\epsilon})$-term. □

Table 8.1 shows the zipping angle for the equilibria points for our several curve families for data $\xi \in C^{3/2+\epsilon}$. Notice that the α_{nk} are uniformly close to $1/2$ if the true time increments τ_{nk} are uniformly small.

Definition 8.1. The *zipper welding energy* $I_W(\mathcal{P}, \mathcal{C})$, or *welding energy* for short, for the $\mathcal{C}$-zipper run on data $\mathcal{P} = \{(x_k, y_k)\}_{k=1}^N$ is

$$I_W(\mathcal{P}, \mathcal{C}) := \sum_{k=1}^{N} \left(\alpha_k - \frac{1}{2}\right)^2. \tag{8.3}$$

Our main theorem in this section is that the welding energy, when run on the equilibria points, converges to a multiple of the Loewner energy.

Theorem 8.2. *Let γ and ξ be as in Theorem 1.1, with $\{\mathcal{P}_n\}_{n=1}^\infty$ a sequence of discretizations of γ's welding whose x-values satisfy* (1.1)*. Fix a tractable curve family $\mathcal{C}$ and let $\{\mathcal{Q}_n\}_{n=1}^\infty$ be the corresponding equilibria-point partitions, with α_{nk} the zipping angle for the kth zip in $\mathcal{Q}_n$. Then*

$$\lim_{n\to\infty} \sum_{k=1}^{N(n)} \left(\alpha_{nk} - \frac{1}{2}\right)^2 = \frac{1}{64c^2} \int_0^T \dot{\xi}(t)^2 dt = \frac{1}{32c^2} I(\gamma), \tag{8.4}$$

where c is the curve-family constant in (5.1)*.*

Note in this theorem that we are using a single curve family for all zips; "mixing and matching" between different flavors of curves is not allowed. See Table 8.1 for the constants $\frac{1}{64c^2}$ for our curve families.

Curve family	*Zipping angle* α_k	*Limit of* $I_W(\mathcal{Q}_n)$
EMW	$\frac{1}{2} + \frac{3}{16}\dot{\xi}(t_{k-1})\sqrt{\tau_k} + O(\tau_k^{1+\epsilon})$	$\frac{9}{128}I(\gamma)$
Circular arc	$\frac{1}{2} + \frac{1}{6}\dot{\xi}(t_{k-1})\sqrt{\tau_k} + O(\tau_k^{1+\epsilon})$	$\frac{1}{18}I(\gamma)$
Wang minimizer	$\frac{1}{2} + \frac{3\pi}{64}\dot{\xi}(t_{k-1})\sqrt{\tau_k} + O(\tau_k^{1+\epsilon})$	$\frac{9\pi^2}{2048}I(\gamma)$
Straight slit	$\frac{1}{2} + \frac{1}{8}\dot{\xi}(t_{k-1})\sqrt{\tau_k} + O(\tau_k^{1+\epsilon})$	$\frac{1}{32}I(\gamma)$

Table 8.1: Zipping angles (8.1) for the equilibria points of our several curve families. Here t_{k-1} is the time elapsed for the true curve through the point corresponding to $k-1$ zips, and τ_k is the time corresponding to the kth zip on the true curve. All the $O(\tau_k^{1+\epsilon})$ terms are quantitative. These are calculated from Theorem 3.5 and Table 6.1.

Proof. Using (8.2), we compute

$$\begin{aligned} I_W(\mathcal{Q}_n, \mathcal{C}) &= \sum_{k=1}^{N(n)} \Big(\frac{1}{8c}\dot{\xi}(t_{n,k-1})\sqrt{\tau_{nk}} + O(\tau_{nk}^{1+\epsilon}) \Big)^2 \\ &= \frac{1}{64c^2} \sum_{k=1}^{N(n)} \dot{\xi}(t_{n,k-1})^2 \tau_{nk} + O\Big(\sum_{k=1}^{N(n)} \tau_{nk}^{3/2+\epsilon} \Big), \end{aligned} \tag{8.5}$$

since we have quantitative control of each $O(\tau_{nk}^{1+\epsilon})$ term, $\dot{\xi}$ is bounded, and τ_{nk} is uniformly small for large n. The first term in (8.5) is a (left) Riemann sum which converges to the desired integral by assumption (1.1) on the τ_{nk}. The second term vanishes in the limit, since

$$\sum_{k=1}^{N(n)} \tau_{nk}^{3/2+\epsilon} \le \max_{1\le j\le N(n)} \tau_{nj}^{1/2+\epsilon} \sum_{k=1}^{N(n)} \tau_{nk} = \big(\max_{1\le j\le N(n)} \tau_{nj}^{1/2+\epsilon} \big) T \to 0. \qquad \square$$

Remark 8.3. The straight-slit curve family satisfies the assumptions in Theorem 8.2, and so we can use its zipper to compute the energy of smooth curves. This is initially surprising, since the constructed curves γ_n^c always have infinite Loewner energy (unless all the angles are $1/2$), owing to the corners between subsequent zips. The welding energy thus offers a

helpful intermediary between the geometry of an approximating curve and the smoothness of the limit.

Example 8.4. Consider the Wang minimizer curve through $\theta = \pi/4$ in Figure 8.2a. Recall from Theorem 5.2 that its Loewner energy is $-8\log(\sin(\pi/4)) = 4\log(2)$. Hence if $\mathcal{C}_s$ and $\mathcal{C}_c$ are the straight-slit and circular-arc curve families, respectively, Theorem 8.2 yields

$$I_W(\mathcal{Q}_n, \mathcal{C}_s) \to \frac{1}{8}\log(2) \qquad \text{and} \qquad I_W(\mathcal{Q}_n, \mathcal{C}_c) \to \frac{1}{9}\log(2)$$

for *equilibria-point* data partitions $\mathcal{Q}_n$. The welding for these curves is explicitly computed in [26], and so we can numerically run the zipper on the true welding points $\mathcal{P}_n$ and compute the associated welding energies. Figure 8.2b shows that the true data points appear to give the same asymptotic welding energy as the equilibria points for the straight-slit zipper, whereas we see in Figure 8.2c that for the circular arc zipper, the true points give asymptotically twice the welding energy of the equilibria points. The reason for this discrepancy is not currently understood. In either case, however, we see a close connection between the flow of the true points $\mathcal{P}_n$ compared to the flow of the equilibria points $\mathcal{Q}_n$.

Example 8.5. For a second example, consider the curve γ which begins at the origin and traces a portion of the circular arc of radius $1/2$ centered at $1/2$, as in Figure 8.3a. One can explicitly compute that this curve has (forward-time) driver $\lambda(t) = \frac{3}{2}(1 - \sqrt{1-8t})$, $0 \le t \le 1/8$, and hence Loewner energy

$$\frac{1}{2}\int_0^T \frac{36}{1-8t}dt = -\frac{9}{4}\log(1-8T)$$

for $0 \le T < 1/8$. Consider the segment with capacity time $T = 0.1$ and thus energy $\frac{9}{4}\log(5)$. Theorem 8.2 yields

$$I_W(\mathcal{Q}_n, \mathcal{C}_s) \to \frac{9}{128}\log(5) \qquad \text{and} \qquad I_W(\mathcal{Q}_n, \mathcal{C}_c) \to \frac{1}{16}\log(5).$$

In Figure 8.3b, we again run the straight-slit zipper on a sequence of true data point meshes $\mathcal{P}_n$, and again see that the welding energies appear to converge to the same multiple of $I(\gamma)$

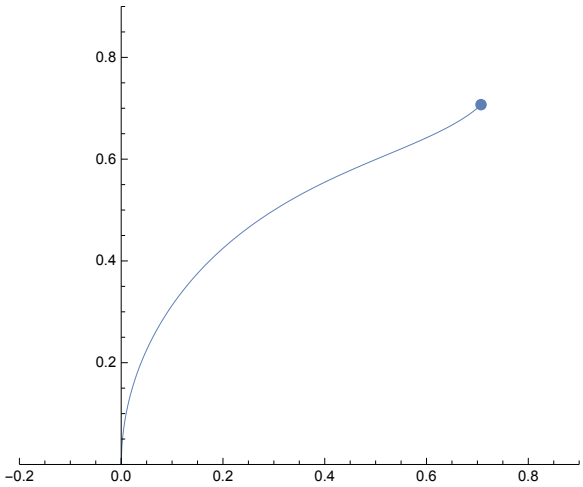

(a) The energy-minimizing curve through $e^{i\pi/4}$.

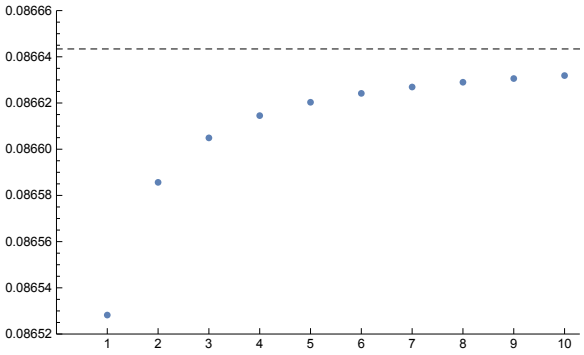

(b) Welding energies for partitioning the welding interval into $100k$ increments, $1 \leq k \leq 10$. The dashed line is $y = \frac{1}{8}\log(2)$, the value for the asymptotic equilibria-point energy.

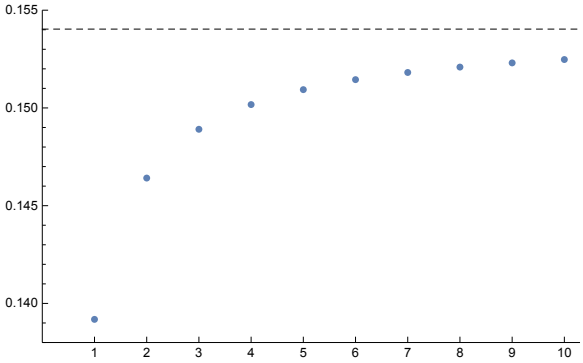

(c) Welding energies for the same partitions with the circular arc zipper. The dashed line is $y = \frac{2}{9}\log(2)$, twice the value of the asymptotic equilibria-point energy.

Figure 8.2: Numerical welding energies from the true welding discretizations $\mathcal{P}_n$ for the Wang minimizer through $\theta = \pi/4$.

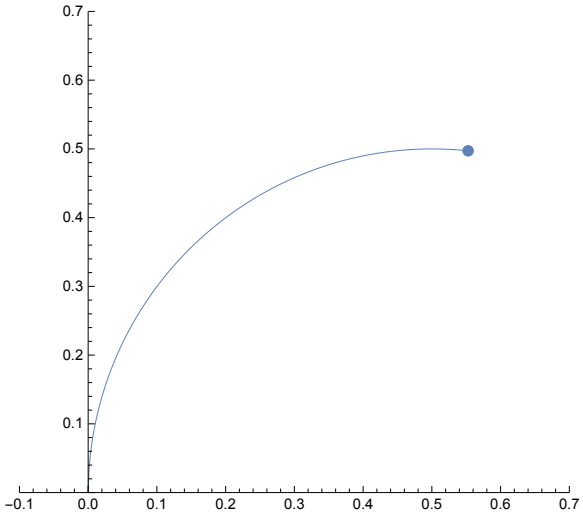

(a) A portion of a hyperbolic geodesic in $\mathbb{H}$.

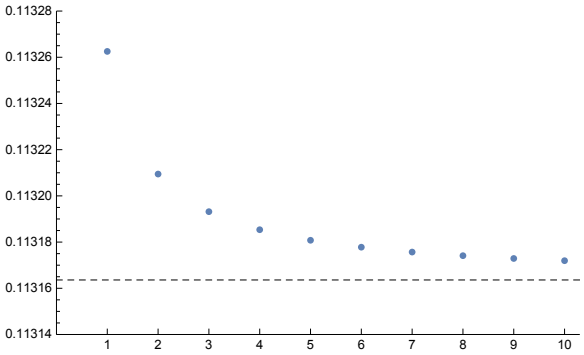

(b) Welding energies for partitioning the welding interval into $100k$ increments, $1 \leq k \leq 10$. The dashed line is $y = \frac{9}{128}\log(5)$, the value for the asymptotic equilibria-point energy..

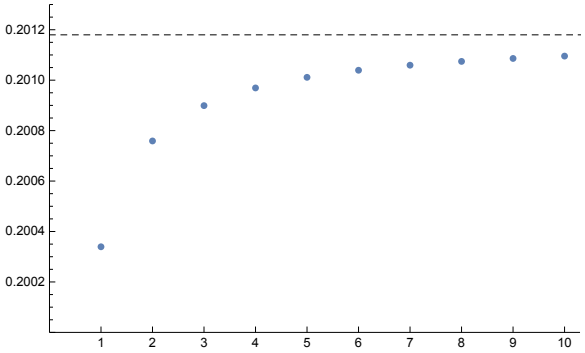

(c) Welding energies for the same partitions with the circular arc zipper. The dashed line is $y = \frac{1}{8}\log(5)$, twice the value of the asymptotic equilibria-point energy.

Figure 8.3: Numerical welding energies for the true welding discretizations $\mathcal{P}_n$ for the circular arc in (A).

as for the equilibria points. Figure 8.3c shows that the energy for the circular arc family on $\mathcal{P}_n$ again converges to twice the energy of the $\mathcal{Q}_n$.

These examples suggest a strong connection between the location of the equilibria points and the true welding points as the curve is zipped up, the full details of which are not currently understood. We conjecture, however, that a result analogous to Theorem 8.2 holds with the actual welding data.

Conjecture 8.6. *Let γ and ξ be as in Theorem 1.1, with $\{\mathcal{P}_n\}_{n=1}^{\infty}$ a sequence of discretizations of γ's welding whose x-values satisfy* (1.1)*. For a fixed tractable curve family $\mathcal{C}$,*

$$\lim_{n\to\infty} I_W(\mathcal{P}_n, \mathcal{C}) = C \int_0^T \dot{\xi}(t)^2 dt = \frac{C}{2} I(\gamma),$$

where $C = C(\mathcal{C})$ is a constant which depends only upon the curve family.

One last example suggests that we could define the Loewner energy via (8.4), in the sense that the limiting welding energy and the integral are either simultaneously finite and equal or simultaneously infinite.

Example 8.7. Consider the line segment γ in $\mathbb{H}$ from 0 to $\gamma(T) = ae^{i\pi/3}$ where $a = (1/3)^{1/3}(2/3)^{2/3}$. The centered upwards Loewner map F is $F(z) = (z - 1/3)^{1/3}(z + 2/3)^{2/3}$ (see [17, Example 4.12]), which maps the intervals $[-2/3, 0]$ and $[0, 1/3]$ onto either side of γ. Solving $F(\varphi(x)) = F(x)$ on $[-2/3, 0]$ yields the explicit welding

$$\varphi(x) = \frac{1}{2}(-1 - x + \sqrt{1 - 2x - 3x^2}) \qquad -2/3 \le x \le 0,$$

which we discretize to form $\mathcal{P}_n$. The driving function for γ is

$$\xi(t) = \sqrt{2(1/18 - t)} - 1/3, \qquad 0 \le t \le 1/18 = T,$$

which has infinite Loewner energy. Figure 8.4 plots φ and the welding energy for the straight-slit zipper for divisions of $I = [-2/3, 0]$ into $100 \cdot 2^{k-1}$ equally-spaced intervals, $1 \le k \le 7$. It thus appears that a partition of n equal sub-intervals of $[-2/3, 0]$ yields welding energy $O(\log(n))$.

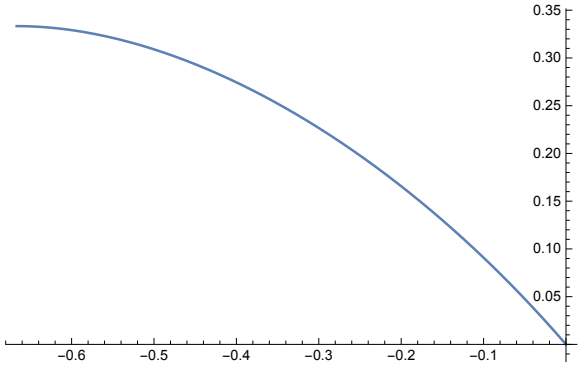

(a) The curve welding φ for a line segment at angle $\pi/3$ from $\mathbb{R}_{\geq 0}$.

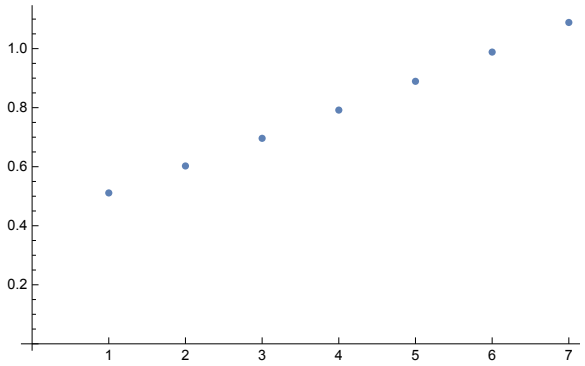

(b) Welding energies for the straight-slit zipper when partitioning the welding interval into $100 \cdot 2^{k-1}$ increments, $1 \leq k \leq 7$.

Figure 8.4: An example where $I(\xi) = \infty$ and the welding energies likewise appear to diverge.

If we have a $C^{3/2+\epsilon}$-driver ξ on all of $[0, \infty)$ instead of just $[0, T]$, we can also consider the sum (8.3) on any sequence of points $\{(x_{nk}, y_{nk})\}_{k=1}^{N(n)}$ welded together by ξ. If

$$I(\xi) := \frac{1}{2} \int_0^\infty \dot{\xi}(t)^2 dt < \infty,$$

ξ expels most of its energy on some compact interval $[0, T]$, and so Theorem 8.2 suggests something akin to (8.4) should hold for the improper integral, so long as we can control $(\alpha_{nk} - 1/2)^2$ for zips "many steps out." We can do so using the EMW family, so long as our starting data points are reasonable. To this end we introduce "locally fine" discretizations. If $\mathcal{P}_n = \{(x_{nk}, y_{nk})\}_{n=1}^{N(n)}$ is a welding discretization, we say a sequence $\{\mathcal{P}_n\}$ is *locally fine* if for every $L < 0$, there exists $M = M(L)$ such that $x_{n,N(n)} < L$ for all $n \geq M$ and

$$\lim_{n \to \infty} \max_{[x_{nj}, x_{n,j-1}] \cap [L,0] \neq \emptyset} \operatorname{hcap}_\gamma(x_{nj}, x_{n,j-1}) = 0. \tag{8.6}$$

We say $\{(x_{nk}, y_{nk})\}_{n=1}^{N(n)}$ is a *welding partition for* ξ if ξ welds each x_{nk} to y_{nk}.

Theorem 8.8. *Let $\xi \in C^{3/2+\epsilon}([0, \infty))$ with $I(\xi) < \infty$, and let $\{\mathcal{P}_n = \{(x_{nk}, y_{nk})\}_{n=1}^{N(n)}\}$ be a sequence of locally fine welding partitions for ξ. Fix a tractable curve family $\mathcal{C}$ and let*

$\{\mathcal{Q}_n\}_{n=1}^{\infty}$ be the corresponding equilibria-point partitions, with α_{nk} the angle for the kth zip in $\mathcal{Q}_n$. Then

$$\lim_{n\to\infty}\sum_{k=1}^{N(n)}\left(\alpha_{nk}-\frac{1}{2}\right)^2=\frac{1}{64c^2}\int_0^{\infty}\dot{\xi}(t)^2dt=\frac{1}{32c^2}I(\xi), \tag{8.7}$$

where c is the curve-family constant in (5.1).

Proof. For a given $0<\epsilon<1$, choose T such that

$$\int_T^{\infty}\dot{\xi}(t)^2dt<\epsilon. \tag{8.8}$$

Let $x_T<0$ be the point hitting ξ at time T, and for each n let $\ell_n\le N(n)$ be the largest index such that $[x_{n,\ell(n)},x_{n,\ell(n)-1}]\cap[x_T,0]\neq 0$. If $t_{n,\ell(n)}:=\sum_{k=1}^{\ell(n)}\tau_{kn}$ is the time of the true curve up to $x_{n,\ell(n)}$, then we can repeat the computation in the proof of Theorem 8.2 to see that $\sum_{k=1}^{\ell_n}\left(\alpha_{nk}-\frac{1}{2}\right)^2$ is close to $\frac{1}{64c^2}\int_0^{t_{n,\ell(n)}}\dot{\xi}(t)^2dt$ (note by our regularity assumption $\dot{\xi}$ is bounded on $[0,\infty)$ and so the expansion in (8.5) is still valid). Since $\{\mathcal{P}_n\}$ is locally fine, applying (8.6) on the interval $[x_T-1,0]$, say, shows that $t_{n,\ell(n)}\searrow T$, and hence

$$\begin{aligned}&\left|\sum_{k=1}^{\ell_n}\left(\alpha_{nk}-\frac{1}{2}\right)^2-\frac{1}{64c^2}\int_0^{T}\dot{\xi}(t)^2dt\right|\\&\qquad\le\left|\sum_{k=1}^{\ell_n}\left(\alpha_{nk}-\frac{1}{2}\right)^2-\frac{1}{64c^2}\int_0^{t_{n,\ell(n)}}\dot{\xi}(t)^2dt\right|+\left|\frac{1}{64c^2}\int_T^{t_{n,\ell(n)}}\dot{\xi}(t)^2dt\right|<\epsilon\end{aligned}$$

for all sufficiently large n (we have uniform control on the first term in the second line by elementary Riemann sum error estimates).

Let ϵ_{nk} be the Loewner energy for ξ corresponding to the interval $[x_{n,k+1},x_{nk}]$,

$$\epsilon_{nk}:=\frac{1}{2}\int_{t_{nk}}^{t_{n,k+1}}\dot{\xi}(t)^2dt.$$

By (8.8), $\sum_{k=\ell_n+1}^{N(n)}\epsilon_{nk}<\epsilon$ for each n, and we claim that $\sum_{k=\ell_n+1}^{N(n)}\left(\alpha_{nk}-\frac{1}{2}\right)^2$ must be small too. To see this, we recall from Theorem 5.5 that the Loewner energy $E(\alpha)$ expelled by the EMW curve for welding two points with angle α is

$$E(\alpha)=-4\log(4\alpha(1-\alpha)),\qquad\text{implying}\qquad\left|\alpha-\frac{1}{2}\right|=\frac{1}{2}\sqrt{1-e^{-E(\alpha)/4}}.$$

So if $|\alpha_{nk} - 1/2| > \frac{1}{2}\sqrt{1 - e^{-\epsilon_{nk}/4}}$, then ξ spends less energy than the energy-minimizing curve on the corresponding segment, a contradiction, yielding

$$\sum_{k=\ell_n+1}^{N(n)} \big(\alpha_{nk} - \frac{1}{2}\big)^2 \leq \sum_{k=\ell_n+1}^{N(n)} \frac{1}{4}(1 - e^{-\epsilon_{nk}/4}) \leq \frac{1}{4} \sum_{k=\ell_n+1}^{N(n)} \frac{\epsilon_{nk}}{4} < \frac{\epsilon}{16}.$$

Altogether, then,

$$\left| \sum_{k=1}^{N(n)} \big(\alpha_{nk} - \frac{1}{2}\big)^2 - \frac{1}{64c^2} \int_0^\infty \dot{\xi}(t)^2 dt \right| \leq \left| \sum_{k=1}^{\ell(n)} \big(\alpha_{nk} - \frac{1}{2}\big)^2 - \frac{1}{64c^2} \int_0^T \dot{\xi}(t)^2 dt \right| + \frac{\epsilon}{16} + \epsilon < \frac{33}{16}\epsilon$$

for all large n. □

As Rohde and Wang [33] extended the Loewner energy of a simple curve $\gamma \subset \mathbb{H} \cup \{0\}$ to the energy of a loop on the Riemann sphere $\hat{\mathbb{C}}$ (which ended up having deep connections in Teichmüller theory [43]), so we hope in future work to extend the welding energy to a loop welding energy. Given the close connection between the welding and Loewner energies, we conjecture the following in the chordal case and hope to extend it to a loop welding energy on the sphere.

Conjecture 8.9. *Let ξ be any driving function and $\{\mathcal{P}_n = \{(x_{nk}, y_{nk})\}_{n=1}^{N(n)}\}$ a sequence of locally fine welding partitions for ξ. Then for a tractable curve family $\mathcal{C}$,*

$$\lim_{n\to\infty} I_W(\mathcal{P}_n, \mathcal{C}) = C \int_0^\infty \dot{\xi}(t)^2 dt,$$

where equality takes place in the extended non-negative reals $[0, +\infty]$. Here $C = C(\mathcal{C})$ is a constant which depends only upon the curve family.

8.2.1 Discussion and questions

While the welding energy originates from the amiable infinitesimal expansions (3.11) and (3.12), the resulting expression $\alpha - 1/2$ is defined independent of smoothness. As we suspect that the finiteness $\sup_n \sum(\alpha_{nk} - 1/2)^2$ characterizes finite-energy curves (Conjecture 8.9), it is also natural to ask if $(\alpha_{nk} - 1/2)$ provides a measure of local curvature which also characterizes

other familiar classes of regularity. For instance, does boundedness of $(\alpha_{nk}-1/2)$ characterize quasislit half-planes? (Here the α_{nk} would have to be expanded to include the "angles" for all the data points, not just the next two to be zipped up.) Is γ an element of the p-summable Teichmüller space (see §9.1) if and only if for every sequence $\{\mathcal{P}_n\}$,

$$\sup_n \sum_{k=1}^{N(n)} \Big(\alpha_{nk} - \frac{1}{2}\Big)^p < \infty?$$

Are asymptotically smooth curves characterized by the vanishing of $\alpha_{nk}-1/2$ on small scales,

$$\lim_{n\to\infty} \max_{1\le k\le N(n)} \Big(\alpha_{nk} - \frac{1}{2}\Big) = 0?$$

Settling these questions is a goal for future work, and may prove relevant for extending our arguments for zipper convergence to the larger classes of drivers.

8.3 The zipper angle energy

The zipper welding energy arises from our expansions for the welding points in Theorem 3.5. These are parallel to the expansion for the curve itself

$$\gamma(t) = 2i\sqrt{t} + \frac{2}{3}\dot\lambda(0)t - \frac{i}{18}\dot\lambda(0)^2 t^{3/2} + \Big(\frac{4}{15}\ddot\lambda(0) + \frac{1}{135}\dot\lambda(0)^3\Big)t^2 + O(t^{5/2}) \tag{8.9}$$

as $t \to 0$ for sufficiently-smooth γ in terms of the driver at zero [24, Prop. 3.3], [22, Prop. 6.2]; the constants are even identical. If $\dot\lambda(0) > 0$, (8.9) immediately yields

$$\arg(\gamma(t)) = \frac{\pi}{2} - \arctan\Big(\frac{\mathrm{Re}(\gamma_\theta(t))}{\mathrm{Im}(\gamma_\theta(t))}\Big) = \frac{\pi}{2} - \frac{1}{3}\dot\lambda(0)\sqrt{t} + O(t^{3/2}),$$

and hence

$$\Big(\arg(\gamma(t)) - \frac{\pi}{2}\Big)^2 = \frac{1}{9}\dot\lambda(0)^2 t + O(t^2). \tag{8.10}$$

So if we run the zipper on a sequence of partitions and denote the curve segment in $\mathbb{H}$ formed by the kth zip in the nth stage as γ_{nk}, we expect, as with the welding energy, that summing

the square deviations of the angle of tip of γ_{nk} from $\pi/2$ will converge to a multiple of the Loewner energy,

$$\lim_{n\to\infty} \sum_{k=1}^{N(n)} \Big(\arg(\gamma_{nk}(\tau_{nk})) - \frac{\pi}{2} \Big)^2 \to C \int_0^\infty \dot{\lambda}(t)^2 dt. \tag{8.11}$$

Working out the details would parallel our work for the welding energy above, but we have not pursued this for lack of time. We also may need more terms in our expansions (3.11) and (3.12) to do the infinitesimal analysis. We immediately see from (8.10), however, that if we zip up with the true curve on every increment, we have the convergence in (8.11) with $C = 1/9$. Note that this gives, by means of the zipper, an explicitly *geometric* way to compute the Loewner energy.

As with the welding energy, the difference $(\arg(\gamma_{nk}(\tau_{nk})) - \pi/2)$ assumes nothing about the regularity of γ, and we could ask the same questions about this energy as for the welding energy in §8.2.1, namely, can we use the angle energy to classify quasi-slit halfplanes, asymptotically conformal curves, finite energy curves, or curves in T_p?

As an aside, we note that the zipper welding energy and the zipper angle energy run conceptually parallel to the EMW and Wang curve families, respectively.

Chapter 9

INTEGRABLE TEICHMÜLLER SPACE AND β-NUMBERS

In this final chapter we extend a result of Bishop [5] from the class of Weil-Petersson curves T_2 to the p-integrable Teichmüller space T_p for any $2 < p < \infty$. Bishop showed that T_2 curves γ are characterized by square summable β-numbers,

$$\sum_{Q \in \mathcal{Q}} \beta_Q(\gamma)^2 < \infty, \tag{9.1}$$

where $\mathcal{Q}$ is the collection of dyadic squares in the plane. See §9.1 and §9.2 below for definitions of T_p and the β-numbers, respectively. We show in Theorem 9.1 that summable β-numbers also characterize T_p for $p > 2$, but with exponent p replacing the square in (9.1).

In what follows, we give background on the p-summable Teichmüller space and the β-numbers in §9.1-§9.2, establish notation in §9.3, and prove Theorem 9.1 in §9.4 and §9.5. We discuss some consequences and questions related to our result in §9.6.

9.1 Background on p-integrable Teichmüller space

Let $\gamma \subset \mathbb{C}$ be a quasicircle, that is, the image of $\partial\mathbb{D}$ under a quasiconformal mapping $q : \mathbb{D} \to \mathbb{D}$. Let $\mu_\gamma = \frac{\overline{\partial} q}{\partial q}$ be the complex dilatation of q on $\mathbb{D}$, and f the conformal map of $\mathbb{D}$ onto the bounded component Ω of $\mathbb{C}\backslash\gamma$. For $1 \leq p < \infty$, the *p-integrable Teichmüller space* T_p is the collection of quasicircles γ for which either of the following equivalent conditions hold:

$$Pf(z)(1 - |z|^2) \in L^p(\mathbb{D}, dA_\rho) \tag{9.2}$$

$$\text{or} \qquad Sf(z)(1 - |z|^2)^2 \in L^p(\mathbb{D}, dA_\rho), \tag{9.3}$$

where $dA_\rho = \frac{4dxdy}{(1-|z|^2)^2}$ is the hyperbolic area measure in $\mathbb{D}$, $Pf = \log(f')' = \frac{f''}{f'}$ is the pre-Schwarzian derivative of f and

$$Sf(z) = (Pf)' - \frac{1}{2}(Pf)^2 = \frac{f'''}{f'} - \frac{3}{2}\Big(\frac{f''}{f'}\Big)^2$$

is the Schwarzian derivative of f. Recalling that the *Besov space* B_p consists of those analytic functions f on $\mathbb{D}$ for which $f'(z)(1-|z|^2) \in L^p(\mathbb{D}, dA_\rho)$, we see that T_p is equivalently characterized by $\log(f') \in B_p$.

The space T_2 was introduced by Cui [8], and Guo generalized to other p in [12]. Guo defined T_p by (9.3) for $1 \le p < \infty$, and proved the equivalence of (9.2) and (9.3) when $1 < p < \infty$ [12, Thm 1]. Jones [14, Lemma 3.2] subsequently showed the conditions are also equivalent when $p = 1$. Guo [12, Thm 2] also showed that $\gamma \in T_p$, $2 \le p < \infty$, if and only if there is a quasiconformal map $q : \mathbb{D} \to \mathbb{D}$ taking $\partial\mathbb{D}$ to γ which is conformal on $\mathbb{D}^*$ and whose complex dilatation μ satisfies

$$\mu \in L^p(\mathbb{D}, dA_\rho).$$

There is also an operator-theoretic characterization from Jones [14] for $1 \le p < \infty$, which states $\gamma \in T_p$ if and only if its Grunsky operator Γ is in the pth Schatten class, which is to say the singular values $\{\sigma_j\}_{j=1}^\infty$ of the Hermitian operator $\sqrt{\Gamma^*\Gamma}$ lie in ℓ^p,

$$\sum_{n=1}^{\infty} \sigma_n^p < \infty.$$

We will not dwell further on the operator theory, other than to note that the philosophy of T_p is clearly "p-summability". Bishop [5] describes T_2 as those quasicircles having "local curvature [that is] square integrable over all locations and scales," and T_p appears to be similar but with 2 replaced by p. Our contribution in this direction is to characterize T_p through a p-summable curvature condition in terms of the *β-numbers* for the curve γ, which measure the local deviation of γ from a straight line in a scale-invariant way.

Theorem 9.1. *A quasicircle $\gamma \subset \mathbb{C}$ is an element of T_p, $2 \leq p < \infty$, if and only if $\{\beta_\gamma(Q)\}_{Q\in\mathcal{Q}} \in \ell^p(\mathcal{Q})$. That is, if and only if*

$$\sum_{Q\in\mathcal{Q}} \beta_\gamma(Q)^p < \infty,$$

where the sum is over all dyadic squares $\mathcal{Q}$ of the plane.

See §9.2 below for precise definitions.

9.1.1 Regularity of $\gamma \in T_p$

Theorem 9.1 offers a fresh perspective on what is known regarding regularity T_p quasicircles. We recall that Guo observed that if $p < q$, $T_p \subsetneq T_q$, and hence regularity in T_p increases as p decreases [12]. In particular, T_p curves for $1 \leq p \leq 2$ are finite energy Weil-Petersson T_2 curves, and hence are *asymptotically smooth*, as noted in [11]. That is, they are rectifiable and if $w_1, w_2 \in \gamma$ and $\ell_\gamma(w_1, w_2)$ is the length of the shorter of the arcs of γ connecting w_1 to w_2,

$$\frac{\ell_\gamma(w_1, w_2)}{|w_1 - w_2|} \to 1 \qquad \text{as} \qquad |w_1 - w_2| \to 0. \tag{9.4}$$

In particular they have no corners, and furthermore they are *chord-arc*, in the sense that the ratio in (9.4) is uniformly bounded over all $w_1, w_2 \in \gamma$.

Our results show that T_p-quasicircles also do not have corners for $p > 2$, although this is deducible from known results. By Lemma 9.4 below, $Pf(z)(1 - |z|^2) \to 0$ as $|z| \to 1$ (as was also noted by Guo [12, Remark 2]), and so by Pommerenke's characterization [31, Thm 1], T_p curves are *asymptotically conformal*, which is to say

$$\max_{w\in\gamma(w_1,w_2)} \frac{|w_1 - w| + |w - w_2|}{|w_1 - w_2|} \to 1 \qquad \text{as} \qquad |w_1 - w_2| \to 0, \tag{9.5}$$

where $\gamma(w_1, w_2)$ is the arc of γ of smaller diameter connecting w_1 and w_2. While this does not imply rectifiability, it does show T_p curves lack corners. Note that we also see this from the β-number characterization: since the β's are p-summable, they tend to zero as the scale goes to zero, and so there cannot be any corners (see Example 9.2 below). It would be useful to settle whether T_p curves are rectifiable and chord-arc when $p > 2$.

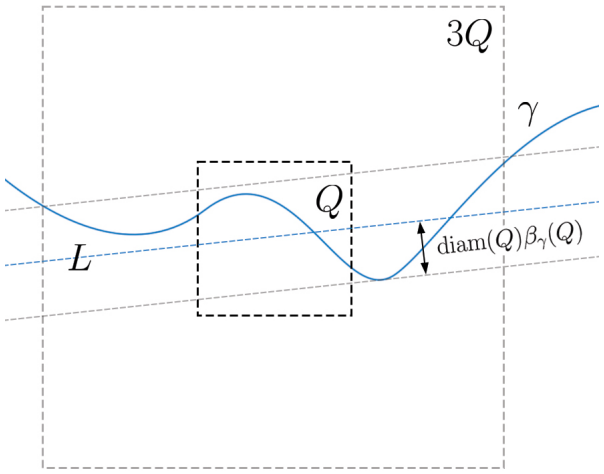

Figure 9.1: The β's quantify the deviation of a curve $\gamma = E$ from the locally best-approximating line L, with $\mathrm{diam}(Q)\beta_\gamma(Q)$ being half the width of the thinnest strip containing $\gamma \cap 3Q$.

9.2 β-numbers

The β-numbers were introduced by Peter Jones in his famous characterization of planar subsets contained in a rectifiable curve, the "travelling salesman theorem," which says that the shortest curve $\gamma \subset \mathbb{R}^2$ passing through a set $E \subset \mathbb{R}^2$ has length $\ell(\gamma)$ comparable to

$$\mathrm{diam}(E) + \sum_{Q \in \mathcal{Q}} \beta_E(Q)\,\mathrm{diam}(Q),$$

and hence E is contained in a rectifiable curve γ if and only if the above sum is finite [12]. Jones' theorem has had a significant impact on modern analysis and has been generalized to $\mathbb{R}^n$ [30], Hilbert space [37], and recently sharpened by Bishop [4] in the case where E is itself a Jordan curve.

The β's for a set $E \subset \mathbb{R}^n$ are precisely defined as follows. For a dyadic cube Q, let $3Q$ be the concentric dilation of Q which has triple the side length, and we set

$$\beta_E(Q) := \frac{1}{\mathrm{diam}(Q)} \inf \Big\{ \sup\{\, \mathrm{dist}(z, L) \;:\; z \in 3Q \cap E \,\} \;:\; L \text{ is a line with } L \cap 3Q \neq \emptyset \Big\}, \tag{9.6}$$

if $E \cap Q \neq \emptyset$, while $\beta_E(Q) = 0$ otherwise.* Note that $0 \leq \beta_E(Q) \leq \frac{3}{2}$, and so the β's give a scale-invariant way to measure the local curvature, or the local deviation from a straight line. Loosely speaking, $\beta_\gamma(Q)$ is telling us the diameter-proportion of $3Q$ that γ takes up. In fact,

$$\frac{2}{3}\beta_\gamma(Q) = \frac{\text{width of the thinnest strip containing } \gamma \cap 3Q}{\text{diam}(3Q)}.$$

See Figure 9.1.

Example 9.2. Suppose γ is a planar curve with one-sided derivatives at $\gamma(t_0)$ that do not agree, i.e. γ has a corner at $\gamma(t_0)$. At fine-enough scales near $\gamma(t_0)$, γ looks like two line segments meeting at a corner with angle $\alpha \neq \pi$. Hence whenever Q is a small square with $\gamma(t_0) \in Q$, the smallest strip containing $\gamma \cap 3Q$ in $3Q$ will have width that is some definite, positive proportion of $\text{diam}(3Q)$, showing

$$\beta_\gamma(Q) \geq \delta = \delta(\alpha) > 0$$

for all sufficiently-small squares Q. So, for example, since $\beta_\gamma(Q)$ tend to zero at small scales for finite-energy γ by Bishop's characterization $\{\beta_\gamma(Q)\} \in \ell^2$, we see that finite-energy curves have no corners.

It will be helpful to have another version of the β's at our disposal which are defined directly in terms of the curve, rather than from dyadic squares. If γ_j is a subarc of γ, let L_j be the line connecting the endpoints of γ_j. We define the β-number for this subarc as

$$\beta(\gamma_j) := \frac{1}{\text{diam}(L_j)} \sup_{z \in \gamma_j} \text{dist}(z, L_j). \tag{9.7}$$

See Figure 9.2. The collection of subarcs we will use form a *multi-resolution family* for γ, which is to say they will cover γ nicely at each scale. The precise definition, from Bishop [5], is as follows.

*This is Bishop's definition; Jones defines β as twice this quantity. As our results only involve the finiteness of the ℓ^p-norm of the β's and not their specific value, the difference is immaterial for us.

Definition 9.1. A *multi-resolution family* $\mathcal{R}(E)$ for a set E in a metric space X is a collection of sets $\{R_j\}$ for which there are constants $1 < M, N < \infty$ and $r_0 > 0$ such that the following three conditions hold.

(i) For each $0 < r < r_0$, E is covered by sets in $\mathcal{R}(E)$ of diameter between r and Mr.

(ii) Each bounded subset F of E intersects at most N of the sets R_j with $\operatorname{diam}(F)/M \leq \operatorname{diam}(R_j) \leq M \operatorname{diam}(F)$.

(iii) Any subset F of E with $0 < \operatorname{diam}(F) < \infty$ is contained in at least one R_j with $\operatorname{diam}(R_j) \leq M \operatorname{diam}(F)$.

As an example, consider dyadic sub-intervals I_{jk} of $\partial\mathbb{D}$ of the form

$$I_{nk} = \{\, e^{i\theta} \;:\; \frac{2\pi}{2^n} k \leq \theta \leq \frac{2\pi}{2^n}(k+1) \,\}$$

where $n \in \{0, 1, \ldots\}$ and $k \in \{0, 1, \ldots, 2^n - 1\}$. The collection of all I_{nk} satisfies properties (i) and (ii) of a multi-resolution family for $\partial\mathbb{D}$ but not (iii), since $\{\, e^{i\theta} \;:\; -\epsilon \leq \theta \leq \epsilon \,\}$ is not contained in a single I_{jk} of comparable diameter for small ϵ. However, if we augment the collection by adding in the rotation of all I_{jk} by a fixed, suitable non-dyadic angle such as $\pi/3$, then the resulting family also satisfies (iii).

Below we work with a finer collection of dyadic sub-intervals and their associated Whitney squares (defined below), starting with $n = 3$. Here adding in one rotation will again yield a family which satisfies (iii) for all sufficiently-small sets F. This will suffice for our purposes, because we only need to show that the tail of the pth power of the β-numbers is summable, and so we are only concerned about small scales.

9.3 Notation

In our estimates below, we write $A \lesssim B$ if there is a constant C independent of A and B such that $A \leq CB$, and $A \asymp B$ if $A \lesssim B$ and $B \lesssim A$, in which case we say "A is comparable to B."

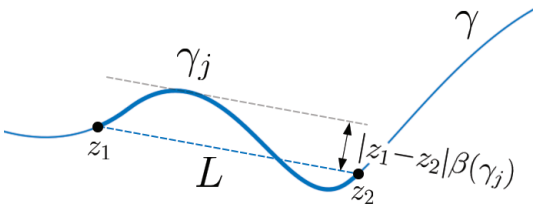

Figure 9.2: A version of the β-numbers for subarcs γ_j of γ. Note $|z_2 - z_1|\beta(\gamma_j)$ is half the width of the thinnest strip *centered on the line* L that contains γ_j. In contrast to $\beta_\gamma(Q)$, we are not free to select an optimal line, and we are only concerned about the portion of γ between z_1 and z_2.

We work with a Whitney decomposition $\mathcal{W}$ of $\mathbb{D}$, defined through the dyadic decomposition $\mathcal{D}$ of $\partial\mathbb{D}$ given by all subarcs $I_{nk} = \{e^{i\theta} \ : \ 2\pi\frac{k}{2^n} \le \theta \le 2\pi\frac{k+1}{2^n}\}$, $k = 0, 1, \ldots, 2^n - 1$, $n = 3, 4, \ldots$. For any $I \in \mathcal{D}$, the associated Carleson square Q_I is

$$Q_I := \left\{ z \in \mathbb{D} \ : \ \frac{z}{|z|} \in I, \, 1 - |I| \le |z| \right\}, \tag{9.8}$$

where $|I_{nk}| = \frac{\pi}{2^{n-1}}$, and $|I|$ is the length of I. The "top half" of Q_I is $Q_I^+ := Q_I \cap \{1 - |I| \le |z| \le 1 - \frac{1}{2}|I|\}$, and Q^* is the reflection of Q across $\partial\mathbb{D}$. Our *Whitney decomposition* is then $\mathcal{W} = \overline{B}(0, 1 - \pi/2) \cup \bigcup_{n,k} Q^+_{I_{nk}}$, a partition of $\mathbb{D}$ into closed sets with disjoint interiors. Each Whitney square $W = Q^+_{I_{nk}}$ has hyperbolic area comparable to 1, Euclidean area comparable to $(1 - |z|^2)^2$ for any $z \in W$, and $\operatorname{diam}(W)$ comparable to $d(z, \partial\mathbb{D})$ for any $z \in W$. While we call W a "square," we note that it is not literally one, although it is asymptotically a rectangle with side-length ratio 2:1 as $|I_{nk}| \to 0$.

For a dyadic interval I, we write rI for the subarc of $\partial\mathbb{D}$ concentric with I but with length $r|I|$. A *dyadic cube* or equivalently a *dyadic square* is a set of the form $Q = [j2^{-n}, (j+1)2^{-n}] \times [k2^{-n}, (k+1)2^{-n}]$, where $j, k \in \mathbb{Z}$ and $n \in \mathbb{N}$. Its side length is $\ell(Q) := 2^{-n}$, and for $\lambda > 0$ we define λQ to be the cube concentric with Q but with side length $\lambda\ell(Q)$ and sides parallel to the axes. We will mostly use $3Q$, which is the union of Q and its eight adjacent neighbors. Note that Q is closed.

For a (measurable) set $C \subset \mathbb{D}$, $|C|$ is the Lebesgue area measure of C, and $|C|_\rho$ is the hyperbolic area $\int_C \frac{dxdy}{(1-|z|^2)^2}$ of C.

9.4 Step one: $\gamma \in T^p$ implies $\beta_\gamma(Q) \in \ell^p$

In this section we take the first step in our argument, proving that T_p quasicircles have p-summable β-numbers when $p > 1$.

Theorem 9.3. *If a quasicircle $\gamma \subset \mathbb{C}$ is an element of T_p, $1 < p < \infty$, then $\{\beta_\gamma(Q)\}_{Q\in\mathcal{Q}} \in \ell^p(\mathcal{Q})$. That is,*

$$\sum_{Q\in\mathcal{Q}} \beta_\gamma(Q)^p < \infty,$$

where the sum is over the collection of dyadic squares $\mathcal{Q}$ of the plane.

Our proof generalizes an argument of Bishop in an earlier version of the preprint [5], which showed that the pre-Schwarzian condition (9.2) for $p = 2$ implies $\sum \beta_\gamma(Q)^2 < \infty$. We closely follow Bishop's logic but adjust to allow for general p.

We break the argument into a series of lemmas; the first says that we can exchange the pre-Schwarzian condition (9.2) for $\sum_{W\in\mathcal{W}} \eta(W)^p < \infty$, where for $W \in \mathcal{W}$,

$$\eta(W) := \max_{z\in W} \left|\frac{f''(z)}{f'(z)}\right| (1-|z|^2). \tag{9.9}$$

Lemma 9.4. *Let $1 \le p < \infty$ and $f : \mathbb{D} \to \Omega$ be conformal. Then*

$$\int_{\mathbb{D}} |Pf(z)|^p \, (1-|z|^2)^p dA_\rho(z) < \infty$$

if and only if

$$\sum_{W\in\mathcal{W}} \eta(W)^p < \infty,$$

where $\mathcal{W}$ is the Whitney decomposition of $\mathbb{D}$.

Proof. For sufficiency, we observe

$$\int_{\mathbb{D}} |Pf(z)|^p \, (1-|z|^2)^p dA_\rho(z) = \sum_{W\in\mathcal{W}} \int_W |Pf(z)|^p \, (1-|z|^2)^p dA_\rho(z)$$
$$\leq \sum_{W\in\mathcal{W}} \eta(W)^p \int_W dA_\rho(z) \lesssim \sum_{W\in\mathcal{W}} \eta(W)^p,$$

as each Whitney square has hyperbolic area comparable to one. For the "only if" direction, we control $\eta(W)^p$ through integrating $|Pf(z)(1-|z|^2)|^p$ over W and a collection of neighboring squares $\{\tilde{W}\}$. Indeed, pick $W \in \mathcal{W}$ and $z_0 \in W$, and set $B_0 := B(z_0, (1-|z_0|)/2)$. Note $|B_0| \asymp (1-|z_0|^2)^2$. By the mean-value property for the holomorphic function Pf,

$$Pf(z_0) = \frac{1}{|B_0|} \int_{B_0} Pf(z) dxdy$$

and hence by Jensen's inequality, and the fact that $1-|z|^2 \asymp 1-|z_0|^2$ for any other $z \in W$,

$$|Pf(z_0)|^p \leq \frac{1}{|B_0|} \int_{B_0} |Pf(z)|^p dxdy \lesssim \frac{1}{|B_0|(1-|z_0|^2)^{p-2}} \int_{B_0} |Pf(z)|^p (1-|z|^2)^{p-2} dxdy.$$

As $|B_0|(1-|z_0|^2)^{p-2} \asymp (1-|z_0|^2)^p$, we have

$$|Pf(z_0)(1-|z_0|^2)|^p \lesssim \int_{B_0} |Pf(z)|^p (1-|z|^2)^{p-2} dxdy.$$

Hence we can control the max $\eta(W)^p$ by integrating the (integrand in the) right-hand side over W and a bounded number of neighboring Whitney squares $\tilde{W}$, enough to cover $\cup_{z\in W} B_0(z)$. When summing over all $W \in \mathcal{W}$, each Whitney square is integrated over a bounded number of times, yielding

$$\sum_{W\in\mathcal{W}} \eta(W)^p \lesssim \int_{\mathbb{D}} |Pf(z)|^p (1-|z|^2)^{p-2} dxdy < \infty. \qquad \square$$

We next recall a version of the Koebe-1/4 theorem, which gives uniform control on the derivative of a conformal map in terms of distances to the boundary in the image and pre-image.

Proposition 9.5. *[17, Cor.3.19] If $\varphi : \Omega_1 \subsetneq \mathbb{C} \to \Omega_2$ is conformal, then for any $z \in \Omega_1$,*

$$\frac{1}{4} \frac{d(\varphi(z), \partial\Omega_2)}{d(z, \partial\Omega_1)} \leq |\varphi'(z)| \leq 4 \frac{d(\varphi(z), \partial\Omega_2)}{d(z, \partial\Omega_1)}. \tag{9.10}$$

We also recall Mori's theorem for the Hölder continuity of K-quasiconformal self-maps of $\mathbb{D}$.

Proposition 9.6. *[1, Thm.III.C] If $G : \mathbb{D} \to \mathbb{D}$ is K-quasiconformal with $G(0) = 0$,*

$$|G(z_1) - G(z_2)| \leq 16|z_1 - z_2|^{1/K} \tag{9.11}$$

for all $z_1, z_2 \in \overline{\mathbb{D}}$.

We also use the fact that K-quasiconformal maps are also η-quasisymmetric away from the boundary. Note that this η is not to be confused with $\eta(W)$ from (9.9).

Proposition 9.7. *[13, Theorem 11.14] A homeomorphism $f : D \to D'$ between domains in $\mathbb{R}^n$, $n \geq 2$, is K-quasiconformal if and only if there is η such that f is η-quasisymmetric in each ball $B(x, \frac{1}{2}d(x, \partial D))$, $x \in D$. The statement is quantitative involving K, η, and the dimension n.*

The previous three propositions combine to give us the next lemma, which we will apply locally to estimate how f distorts arcs close to $\partial\mathbb{D}$.

Lemma 9.8. *Let $I \subset \partial\mathbb{D}$ be a dyadic interval with midpoint x_m and let Q_I the corresponding Carleson square. Suppose f is conformal on $\mathbb{D}$ with K-quasiconformal extension to Q_{2I}^*. Then there exists constant $C = C(K)$ such that for any set $J \subset Q_I$,*

$$\frac{\operatorname{diam}(f(J))}{\operatorname{diam}(f(I))} \leq C\Big(\frac{\operatorname{diam}(J)}{\operatorname{diam}(I)}\Big)^{1/K}. \tag{9.12}$$

Proof. We begin by centering the picture at zero and re-scaling, defining the sets

$$S_1 := \frac{Q_I \cup Q_I^* - x_m}{\operatorname{diam}(I)}, \qquad S_{1.5} := \frac{Q_{1.5I} \cup Q_{1.5I}^* - x_m}{\operatorname{diam}(I)} \quad \text{and} \quad S_2 := \frac{Q_{2I} \cup Q_{2I}^* - x_m}{\operatorname{diam}(I)}.$$

Our normalized version of f is then $g : S_2 \to \frac{f(Q_{2I} \cup Q_{2I}^*)}{\operatorname{diam}(f(I))}$ defined by

$$g(z) := \frac{1}{\operatorname{diam}(f(I))} f\big(\operatorname{diam}(I)z + x_m\big).$$

Let $\varphi : \mathbb{D} \to S_{1.5}$ and $\psi : \mathbb{D} \to g(S_{1.5})$ be conformal with $\varphi(0) = 0$ and $\psi(0) = g(0)$. Then $G := \psi^{-1} \circ g \circ \varphi$ is a quasiconformal self-map of $\mathbb{D}$, fixing zero, and we have the Hölder

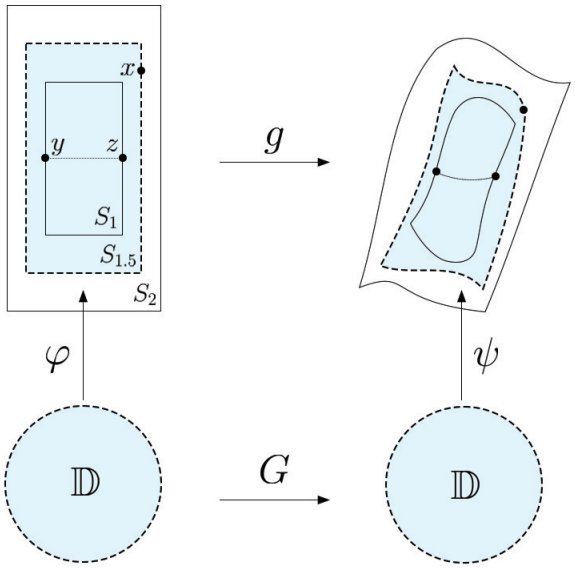

Figure 9.3: The maps in Lemma 9.8.

continuity (9.11). See Figure 9.3. Note there exists δ_1, universal for all dyadic I, such that $z \in S_1$ satisfy

$$0 < \delta_1 \leq d(z, \partial S_{1.5}).$$

By (9.10) we thus have $|(\varphi^{-1})'(z)| \leq \frac{4}{\delta_1}$ on S_1, showing φ^{-1} is $4/\delta_1$-Lipschitz on S_1. Thus whenever $z_1, z_2 \in S_1$,

$$|\psi^{-1} \circ g(z_1) - \psi^{-1} \circ g(z_2)| \leq 16|\varphi^{-1}(z_1) - \varphi^{-1}(z_2)|^{1/K} \leq C_1|z_1 - z_2|^{1/K} \tag{9.13}$$

for a global constant C_1.

We wish to apply a similar argument to remove ψ^{-1} in (9.13). We first note that $d(\partial g(S_1), \partial g(S_2))$ is bounded above. By compactness and Proposition 9.6, we can cover $S_{1.5}$ with a finite number of balls of the form $B(x_k, \frac{1}{2}d(x_k, \partial S_2))$, $x_k \in S_{1.5}$, on each of which g is η_k-quasisymmetric for some homeomorphism $\eta_k : [0, \infty) \to [0, \infty)$. By defining $\eta(t) := \max_k \eta_k(t)$, we have that g is η-quasisymmetric on $S_{1.5}$, which is to say

$$|g(y) - g(x)| \leq \eta\Big(\frac{|y - x|}{|y - z|}\Big)|g(y) - g(z)| \tag{9.14}$$

for any $x, y, z \in S_{1.5}$. Here η only depends on K. Write $I_1 = \frac{I - x_m}{\operatorname{diam}(I)}$, and let y and z be the endpoints of I_1. Noting that $\operatorname{diam}(g(I_1)) = 1$, we have that for any $x \in \partial g(S_{1.5})$,

$$d(\partial g(S_1), \partial g(S_{1.5})) \leq |g(y) - g(x)| \leq \eta\Big(\frac{|y-x|}{|y-z|}\Big)|g(y) - g(z)| \leq C_3 \cdot 1$$

for a universal constant C_3. Thus by Proposition 9.5,

$$|\psi'(z)| \lesssim \frac{1}{d(z, \partial\mathbb{D})} \tag{9.15}$$

for $z \in \psi^{-1} \circ g(S_1)$.

We also wish to bound $d(z, \partial\mathbb{D})$ below, and first note that we also have a lower bound on $d(\partial g(S_1), \partial g(S_{1.5}))$. Indeed, for $x \in \partial S_{1.5}, y \in \partial S_1$ and $z \in S_1$, $\eta\big(\frac{|x-z|}{|x-y|}\big) \leq c$ for some $c = c(K) > 0$ independent of the dyadic square, and so

$$|g(x) - g(y)| \geq \frac{|g(x) - g(z)|}{c} \geq \frac{1}{2c},$$

where the last inequality is because $\operatorname{diam}(\{g(x)\} \cup g(S_1)) \geq 1$. Thus $g(S_{1.5}) \backslash g(S_1)$ is an annulus of bounded modulus, and so its image under the conformal map ψ^{-1} is an annulus of the same modulus that has circular outer boundary and the point zero in the bounded component of its complement. By considering extermal configurations of annuli (see [1, Ch.III]), we conclude $d(z, \partial\mathbb{D})$ is bounded below for $z \in \psi^{-1} \circ g(S_1)$.

By (9.15), we thus have that ψ is Lipschitz on $\psi^{-1} \circ g(S_1)$, and so ψ^{-1} satisfies the lower Lipschitz bound $M_2|z_1 - z_2| \leq |\psi^{-1}(z_1) - \psi^{-1}(z_2)|$ on $g(S_1)$, and applied to (9.13) we have

$$|g(z_1) - g(z_2)| \leq C_4|z_1 - z_2|^{1/K}$$

for any $z_1, z_2 \in S_1$, where C_4 is a universal constant. For $w_j \in Q_I$, $z_j := \frac{w_j - x_m}{\operatorname{diam}(I)} \in S_1$, and hence the above yields

$$\frac{|f(w_1) - f(w_2)|}{\operatorname{diam}(f(I))} \leq C_2\Big(\frac{|w_1 - w_2|}{\operatorname{diam}(I)}\Big)^{1/K},$$

implying (9.12). □

At the end of the argument for Theorem 9.3 will we need that the image of a multi-resolution family of $\partial\mathbb{D}$ under a nice conformal map is a multi-resolution for the $f(\partial\mathbb{D})$. We include this simple observation and its proof for completeness.

Lemma 9.9. *If $\mathcal{R}'$ is a multi-resolution family for $\partial\mathbb{D}$ and $f : \mathbb{D} \to \Omega \subset \mathbb{C}$ is a conformal map onto a quasidisk Ω, then $\mathcal{R} := \{f(R')\}_{R'\in\mathcal{R}'}$ is a multi-resolution family for $\gamma := f(\partial\mathbb{D})$.*

Proof. Since f maps to a quasidisk, f is quasisymmetric on $\partial\mathbb{D}$ and satisfies (9.14) with g replaced by f and some homeomorphism $\eta : [0,\infty) \to [0,\infty)$ which only depends on K, the quasidisk constant of Ω [32, Thm.5.11]. The lemma readily follows. Start with property (iii) of Definition 9.1: for $F \subset \gamma$ of positive diameter, pull back to $F' := f^{-1}(F)$ and choose $R'_j \in \mathcal{R}'$ such that $F' \subset R'_j$ and $\operatorname{diam}(R'_j) \le M' \operatorname{diam}(F')$. Let $z_1, z_2 \in F'$ such that $\frac{1}{2}\operatorname{diam}(F') \le |z_1 - z_2|$. Then for $z_3 \in R'_j$, quasisymmetry (9.14) yields

$$\begin{aligned}|f(z_2) - f(z_3)| &\le \eta\Big(\frac{|z_2 - z_3|}{|z_1 - z_2|}\Big)|f(z_1) - f(z_2)| \\ &\le \eta\Big(2\frac{\operatorname{diam}(R'_j)}{\operatorname{diam}(F')}\Big)\operatorname{diam}(F) \le \eta(2M')\operatorname{diam}(F).\end{aligned}$$

By choosing z_3 such that $\frac{1}{2}\operatorname{diam}(f(R'_j)) \le |f(z_2) - f(z_3)|$, we thus have

$$\operatorname{diam}(f(R'_j)) \le 2\eta(2M')\operatorname{diam}(F),$$

yielding (iii).

Property (i) immediately follows: cover γ by sets F_j of diameter r. For each F_j, we now have $R_j \in \mathcal{R}$ covering F_j with $\operatorname{diam}(R_j) \lesssim \operatorname{diam}(F_j)$, and these R_j form the desired cover for γ.

For (ii), note that our argument above for (i) only assumed that $F' \cap R'_j \neq \emptyset$, and so we can also reverse the roles of F' and R'_j and see that if $\operatorname{diam}(F') \asymp \operatorname{diam}(R'_j)$, then

$$\operatorname{diam}(f(F')) \asymp \operatorname{diam}(f(R'_j)). \tag{9.16}$$

Since f^{-1} is also quasisymmetric [13, Prop.10.6], if $\operatorname{diam}(F) \asymp \operatorname{diam}(R_j)$, we also have $\operatorname{diam}(f^{-1}(F)) \asymp \operatorname{diam}(f^{-1}(R_j))$ (although the constant of proportionality may be differ-

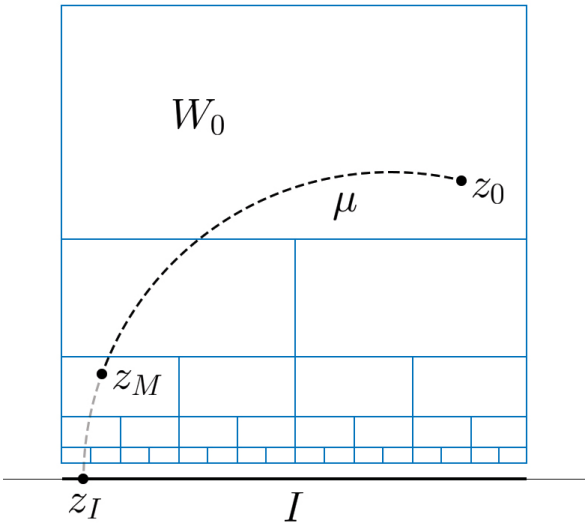

Figure 9.4: We show f is approximately linear on I by first showing $f(z_0) - f(z_I) \approx z_0 - z_I$.

ent than in (9.16)). So if $F \subset \gamma$ and $R_j \cap F \neq \emptyset$ with $\operatorname{diam}(R_j) \asymp \operatorname{diam}(F)$, we have $\operatorname{diam}(f^{-1}(R_j)) \asymp \operatorname{diam}(f^{-1}(F))$, and there are only a bounded number N of such sets. □

Proof of Theorem 9.3. As discussed above in §9.1.1, γ is asymptotically conformal, and hence the conformal map f from $\mathbb{D}$ to the bounded component Ω of $\mathbb{C}\backslash\gamma$ has a quasiconformal extension to $\mathbb{C}$ which satisfies $\mu_f(z) = \frac{\overline{\partial} f}{\partial f}(z) \to 0$ as $|z| \to 1^+$ [32, Thm.11.1(v)]. Hence for fixed $\alpha \in (1/p, 1)$, we may choose an interval width δ small enough such that f extends $K := 1/\alpha$-quasiconformally on Q^*_{2I} whenever

$$|I| < \delta, \tag{9.17}$$

thus yielding (9.12) for all such dyadic I. We will show that $\gamma_I := f(I)$ is approximately a line segment with small, explicit error, which will enable us to estimate $\beta(\gamma_I)$.

Let I be one of these intervals, pick $z_I \in I$, let Q_I the corresponding square (9.8), and fix $z_0 \in Q_I^+ =: W_0$. Since re-scaling f does not change the η's or our estimate (9.12), we may assume $f'(z_0) = 1$. Consider the hyperbolic geodesic μ in $\mathbb{D}$ from z_0 to z_I, with $\{W_k\}_{k=0}^{\infty}$ the chain of Whitney squares that μ passes through, listed in increasing distance from z_0. See

Figure 9.4. For a square W_M in this chain to be determined below and any point $z_M \in W_M$, we start by showing

$$|f(z_M) - f(z_0) - (z_M - z_0)| \lesssim \sum_{k=0}^{M} \eta(W_k) \operatorname{diam}(W_0) e^{-\alpha\rho(W_0, W_k)}, \tag{9.18}$$

our first "approximately linear" result for f. Start by writing hyperbolic distance as $\rho(\cdot, \cdot)$, and note that whenever δ in (9.17) is sufficiently small,

$$\rho(W_0, W_n) \leq n \log(2),$$

and hence

$$\operatorname{diam}(W_n) \lesssim \operatorname{diam}(W_0) 2^{-n} \ \leq \ \operatorname{diam}(W_0) e^{-\rho(W_0, W_n)}. \tag{9.19}$$

Let z_n be any point in $\mu \cap W_n$ and let μ_n be the portion of μ from z_0 up to z_n. Using the $\eta(W)$ of (9.9), we see

$$\begin{aligned} |\log(f'(z_n))| \leq \int_{\mu_n} \left| \frac{f''(z)}{f'(z)} \right| |dz| &= \sum_{k=0}^{n} \int_{\mu_n \cap W_k} \left| \frac{f''(z)}{f'(z)} \right| |dz| \\ &\lesssim \sum_{k=0}^{n} \int_{\mu_n \cap W_k} \frac{\eta(W_k)}{\operatorname{diam}(W_k)} |dz| \lesssim \sum_{k=0}^{n} \eta(W_k). \end{aligned}$$

The elementary estimate $|e^w - 1| \leq e^{|w|} - 1$ obtained from the series expansion of e^w then yields

$$|f'(z_n) - 1| \leq \exp\Big(C \sum_{k=0}^{n} \eta(W_k) \Big) - 1.$$

Either $\sum_{k=0}^{\infty} \eta(W_k) \leq 1$ or $\sum_{k=0}^{\infty} \eta(W_k) > 1$. In the former case, since C is a global constant and

$$e^x - 1 \lesssim x \tag{9.20}$$

for $x \in [0, C]$, integration along μ up to any point $z_M \in W_M$ for any square W_M in the chain yields

$$|f(z_M) - f(z_0) - (z_M - z_0)| = \left| \int_{\mu_M} (f'(z) - 1) dz \right|$$

$$
\begin{aligned}
&= \left| \sum_{n=0}^{M} \int_{\mu_M \cap W_n} (f'(z) - 1) dz \right| \\
&\lesssim \sum_{n=0}^{M} \int_{\mu_M \cap W_n} \sum_{k=0}^{n} \eta(W_k) |dz| \\
&\lesssim \sum_{n=0}^{M} \operatorname{diam}(W_n) \sum_{k=0}^{n} \eta(W_k) \\
&= \sum_{k=0}^{M} \eta(W_k) \sum_{n=k}^{M} \operatorname{diam}(W_n) \\
&\lesssim \sum_{k=0}^{M} \eta(W_k) \operatorname{diam}(W_k), \qquad (9.21) \\
&\lesssim \sum_{k=0}^{M} \eta(W_k) \operatorname{diam}(W_0) e^{-\rho(W_0, W_k)} \qquad (9.22) \\
&\leq \sum_{k=0}^{M} \eta(W_k) \operatorname{diam}(W_0) e^{-\alpha\rho(W_0, W_k)},
\end{aligned}
$$

where we use the fact in (9.21) that the geometric sum $\sum_{n=k}^{M} \operatorname{diam}(W_n)$ is bounded by a multiple of its first term, and in (9.22) we use (9.19), and for the last line we recall $\alpha \leq 1$. Hence we obtain (9.18) when $\sum_{k=0}^{\infty} \eta(W_k) < 1$ for any choice of W_M. Since the constant in (9.18) does not depend on M, sending $M \to \infty$ yields

$$
|f(z_I) - f(z_0) - (z_I - z_0)| \lesssim \sum_{k=0}^{\infty} \operatorname{diam}(W_0) \eta(W_k) e^{-\alpha\rho(W_0, W_k)} \qquad (9.23)
$$

in this case.

We also wish to show (9.23) when $\sum_{k=0}^{\infty} \eta(W_k) > 1$, but with the sum terminating at some finite M, and we start by showing (9.18). In this case define M to be the first index where

$$
\sum_{k=0}^{M} \eta(W_k) \geq 1. \qquad (9.24)
$$

Since $\eta(W) \to 0$ as W approaches $\partial\mathbb{D}$, we may further suppose that $\sum_{k=1}^{M} \eta(W_n) < 2$, by shrinking δ in (9.17), if necessary. Then we still obtain (9.18) upon increasing the $O(\cdot)$-constant, if needed, as (9.20) still holds for $x \in [0, 2C]$ with a larger constant. To obtain

our version of (9.23) here, we also need to estimate $|z_M - z_I|$ and $|f(z_M) - f(z_I)|$, and we proceed to show both are $O\big(\sum_{k=0}^{M} \operatorname{diam}(W_0)\eta(W_k)e^{-\alpha\rho(W_0,W_k)}\big)$.

For $|z_M - z_I|$, observe

$$\begin{aligned}
|z_M - z_I| &\lesssim \operatorname{diam}(W_M) \\
&\lesssim \operatorname{diam}(W_0)e^{-\rho(W_0,W_M)} \\
&\leq \operatorname{diam}(W_0)\Big(\sum_{k=0}^{M}\eta(W_k)\Big)e^{-\rho(W_0,W_M)} \qquad (9.25)\\
&\leq \operatorname{diam}(W_0)\sum_{k=0}^{M}\eta(W_k)e^{-\rho(W_0,W_k)}, \\
&\leq \operatorname{diam}(W_0)\sum_{k=0}^{M}\eta(W_k)e^{-\alpha\rho(W_0,W_k)}, \qquad (9.26)
\end{aligned}$$

where we used (9.24) in (9.25). For $|f(z_M) - f(z_I)|$, we similarly observe, using Lemma 9.8 and (9.19) as well, that

$$\begin{aligned}
|f(z_M) - f(z_I)| &\lesssim \operatorname{diam}(f(I))\Big(\frac{\operatorname{diam}(W_M)}{\operatorname{diam}(W_0)}\Big)^{\alpha} \\
&\lesssim \operatorname{diam}(f(I))e^{-\alpha\rho(W_0,W_M)} \qquad (9.27)\\
&\leq \operatorname{diam}(f(I))\Big(\sum_{k=0}^{M}\eta(W_k)\Big)e^{-\alpha\rho(W_0,W_M)} \\
&\leq \operatorname{diam}(f(I))\sum_{k=0}^{M}\eta(W_k)e^{-\alpha\rho(W_0,W_k)}. \qquad (9.28)
\end{aligned}$$

We furthermore claim that

$$\operatorname{diam}(f(I)) \asymp \operatorname{diam}(W_0). \qquad (9.29)$$

For $\operatorname{diam}(f(I)) \lesssim \operatorname{diam}(W_0)$, we use a harmonic measure estimate and the fact that $\partial\Omega$ is a quasicircle. Indeed, consider the two dyadic arcs I_1 and I_2 adjacent to I on either side and of the same generation as I. A result of Pommerenke [32, Cor. 4.18] implies that, for $j = 1, 2$,

$$d(f(z_0), f(I_j)) \leq d(f(z_0), \partial\Omega)e^{C/\omega(z_0,I_j,\mathbb{D})},$$

where $\omega(z_0, I_j, \mathbb{D})$ is the harmonic measure of I_j in $\mathbb{D}$ as seen from z_0. Since $\omega(z_0, I_j, \mathbb{D})$ is globally bounded below over all I, and as $d(f(z_0), \partial\Omega) \asymp d(z_0, I) \asymp \operatorname{diam}(W_0)$ by (9.10) and the construction of the Whitney squares, we have

$$d(f(z_0), f(I_j)) \lesssim \operatorname{diam}(W_0).$$

Choose $z_j \in I_j$ such that $|f(z_0) - f(z_j)| \leq 2d(f(z_0), f(I_j))$. As $f(\partial\mathbb{D})$ is a quasicircle, by Ahlfor's three-point characterization there exists M such that $|f(z_1) - w| \leq M|f(z_1) - f(z_2)|$ whenever $w \in f(I)$. Hence for $w_1, w_2 \in f(I)$,

$$|w_1 - w_2| \leq 2M|f(z_1) - f(z_2)| \leq 4Md(f(z_0), f(I_1)) + 4Md(f(z_0), f(I_2)) \lesssim \operatorname{diam}(W_0),$$

yielding $\operatorname{diam}(f(I)) \lesssim \operatorname{diam}(W_0)$, as claimed.

For the other direction, we again use the 3-point property. Let z_l and z_r be the left and right end-points of I. Then the curve formed from the two line segments $[z_l, z_0] \cup [z_0, z_r]$ is a K-quasiarc with bounded K, and so we have

$$\operatorname{diam}(W_0) \lesssim d(z_0, I) \lesssim d(f(z_0), \partial\Omega) \leq |f(z_0) - f(z_l)| \leq M|f(z_l) - f(z_r)| \leq M \operatorname{diam}(f(I)),$$

as claimed, completing the proof of (9.29).

Applied to (9.28) we have

$$|f(z_M) - f(z_I)| \lesssim \operatorname{diam}(W_0) \sum_{k=0}^{M} \eta(W_k) e^{-\alpha\rho(W_0, W_k)}, \tag{9.30}$$

and so in this second case (when $\sum_{k=0}^{\infty} \eta(W_k) > 1$) we find

$$\begin{aligned} |f(z_I) - f(z_0) - (z_I - z_0)| &\leq |f(z_M) - f(z_0) - (z_M - z_0)| + |f(z_I) - f(z_M)| + |z_M - z_I| \\ &\lesssim \operatorname{diam}(W_0) \sum_{k=0}^{M} \eta(W_k) e^{-\alpha\rho(W_0, W_k)} \end{aligned}$$

by (9.18), (9.26) and (9.30).

Whether or not $\sum_{k=0}^{\infty} \eta(W_k)$ is bounded by one, then, we find that f is approximately linear on I, with the deviation from linearity controlled by a fixed multiple of

$$\sup_{z \in I} \sum_{k=0}^{M(z)} \operatorname{diam}(W_0) \eta(W_k) e^{-\alpha\rho(W_0, W_k)},$$

where the sum is over the chain $\mathcal{C}(z)$ of Whitney squares from a fixed point $z_0 \in W_0 = Q_I^+$ to z, and $M(z) \in \mathbb{N} \cup \{\infty\}$. Let z_I be a point where the sum is within a factor of two of this supremum. For $\gamma_I := f(I)$, we can now estimate the associated $\beta(\gamma_I)$ defined by (9.7). If z_l, z_r are the left- and right-endpoints of I, we have

$$\frac{\operatorname{diam}(W_0)}{|f(z_l) - f(z_r)|} \lesssim \frac{\operatorname{diam}(f(I))}{|f(z_l) - f(z_r)|} \lesssim 1$$

by (9.29) and the fact that $\partial\Omega$ is a quasicircle. For $w \in I$, we note there exists $t \in [0,1]$ such that

$$|tz_l + (1-t)z_r - w| \lesssim |I|^2 \lesssim \operatorname{diam}(W_I)^2$$

where $W_I = Q_I^+ = W_0$, and the same constant works for all sufficiently-small I. Therefore

$$\begin{aligned}
&|tf(z_l) + (1-t)f(z_r) - f(w)| \\
&\quad \le t|f(z_l) - f(w) - (z_l - w)| + (1-t)|f(z_r) - f(w) - (z_r - w)| + |tz_l + (1-t)z_r - w| \\
&\quad \lesssim \sum_{k=0}^{M(z_I)} \operatorname{diam}(W_I)\eta(W_k)e^{-\alpha\rho(W_I, W_k)} + \operatorname{diam}(W_I)^2
\end{aligned}$$

for small I, and we see

$$\beta(\gamma_I) \lesssim \max\Big\{ \sum_{W \in \mathcal{C}(z_I)} \eta(W_k)e^{-\alpha\rho(W_I, W)},\, \operatorname{diam}(W_I)\Big\}.$$

Summing $\operatorname{diam}(W_I)^p$ over all dyadic intervals $\mathcal{I}$ of $\partial\mathbb{D}$ yields $\sum_n 2^n \frac{\pi^p}{2^{pn}} < \infty$ since $p > 1$, and so to show $\{\beta(\gamma_I)\} \in \ell^p$ we only have to show that the first member in this maximum is p-summable. Choosing r such that $1 < r < p\alpha$, we sum over all small dyadic intervals and find

$$\begin{aligned}
&\sum_{I:|I|<\delta} \Big(\sum_{W \in \mathcal{C}(z_I)} \eta(W)e^{(-\alpha + \frac{r}{p} - \frac{r}{p})\rho(W_I, W)} \Big)^p \\
&\qquad\qquad \le \sum_{I:|I|<\delta} \Big(\sum_{W \in \mathcal{C}(z_I)} \eta(W)^p e^{-r\rho(W_I, W)} \Big) \Big(\sum_{W \in \mathcal{C}(z_I)} e^{q(-\alpha + r/p)\rho(W_I, W)} \Big)^{p/q}
\end{aligned}$$

by Hölder's inequality, where $q = \frac{p}{p-1}$. Since $\rho(W_I, W) = \rho(W_I, W_k) \lesssim k$ as $k \to \infty$ and $-\alpha + r/p < 0$, the second inside sum is dominated by a convergent geometric series, showing

$$\sum_{I:|I|<\delta} \Big(\sum_{W \in \mathcal{C}(z_I)} \eta(W) e^{-\alpha\rho(W_I,W)} \Big)^p \lesssim \sum_{I:|I|<\delta} \sum_{W \in \mathcal{C}(z_I)} \eta(W)^p e^{-r\rho(W_I,W)}$$
$$= \sum_W \eta(W)^p \sum_{\substack{I\,:\,|I|<\delta,\\ W \in \mathcal{C}(z_I)}} e^{-r\rho(W_I,W)}.$$

Since $r > 1$, the sum over all dyadic intervals $\sum_I e^{-r\rho(W_I,W)}$ is bounded by a constant independent of W, and therefore the sum above is controlled by a multiple of $\sum_W \eta(W)^p$. By assumption and Lemma 9.4 this is finite, and we conclude

$$\sum_{I \in \mathcal{I}} \beta(\gamma_I)^p < \infty.$$

The dyadic intervals $\mathcal{I}$ of $\partial\mathbb{D}$ do not form a multi-resolution family for $\partial\mathbb{D}$, but supplementing $\mathcal{I}$ by an appropriate rotated version of itself generates one (see the discussion following Definition 9.1). The collective image under f of all these intervals forms a multi-resolution family for γ by Lemma 9.9, and the above argument applies to both the image of $\mathcal{I}$ under f and the image of the rotated family. We thus have a multi-resolution family $\Gamma = \{\gamma_j\}$ for γ for which $\sum_j \beta(\gamma_j)^p < \infty$.

We conclude by noting that this implies that the sum of the dyadic-square β's of (9.6) is likewise finite,

$$\sum_{Q \in \mathcal{Q}} \beta_\gamma(Q)^p < \infty.$$

Indeed, let Q_j be a dyadic square such that $3Q_j \cap \gamma \neq \emptyset$. Since Γ is a multi-resolution family, there exists $\gamma_{k(j)} \in \Gamma$ such that $3Q_j \cap \gamma \subset \gamma_{k(j)}$ and

$$\operatorname{diam}(\gamma_{k(j)}) \lesssim \operatorname{diam}(3Q_j). \tag{9.31}$$

Let $L_{k(j)}$ be the line connecting the endpoints of $\gamma_{k(j)}$. If $L_{k(j)} \cap 3Q_j \neq \emptyset$, we have

$$\inf_{L \cap 3Q_j \neq \emptyset} \sup_{z \in 3Q_j \cap \gamma} d(z, L) \leq \sup_{z \in 3Q_j \cap \gamma} d(z, L_{k(j)}) \leq \sup_{z \in \gamma_{k(j)}} d(z, L_{k(j)}), \tag{9.32}$$

and so by (9.31) we conclude

$$\beta_\gamma(Q_j) \lesssim \beta(\gamma_{k(j)}). \tag{9.33}$$

If $L_{k(j)} \cap 3Q = \emptyset$, the second inequality in (9.32) still holds, and we may reduce this distance over $z \in 3Q_j \cap \gamma$ by choosing a line L intersecting $3Q_j$, showing that the first inequality also holds, and so we again have (9.33). By (9.31), this specific γ_k is chosen as $\gamma_{k(j)}$ a bounded number of times, and hence

$$\sum_{Q_j \in \mathcal{Q}} \beta_\gamma(Q_j)^p \lesssim \sum_j \beta(\gamma_{k(j)})^p \leq \sum_k \beta(\gamma_k)^p < \infty. \qquad \square$$

9.5 *Step two:* $\beta_\gamma(Q) \in \ell^p$ *implies* $\mu \in L^p(\mathbb{D}, dA_\rho)$

In the next stage of the argument, we prove that $\{\beta_\gamma(Q)\} \in \ell^p$ implies the dilatation condition $\mu \in L^p(\mathbb{D}, dA_\rho)$. We again follow Bishop's reasoning from an earlier version of [5], although we fill in many of the details that were omitted. This may frustrate the expert, but we hope it aids those less familiar with the subject matter.

Theorem 9.10. *Suppose $\gamma \subset \mathbb{C}$ is a quasicircle for which*

$$\sum_{Q \in \mathcal{Q}} \beta_\gamma(Q)^p < \infty \tag{9.34}$$

for some $1 < p < \infty$. Then there exists a quasiconformal map $q : \mathbb{C} \to \mathbb{C}$, conformal on $\mathbb{D}^*$ and taking $\partial\mathbb{D}$ to γ, whose complex dilatation μ satisfies

$$\int_{\mathbb{D}} \frac{|\mu(z)|^p}{(1-|z|^2)^2} dx\, dy < \infty. \tag{9.35}$$

In particular, $\gamma \in T_p$ when $p \geq 2$.

The idea for the proof is to define a quasiconformal reflection across γ, using the $\beta_\gamma(Q)$'s, which has p-integrable dilatation. More specifically, we start with a triangulation determined by a Whitney decomposition of dyadic squares, and reflect the triangles in a square Q across an approximating line determined by $\beta_\gamma(R)$ for a nearby dyadic square R which intersects γ (see Figures 9.5 and 9.6). The p-summability of β will imply the p-integrability of μ.

Proof. Start with the following Whitney decomposition $\mathcal{W}$ of the bounded component Ω of $\mathbb{C}\backslash\gamma$. Set $\mathcal{Q}_k$ to be the collection of dyadic squares $Q \in \mathcal{Q}$ with side length $\ell(Q) = 2^{-k}$, and let $\mathcal{W}_0$ be the union of all $Q \in \mathcal{Q}_0$ satisfying $2Q \subset \Omega$ (which may be the empty set). For $Q \in \mathcal{Q}_0$ not satisfying this condition, we subdivide to the next smaller generation and define $\mathcal{W}_1$ to be the collection of all subsquares $Q' \in \mathcal{Q}_1$ of Q for which $2Q' \subset \Omega$, where Q is any element of $\mathcal{Q}_0\backslash\mathcal{W}_0$. Similarly, having constructed $\mathcal{W}_0, \ldots, \mathcal{W}_k$, we define $\mathcal{W}_{k+1}$ as the union of those $Q \in \mathcal{Q}_{k+1}$ such that $2Q \subset \Omega$ and $Q^+ \notin \mathcal{W}_k$, where Q^+ is the unique element of $\mathcal{Q}_k$ such that $Q \subset Q^+$. Our decomposition is then the collection of all these dyadic squares, $\mathcal{W} = \bigcup_{k\geq 0} \mathcal{W}_k$, which possesses the following standard properties:

(*i*) For any $Q \in \mathcal{W}$,

$$\frac{1}{2}\ell(Q) \leq d(Q, \gamma) \leq 2\sqrt{2}\ell(Q). \tag{9.36}$$

(*ii*) For any $Q \in \mathcal{W}$, either Q^+ or one of its eight neighbors of the same generation intersect γ, and any of these nine squares R satisfy $Q \subset 3R$.

(*iii*) If Q_1 and Q_2 are adjacent in $\mathcal{W}$, then

$$\frac{1}{4} \leq \frac{\ell(Q_1)}{\ell(Q_2)} \leq 4. \tag{9.37}$$

The proofs are immediate. For (*i*), since $2Q \in \Omega$, the closest γ can be is $\ell(Q)/2$ away from one of its edges. Since $2(Q^+) \not\subset \Omega$, the extreme case of γ intersecting the corner of $2(Q^+)$ furthest from Q yields the upper bound in (9.36). For (*ii*), we note $2(Q^+) \not\subset \Omega$ and $2(Q^+) \subset Q^+ \cup \bigcup_{j=1}^{8} Q_j^+$, where Q_j^+ are the neighbors of Q^+ of the same generation. Lastly, for (*iii*), since $2Q_1 \subset \Omega$, there is a "square annulus" around Q_1 of width $\frac{1}{2}\ell(Q_1)$ contained in Ω. Hence all neighboring squares Q_2 two generations down have $2Q_2 \subset \Omega$, and so there is no need to subdivide any further. Thus $\ell(Q_2) \geq \frac{1}{4}\ell(Q_1)$ and (9.37) follows by symmetry.

We use $\mathcal{W}$ to define a triangulation that we will reflect across γ using lines determined by the $\beta_\gamma(Q)$'s. Indeed, triangulate Ω by attaching the center of each $Q \in \mathcal{W}$ to its four vertices

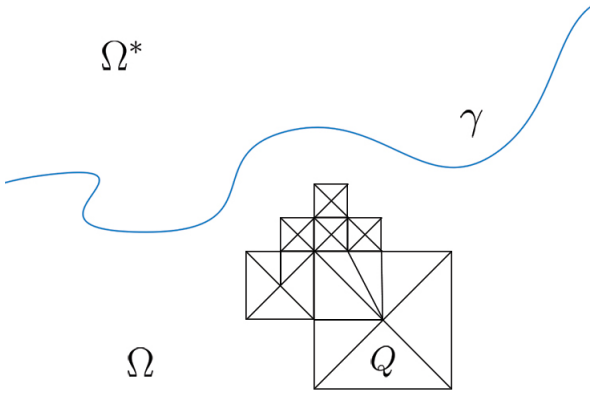

Figure 9.5: Selected squares of the Whitney decomposition and the corresponding triangulation of Ω.

and any other vertices on ∂Q from the corners of neighboring squares, as in Figure 9.5. By (9.37), adjacent squares have nearby generation, and so all triangles have angles uniformly bounded above 0 and below π.

Enumerate the dyadic squares in each $\mathcal{W}_k$ as Q_{kj} and start with the first square $Q_{i1} \in \mathcal{W}_i$, where i is the lowest index such that $\mathcal{W}_i \neq \emptyset$. By property (ii), we know at least one neighboring square of Q_{i1}^+'s generation intersects γ; let R_{i1} be any of these. Let L_{i1} be a line in $3R_{i1}$ which is a minimizer in the definition of $\beta_\gamma(R_{i1})$, and reflect all the vertices in Q_{i1} across L_{i1} (our dyadic squares are closed, and so this is the center of Q_{i1} and any vertices on its boundary). As we proceed to latter Q_{jk}, reflect any vertices in Q_{jk} yet to be reflected across the line L_{jk} from R_{jk}. See Figure 9.6.

A single triangle T may have a different reflection line for each of its three vertices, but we show these lines are $O(\beta_T \operatorname{diam}(Q_j))$ apart and intersect at angle $O(\beta_T)$, where Q_j is any one of the dyadic squares associated to the vertices of T and β_T is the largest of several local β-numbers. This will imply that we can paste together the affine reflecting maps $T \mapsto T^*$, where T^* is the triangle whose vertices are the reflections of those of T, and obtain an injective

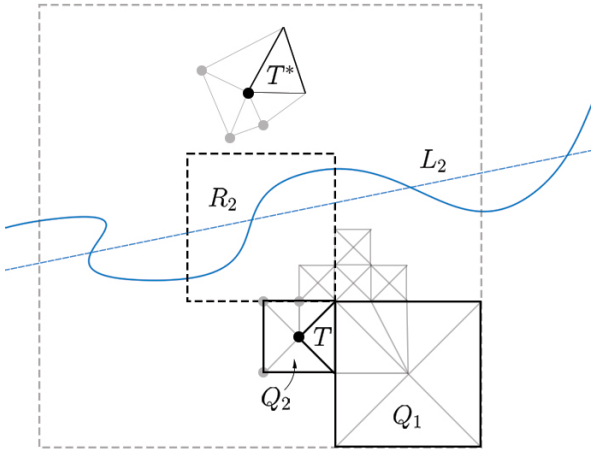

Figure 9.6: An example triangle T and its two associated Whitney squares Q_1 and Q_2. Here the vertex of T at the center of Q_2 is reflected across the best-fitting line L_2 for γ in $3R_2$ (along with the other vertices in Q_2, in this instance). The other two vertices of T are reflected across the non-pictured line L_1 for $3R_1$. Our proof shows L_1 and L_2 are distance $O(\beta_T \operatorname{diam}(Q_1))$ apart and intersect at angle $O(\beta_T)$, where $\beta_T := \max\{\beta_\gamma(R_1), \beta_\gamma(R_2)\}$, which implies that the reflecting map $T \mapsto T^*$ has reflection-dilatation $O(\beta_T)$.

quasiconformal reflection φ in a small neighborhood of γ whose "reflection-dilatation" is controlled by $C\beta_T$ on each triangle T.[†] We proceed with the details.

Begin by considering a fixed triangle T and the squares $\{Q_j\}_{j=1}^{n_T}$, $n_T \in \{1, 2, 3\}$, that generate the reflection of the vertices of T. Let R_j be the square for Q_j which intersects γ, and L_j the line from $\beta_\gamma(R_j)$. Our first observation is that when we restrict to dyadic squares in small neighborhood of γ, T^* is entirely in Ω^*, the unbounded component of the complement of γ. Indeed, since $L_j \cap 3R_j \neq \emptyset$, the distance from each reflected vertex v^* to L_j is $\lesssim \operatorname{diam}(Q_1)$, and thus the distance of v^* to γ is likewise $\lesssim \operatorname{diam}(Q_1)$. Since γ is a quasicircle, it has an "ϵ-collar" around itself, in the sense that there exists a fixed $\epsilon > 0$ such that $B(z, \epsilon) \cap \gamma$ is connected for every $z \in \gamma$ (if not, then γ comes arbitrarily-close to touching back upon itself, violating Ahlfors' 3-point condition for quasicircles). Hence by

[†]Note that by "paste together," we mean define a piecewise function φ which is the affine map $T \mapsto T^*$ on each triangle T. Each of these affine maps is unique, and they agree on the common edges between triangles because the vertices of a shared edge have the same reflections.

starting with squares Q_j with $C\operatorname{diam}(Q_j) < \epsilon$, we have $T^* \subset \Omega^*$ for every T.

Next we consider how far apart the different lines L_j can be. By moving a bounded number of generations up from any of the Q_j, we can find a dyadic square S such that $3S$ contains $\bigcup_{j=1}^{n_T} 3Q_j^+$, and so, in particular, $3S$ contains $3R_j$ for each j. If L is a minimizing line for $\beta_\gamma(S)$, we first note each of the L_j's is close to L. Indeed, for $z_j \in L_j \cap 3R_j$, let z_γ be the closest point on γ to z_j in $3R_j$, and z_L the closest point on L to z_γ. Then

$$|z_j - z_L| \leq |z_j - z_\gamma| + |z_\gamma - z_L| \leq \beta_\gamma(R_j)\operatorname{diam}(R_j) + \beta_\gamma(S)\operatorname{diam}(S) \lesssim \beta_T \operatorname{diam}(R_j),$$

where β_T is the max of the $\beta_\gamma(R_j)$'s and $\beta_\gamma(S)$. Thus L_j is contained in a strip of width $C\beta_T \operatorname{diam}(R_j)$ around L inside of $3R_j$, and so in particular the angle α_j between them is dominated by

$$\arctan\Big(\frac{C\beta_T \operatorname{diam}(R_j)/2}{3\operatorname{diam}(R_j)/2}\Big) \lesssim \beta_T \tag{9.38}$$

when all the β's we maximize over for β_T are sufficiently small. Since $\operatorname{diam}(S) \lesssim \operatorname{diam}(R_j)$, we see that L_j is contained in a strip of width $\lesssim \beta_T \operatorname{diam}(3S) \lesssim \beta_T \operatorname{diam}(Q_1)$ around L in all of $3S$, and hence any L_k is similarly contained within a strip of width $\lesssim \beta_T \operatorname{diam}(Q_1)$ around L_j in all of $3S$. Furthermore, the angle α_{jk} between L_j and L_k is $\lesssim \beta_T$ by (9.38) when the β's are small.

From elementary linear algebra we can conclude that a fixed vertex v of T has reflections under any two of the lines L_j and L_k that are at most $O(\beta_T \operatorname{diam}(Q_1))$ apart. Indeed, if $\operatorname{proj}_\ell(v)$ is the orthogonal projection of v onto a line ℓ, then the reflection v_i^* of v across L_i is $v_i^* = 2\operatorname{proj}_{L_i}(v) - v$, and so $|v_j^* - v_k^*| \lesssim |\operatorname{proj}_{L_j}(v) - \operatorname{proj}_{L_k}(v)|$. Without loss of generality $\operatorname{proj}_{L_k}(v) = 0$. Writing $L_j = \operatorname{span}\{u_j\} + w$ for some unit vector u_j and $w \perp u_j$, see Figure 9.7, we have

$$|\operatorname{proj}_{L_j}(v)| = |\langle u_j, v\rangle u_j + w| \leq |v||\cos(\pi/2 \pm \alpha_{jk})| + C\beta_T \operatorname{diam}(Q_1) \lesssim \beta_T \operatorname{diam}(Q_1) \tag{9.39}$$

by (9.38), when the β's are sufficiently small. Note that this implies that the map formed by gluing together the affine maps $T \mapsto T^*$ is injective when we restrict to a neighborhood of γ where the β's are very small.

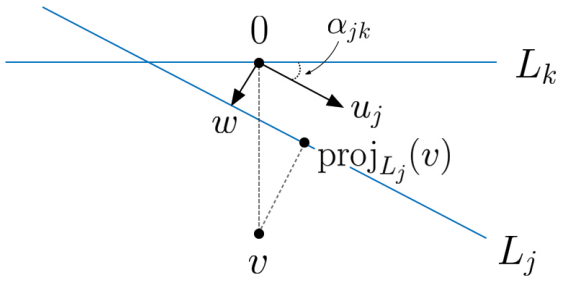

Figure 9.7: The distance between reflections of the same point in different lines is $O(\beta_T \operatorname{diam}(Q_1))$.

This map is a homeomorphism, reflecting a small neighborhood U_ϵ of $\partial\Omega$ in Ω across γ to a small neighborhood of $\partial\Omega^*$ in Ω^*. We claim it has reflection-dilatation $O(\beta_T)$. Let $w_j = (v_j)^*_j = 2\,\mathrm{proj}_{L_j}(v_j) - v_j$ be the reflection of v_j across L_j, $j = 1, 2, 3$, where v_i^*, recall, denotes reflection of a point v across L_i. That is, the w_j are the vertices of T^*. Writing

$$w_i - w_j = (v_i)^*_i - (v_j)^*_j = (v_i)^*_i - (v_j)^*_i + (v_j)^*_i - (v_j)^*_j,$$

we see by (9.39) that

$$\left|\frac{w_i - w_j}{(v_i)^*_i - (v_j)^*_i} - 1\right| = \frac{|(v_j)^*_i - (v_j)^*_j|}{|(v_i)^*_i - (v_j)^*_i|} = \frac{|(v_j)^*_i - (v_j)^*_j|}{|v_i - v_j|} \lesssim \beta_T \tag{9.40}$$

for small β's. Also, note

$$\begin{aligned} |w_i - w_j| &= |2(\mathrm{proj}_{L_i}(v_i) - \mathrm{proj}_{L_j}(v_j)) + v_j - v_i| \\ &\geq |v_j - v_i| - 2|\,\mathrm{proj}_{L_i}(v_i) - \mathrm{proj}_{L_j}(v_j)| \\ &\gtrsim \operatorname{diam}(Q_1) - \beta_T \operatorname{diam}(Q_1) \\ &\gtrsim \operatorname{diam}(Q_1) \end{aligned} \tag{9.41}$$

when the β's are sufficiently small.

To bound the distortion of the affine map which extends $v_i \mapsto w_i$, we first consider the dilatation of the map taking the triangle with vertices $0, 1$ and $a \in \mathbb{H}$ to that with vertices $0, 1$ and $b \in \mathbb{H}$. This linear map is explicitly

$$M(z) = \frac{b - \bar{a}}{a - \bar{a}} z + \frac{a - b}{a - \bar{a}} \bar{z},$$

and hence has dilatation

$$|\mu_M(z)| = \left|\frac{\overline{\partial} M}{\partial M}(z)\right| = \left|\frac{a-b}{b-\bar{a}}\right| \lesssim |a-b| \tag{9.42}$$

when both triangles have angles bounded above 0 and below π.

In our case, we compare T^* with the reflection T_1^* of T across L_1. By pre- and post-composing with translations, we may assume $w_1 = 0$, and so re-scaling by the second vertex yields vertices $a = \frac{w_3}{w_2}$ and $b = \frac{(v_3)_1^*}{(v_2)_1^*}$. Using (9.42), (9.39), (9.40) and (9.41), the linear map M taking T_1^* to T^* thus has dilatation

$$\begin{aligned}
|\mu_M(z)| \lesssim \left|\frac{w_3}{w_2} - \frac{(v_3)_1^*}{(v_2)_1^*}\right| &= \frac{1}{|w_2|}\left|w_3 - \frac{w_2}{(v_2)_1^*}(v_3)_1^*\right| \\
&\leq \frac{1}{|w_2|}\left(|w_3 - (v_3)_1^*| + |(v_3)_1^*|\left|1 - \frac{w_2}{(v_2)_1^*}\right|\right) \\
&\lesssim \frac{1}{\operatorname{diam}(Q_1)}\Big(\beta_T \operatorname{diam}(Q_1) + \operatorname{diam}(Q_1)\beta_T\Big) \lesssim \beta_T.
\end{aligned}$$

Our actual affine map of interest φ_T is the reflection taking T to T^*, and by pre- and post-composing by complex-affine maps $z \mapsto az + b$, we see the dilatation of φ_T is the same as the dilatation of the composition of M and $z \mapsto \bar{z}$. Hence the "reflection-dilatation" $\mu^*_{\varphi_T} := \frac{\partial \varphi_T}{\overline{\partial}\varphi_T}$ has modulus

$$|\mu^*_{\varphi_T}(z)| = \left|\frac{\partial(M(\bar{z}))}{\overline{\partial}(M(\bar{z}))}\right| = \left|\frac{(\overline{\partial} M)(\bar{z})}{(\partial M)(\bar{z})}\right| \lesssim \beta_T.$$

Since $\{\beta_\gamma(Q)\} \in \ell^p$, the β's are very small for all small dyadic squares Q. Hence by restricting to a small neighborhood of γ, we have $|\mu^*_{\varphi_T}(z)|^p \lesssim \beta_T^p$ for all triangles T in this neighborhood, and since the hyperbolic area of each triangle is comparable to 1 by the Koebe distortion theorem, we see

$$\int_T |\mu_T(z)|^p dA_\rho(z) \lesssim \beta_T^p.$$

By moving to an even smaller neighborhood if necessary, we glue these maps together and obtain an injective quasiconformal reflection defined in a small neighborhood $U_\epsilon \subset \Omega$ of γ in Ω which satisfies

$$\int_{U_\epsilon} |\mu^*(z)|^p dA_\rho(z) \lesssim \sum_{T \in U_\epsilon} \beta_T^p < \infty,$$

as each square chosen for β_T can only occur a bounded number of times, and $\{\beta_\gamma(Q)\} \in \ell^p$ by assumption. Note that we can extend this map quasiconformally to the rest of Ω. The underlying reason is that a quasisymmetric mapping $\psi : \mathbb{R} \to \mathbb{R}$ is extendable to a quasiconformal map $\tilde{\psi} : \overline{\mathbb{H}} \to \overline{\mathbb{H}}$ [19, Thm. 5.2], from which it follows that a quasisymmetric map between quasicircles is extendable to either side of the domain quasicircle. In our case, draw a quasicircle $\tilde{\gamma}$ in U_ϵ and observe that our reflection is quasisymmetric on $\tilde{\gamma}$ and maps it to another quasicircle, and hence we can extend our reflection from $\tilde{\gamma}$ inwards to all of Ω. We thus obtain a quasiconformal reflection $\varphi : \Omega \to \Omega^*$, which we can consider as an involution Φ of $\Omega \cup \Omega^*$,

$$\Phi(z) := \begin{cases} \varphi(z) & z \in \Omega \\ \varphi^{-1}(z) & z \in \Omega^*, \end{cases}$$

and which satisfies

$$\int_{\Omega \cup \Omega^*} |\mu^*_\Phi(z)|^p dA_\rho(z) < \infty.$$

To obtain (9.35), take a conformal map $f : \mathbb{D}^* \to \Omega^*$ which fixes infinity, set $j(z) := \frac{1}{\bar{z}}$, and note the composition $\Phi \circ f \circ j : \mathbb{D} \to \Omega$ is quasiconformal with dilatation

$$|\mu_{\Phi \circ f \circ j}(z)| = \left| \frac{\overline{\partial}(\Phi \circ f \circ j)}{\partial(\Phi \circ f \circ j)}(z) \right| = \left| \mu^*_\Phi(f(1/\bar{z})) \cdot \frac{f'(1/\bar{z})}{\overline{f'(1/\bar{z})}} \cdot \frac{z^2}{\bar{z}^2} \right| = |\mu^*_\Phi(f(1/\bar{z}))|,$$

and thus

$$\begin{aligned} \int_{\mathbb{D}} |\mu_{\Phi \circ f \circ j}(z)|^p dA_\rho(z) &= \int_{\mathbb{D}} |\mu^*_\Phi(f(1/\bar{z}))|^p dA_\rho(z) \\ &= \int_{\mathbb{D}^*} |\mu^*_\Phi(f(z))|^p dA_\rho(z) \\ &= \int_{\Omega^*} |\mu^*_\Phi(z)|^p dA_\rho(z) < \infty, \end{aligned}$$

where in each case dA_ρ is hyperbolic area in the domain of the given integral. □

As an aside, we note that this proof never uses the fact that $p > 1$, and hence Theorem 9.10 holds for all positive p. However, p-summability assumption becomes vacuous when

$0 < p \leq 1$, as curves γ which are not straight line segments do not satisfy (9.34) for such p. For example, it is not hard to see that $\gamma = \partial\mathbb{D}$ has $\sum_{Q\in\mathcal{Q}} \beta_\gamma(Q)^p < \infty$ for all $p > 1$, but $\sum_{Q\in\mathcal{Q}} \beta_\gamma(Q) = \infty$.

Proof of Theorem 9.1. If $\gamma \in T_p$, $2 \leq p < \infty$, by Theorem 9.3 we have $\{\beta_\gamma(Q)\}_\mathcal{Q} \in \ell^p$, and hence by Theorem 9.10 we see $\mu \in L^p(\mathbb{D}, dA_\rho)$. As noted above, it is known that this implies the pre-Schwarzian condition (9.2). □

We note that theorems 9.3 and 9.10 together show that $\mu \in L^p(\mathbb{D}, dA_\rho)$ is a necessary condition for membership in T_p for all $p > 1$. This appears to be a new result for $1 < p < 2$, and we hope in future work to show that this implies the pre-Schwarzian condition (9.2), thus completing the β-number characterization of T_p for all $p > 1$.

9.6 Corollaries and commentary

9.6.1 T_p in $\mathbb{R}^n$

As a consequence, we note that we can extend the definition of T_p from the plane to $\mathbb{R}^n$, as the β-numbers $\beta_\gamma(Q)$ are defined exactly as in (9.6) in any dimension n, with the dyadic squares replaced by n-dimensional dyadic cubes.

Definition 9.2. A Jordan arc $\gamma \subset \mathbb{R}^n$ belongs to the p-summable Teichmüller space $T_p(\mathbb{R}^n)$, $2 \leq p < \infty$, if

$$\sum_{Q\in\mathcal{Q}} \beta_Q(\gamma)^p < \infty.$$

By our characterization this coincides with the usual definition when $n = 2$.

9.6.2 A T_p-Loewner Teichmüller space

What characterizes the driving function ξ of $\gamma \in T_p$? By Wang's work [43], we know T_2 corresponds to $\int_{-\infty}^{\infty} \dot{\xi}(t)^2 dt < \infty$, and a naïve guess for T_p is that it corresponds to $\int_{-\infty}^{\infty} \dot{\xi}(t)^p dt < \infty$. However, we can immediately see this is incorrect, as local regularity

increases as local p-integrability of $\dot{\xi}$ increases, whereas regularity *decreases* as p increases for T_p. A second guess would be $\int_{-\infty}^{\infty} \dot{\xi}(t)^q dt < \infty$, where q is dual to p, but this is also wrong. Indeed, consider a vertical line segment in $\mathbb{H}$ which is followed by another line segment making a corner of any angle $\alpha \neq \pi$ with the vertical one. The driver ξ has derivative in L^q for any $q < 2$, but we know T_p curves do not have corners for any $1 \leq p < \infty$. This suggests the spaces defined by

$$\int_{-\infty}^{\infty} \dot{\xi}(t)^q dt < \infty. \tag{9.43}$$

are distinct from T_p for $p \neq 2$.

It would be interesting to investigate these spaces and see if they define a "q-summable-Loewner-Teichmüller space." One would have to verify that if (9.43) holds independent of the choice of root, much like the process for proving the Loewner loop energy is well defined in [33]. The numerical value of the "L^q-Dirichlet norm" in (9.43) is not well defined, as it is not invariant under scaling for $q \neq 2$, but its finiteness may be.

Problem 9.11. Determine if (9.43) defines a class of "q-summable-Loewner" quasicircles. How do these spaces relate to T_q? What properties characterize their conformal maps?

Problem 9.12. Characterize the driving functions of $\gamma \in T_p$, $p \neq 2$.

BIBLIOGRAPHY

[1] Lars V. Ahlfors. *Lectures on quasiconformal mappings,*. Van Nostrand mathematical studies, no. 10. Van Nostrand, Princeton, N.J., 1966.

[2] Kari Astala. *Elliptic Partial Differential Equations and Quasiconformal Mappings in the Plane (PMS-48)*. Princeton Mathematical Series. Princeton University Press, Princeton, NJ, 2008.

[3] Dmitry Beliaev, Atul Shekhar, and Vlad Margarint. Continuity of zero-hitting times of Bessel processes and welding homeomorphisms of SLE_κ. 2020.

[4] Christopher Bishop. The traveling salesman theorem for jordan curves. *Preprint*.

[5] Christopher Bishop. Weil-petersson curves, β-numbers, and minimal surfaces. *Preprint*.

[6] Christopher J Bishop. Conformal welding and Koebe's theorem. *Annals of mathematics*, 166(3):613–656, 2007.

[7] Girolamo Cardano. *Artis Magnae, Sive de Regulis Algebraicis Liber Unus*. Italy, 1545.

[8] Guizhen Cui. Integrably asymptotic affine homeomorphisms of the circle and teichmüller spaces. *Science in China. Series A, Mathematics, physics, astronomy*, 43(3):267–279, 2000.

[9] Peter L. Duren. *Univalent functions*. Grundlehren der mathematischen Wissenschaften; 259. Springer-Verlag, New York, 1983.

[10] Lawrence Craig Evans and Ronald F Gariepy. *Measure Theory and Fine Properties of Functions, Revised Edition*. CRC Press LLC, Oakville, 2015.

[11] Eva A Gallardo-Gutiérrez, María J González, Fernando Pérez-González, Christian Pommerenke, and Jouni Rättyä. Locally univalent functions, VMOA and the Dirichlet space. *Proceedings of the London Mathematical Society*, 106(3):565–588, 2013.

[12] Hui Guo. Integrable Teichmüller spaces. *Science in China. Series A, Mathematics, physics, astronomy*, 43(1):47–58, 2000.

[13] Juha Heinonen. *Lectures on analysis on metric spaces*. Universitext. Springer, New York, 2001.

[14] Gavin L Jones. The Grunsky operator and the Schatten ideals. *The Michigan mathematical journal*, 46(1):93–100, 1999.

[15] W Kager and B Nienhuis. A guide to stochastic Löwner evolution and its applications. *Journal of statistical physics*, 115(5):1149–1229, 2004.

[16] W Kager, B Nienhuis, and L.P Kadanoff. Exact solutions for Loewner evolutions. *Journal of statistical physics*, 115(3):805–822, 2004.

[17] Gregory F. Lawler. *Conformally invariant processes in the plane*. Mathematical surveys and monographs; no. 114. American Mathematical Society, Providence, R.I., 2005.

[18] Gregory F Lawler. Conformal invariance and 2d statistical physics. *Bulletin (new series) of the American Mathematical Society*, 46(1):35–54, 2009.

[19] O Lehto. *Univalent Functions and Teichmüller Spaces*, volume 109 of *Graduate Texts in Mathematics*. Springer, 2012.

[20] Olli Lehto. *Quasiconformal mappings in the plane*. Grundlehren der mathematischen Wissenschaften in Einzeldarstellungen mit besonderer Berücksichtigung der Anwendungsgebiete; Bd. 126. Springer, Berlin, Heidelberg, New York, 2nd ed. edition, 1973.

[21] Joan Lind, Donald E Marshall, and Steffen Rohde. Collisions and spirals of Loewner traces. *Duke mathematical journal*, 154(3):527–573, 2010.

[22] Joan Lind and Huy Tran. Regularity of Loewner curves. *Indiana University mathematics journal*, 65(5):1675–1712, 2016.

[23] Joan R Lind. A sharp condition for the Loewner equation to generate slits. *Annales Academiæ Scientiarum Fennicæ Mathematica*, 30:143–158, 2005.

[24] Joan R Lind and Steffen Rohde. Loewner curvature. *Mathematische annalen*, 364(3):1517–1534, 2016.

[25] Karl Löwner. Untersuchungen über schlichte konforme abbildungen des einheitskreises. i. *Mathematische Annalen volume*, 89:103–121, 1923.

[26] Don Marshall, Steffen Rohde, and Yilin Wang. Hyperbolic geodesic pairs. *In preparation*.

[27] Donald E. Marshall and Steffen Rohde. The Loewner differential equation and slit mappings. *Journal of the American Mathematical Society*, 18(4):763–778, 2005.

[28] Donald E. Marshall and Steffen Rohde. Convergence of a variant of the zipper algorithm for conformal mapping. *SIAM journal on numerical analysis*, 45(6):2577–2609, 2007.

[29] Peter Mörters and Yuval Peres. *Brownian Motion*, volume 30 of *Cambridge series in statistical and probabilistic mathematics*. Cambridge University Press, Cambridge, 2010.

[30] Kate Okikiolu. Characterization of subsets of rectifiable curves in $\mathbb{R}^n$. *Journal of the London Mathematical Society.*, 46(2):336–348, 1992.

[31] Christian Pommerenke. On univalent functions, Bloch functions and VMOA. *Mathematische annalen*, 236(3):199–208, 1978.

[32] Christian Pommerenke. *Boundary behaviour of conformal maps*. Grundlehren der mathematischen Wissenschaften ; 299. Springer-Verlag, Berlin ; New York, 1992.

[33] Steffen Rohde and Yilin Wang. The Loewner energy of loops and regularity of driving functions. *International mathematics research notices*, 2019.

[34] Steffen Rohde and Carto Wong. Half-plane capacity and conformal radius. *Proceedings of the American Mathematical Society*, 142(3):931–938, 2014.

[35] Oded Schramm. Scaling limits of loop-erased random walks and uniform spanning trees. *Israel journal of mathematics*, 118(1):221–288, 2000.

[36] Oded Schramm. A percolation formula. *Electronic communications in probability*, 6, 2001.

[37] Raanan Schul. Subsets of rectifiable curves in Hilbert space-the analyst's TSP. *Journal d'analyse mathématique (Jerusalem)*, 103(1):331–375, 2007.

[38] Yuliang Shen. Weil-Petersson Teichmüller space. *American journal of mathematics*, 140(4):1041–1074, 2018.

[39] Leon A. Takhtajan and Lee-Peng Teo. *Weil-Petersson metric on the universal Teichmüller space*. Memoirs of the American Mathematical Society; no. 861. American Mathematical Society, Providence, R.I., 2006.

[40] Terrance Tao. Oded Schramm. `https://terrytao.wordpress.com/2008/09/03/oded-schramm/#more-645`, 2008.

[41] Huy Tran and Yizheng Yuan. A support theorem for SLE curves. *Electronic journal of probability*, 25, 2020.

[42] Yilin Wang. The energy of a deterministic Loewner chain: Reversibility and interpretation via SLE_{0+}. *Journal of the European Mathematical Society : JEMS*, 21(7):1915–1941, 2019.

[43] Yilin Wang. Equivalent descriptions of the Loewner energy. *Inventiones mathematicae*, 218(2):573–621, 2019.

[44] Malik Younsi. Removability and non-injectivity of conformal welding. *Annales Academiae scientiarum Fennicae. Mathematica*, 43:463–473, 2018.